UNIVERSIDADE FEDERAL DE UBERLÂNDIA

FACULDADE DE ENGENHARIA ELÉTRICA

MARIANA CARDOSO MELO

DECODING CORTICAL RESPONSE DURING MOTOR TASKS USING BRAIN CONNECTIVITY

UFU

2020

MARIANA CARDOSO MELO[1]

DECODING CORTICAL RESPONSE DURING MOTOR TASKS USING BRAIN CONNECTIVITY

PhD thesis presented to the Graduate Program of Electrical Engineering at the Federal University of Uberlândia as part of the requirements for obtaining the title of Doctor of Science.

Area: Biomedical Engineering

Supervisor: Prof. Dr. Alcimar Barbosa Soares

Examination Board:

Dr. Alcimar Barbosa Soares – UFU (Supervisor)
Dr. Adriano de Oliveira Andrade – UFU
Dr. Ailton Luiz Dias Siqueira Junior – IFTM
Dr. Sérgio Ricardo de Jesus Oliveira – UFU
Dr. Teodiano Freire Bastos Filho - UFES

Uberlândia

2020

[1] This reseach was funded by CAPES - Brasil, and ELAP - Canada.

Dados Internacionais de Catalogação na Publicação (CIP)
Sistema de Bibliotecas da UFU, MG, Brasil.

M528d 2020

Melo, Mariana Cardoso, 1990-
Decoding cortical response during motor tasks using brain connectivity [recurso eletrônico] / Mariana Cardoso Melo. - 2020.

Orientador: Alcimar Barbosa Soares.
Tese (Doutorado) - Universidade Federal de Uberlândia, Programa de Pós-Graduação em Engenharia Elétrica.
Modo de acesso: Internet.
Disponível em: http://doi.org/10.14393/ufu.te.2020.3003
Inclui bibliografia.
Inclui ilustrações.

1. Engenharia elétrica. I. Soares, Alcimar Barbosa, 1965-, (Orient.). II. Universidade Federal de Uberlândia. Programa de Pós-Graduação em Engenharia Elétrica. III. Título.

CDU: 621.3

Rejâne Maria da Silva – CRB6/1925

UNIVERSIDADE FEDERAL DE UBERLÂNDIA
Coordenação do Programa de Pós-Graduação em Engenharia Elétrica
Av. João Naves de Ávila, 2121, Bloco 3N - Bairro Santa Mônica, Uberlândia-MG, CEP 38400-902
Telefone: (34) 3239-4707 - www.posgrad.feelt.ufu.br - copel@ufu.br

ATA DE DEFESA - PÓS-GRADUAÇÃO

Programa de Pós-Graduação em:	Engenharia Elétrica				
Defesa de:	Tese de Doutorado, 270, PPGEELT				
Data:	Trinta de junho de dois mil e vinte	Hora de início:	09:00	Hora de encerramento:	13:15
Matrícula do Discente:	11423EEL011				
Nome do Discente:	Mariana Cardoso Melo				
Título do Trabalho:	Decoding Cortical Response During Motor Tasks Using Brain Connectivity				
Área de concentração:	Processamento da informação				
Linha de pesquisa:	Engenharia biomédica				
Projeto de Pesquisa de vinculação:	Título: Eletroencefalografia de Alta Definição para Decodificação da Atividade Cortical Aplicada a Reabilitação e Avaliação Neuromotora. Agência Financiadora: CAPES Início: 03/2014 Término: 12/2018 Coordenador: Alcimar Barbosa Soares				

Reuniu-se por meio de videoconferência, a Banca Examinadora, designada pelo Colegiado do Programa de Pós-graduação em Engenharia Elétrica, assim composta: Professores Doutores: Adriano de Oliveira Andrade - FEELT/UFU; Sérgio Ricardo de Jesus - FEELT/UFU; Ailton Luiz Dias Siqueira Junior - IFTM; Teodiano Freire Bastos Filho - UFES; Alcimar Barbosa Soares - FEELT/UFU, orientador da candidata.

Iniciando os trabalhos o presidente da mesa, Dr. Alcimar Barbosa Soares, apresentou a Comissão Examinadora e o candidato, agradeceu a presença do público, e concedeu à Discente a palavra para a exposição do seu trabalho. A duração da apresentação da Discente e o tempo de arguição e resposta foram conforme as normas do Programa.

A seguir o senhor(a) presidente concedeu a palavra, pela ordem sucessivamente, aos(às) examinadores(as), que passaram a arguir o(a) candidato(a). Ultimada a arguição, que se desenvolveu dentro dos termos regimentais, a Banca, em sessão secreta, atribuiu o resultado final, considerando o(a) candidato(a):

Aprovada.

Esta defesa faz parte dos requisitos necessários à obtenção do título de Doutor.

O competente diploma será expedido após cumprimento dos demais requisitos, conforme as normas do Programa, a legislação pertinente e a regulamentação interna da UFU.

Nada mais havendo a tratar foram encerrados os trabalhos. Foi lavrada a presente ata que após lida e achada conforme foi assinada pela Banca Examinadora.

Documento assinado eletronicamente por **Alcimar Barbosa Soares**, **Professor(a) do Magistério Superior**, em 30/06/2020, às 13:45, conforme horário oficial de Brasília, com fundamento no art. 6º, § 1º, do Decreto nº 8.539, de 8 de outubro de 2015.

Documento assinado eletronicamente por **Adriano de Oliveira Andrade**, **Professor(a) do Magistério Superior**, em 30/06/2020, às 14:15, conforme horário oficial de Brasília, com fundamento no art. 6º, § 1º, do Decreto nº 8.539, de 8 de outubro de 2015.

Documento assinado eletronicamente por **Sergio Ricardo de Jesus Oliveira**, **Membro de Comissão**, em 30/06/2020, às 15:30, conforme horário oficial de Brasília, com fundamento no art. 6º, § 1º, do Decreto nº 8.539, de 8 de outubro de 2015.

Documento assinado eletronicamente por **Ailton Luiz Dias Siqueira Junior**, **Usuário Externo**, em 30/06/2020, às 19:51, conforme horário oficial de Brasília, com fundamento no art. 6º, § 1º, do Decreto nº 8.539, de 8 de outubro de 2015.

Documento assinado eletronicamente por **TEODIANO FREIRE BASTOS FILHO**, **Usuário Externo**, em 01/07/2020, às 11:24, conforme horário oficial de Brasília, com fundamento no art. 6º, § 1º, do Decreto nº 8.539, de 8 de outubro de 2015.

A autenticidade deste documento pode ser conferida no site https://www.sei.ufu.br/sei/controlador_externo.php?acao=documento_conferir&id_orgao_acesso_externo=0, informando o código verificador **2093364** e o código CRC **976D7F40**.

Referência: Processo nº 23117.035874/2020-28 SEI nº 2093364

DECODING CORTICAL RESPONSE DURING MOTOR TASKS USING BRAIN CONNECTIVITY

MARIANA CARDOSO MELO

PhD thesis presented to the Graduate Program of Electrical Engineering at the Federal University of Uberlândia as part of the requirements for obtaining the title of Doctor of Science.

Prof. Alcimar Barbosa Soares, PhD	Prof. José Roberto Camacho, PhD
Supervisor	Head of the Graduate Program

ACKNOWLEDGMENTS

I would like to thank my family and my friends, and everyone who has been part of my journey. I would like to thank Biolab colleagues. My supervisor Alcimar Soares, for providing me an incredible learning process during my PhD studies. Thank you for your patience and trust in my work. And I would like to thank all the professors and technicians from the Electrical Engineering Faculty that helped me. In addition, thanks to Dr. Sridhar Krishnan, SAR lab supervisor, and all colleagues from Canada for receiving me. In special, I would like to thank Dharmendra Gurve, Vytautas Abromavicius, Marco Tullio, Dhainner, Eduardo Carvalho, Gabriela Dyonísio, Gustavo Moreira, Letícia Segatto, Gaetan Daevout, Nathália Fernandes, Ludymila Borges, Amanda Rabelo, Everton Lira and Denis Deslile for the friendship no matter the distance. I would also like to thank my São Paulo's colleagues, especially, Karina Abrahão, Andréia Bezerra, Gisele Cardoso, Marianna Cecyn, Bruna Franchi, Erica Garisto, Susy Tassini, and Johnny Carvalho!

"A person who never made a mistake never tried anything new.".

Albert Einstein

"Our greatest weakness lies in giving up. The most certain way to succeed is always to try just one more time."

Thomas A. Edison

ABSTRACT

Sensorimotor integration is defined as the capacity of the central nervous system to integrate different sources of stimuli and transform such inputs in motor actions. Traditional approaches to measure sensorimotor dynamics are based on sensorimotor rhythms detected by Electroencephalography (EEG), such as the Event-Related Desynchronization (ERD) and Event-Related Synchronization (ERS). However, it is still not clear what are the underlying cortical dynamics involved in voluntary movements, and there is a lack of understanding of the temporal flow patterns related to a task. Although the models for motor decoding have improved considerably over the past decade, Brain-Machine Interfaces (BMIs), such as those attempting to control upper-limb prostheses, are still far from the goal of reaching naturalistic and dexterous control like our natural limbs.

In this thesis, a model using connectivity estimators on EEG signals is proposed, with the aim of mapping cortical dynamics involved in sensorimotor integration while performing motor tasks. Here, special focus is given to wrist movements, since they are extremely important for proper handling of objects and have not been adequately explored in current literature associated with neural and standard control models used for upper-limb prosthesis. After initial screening, Mutual Information (MI) was chosen as the connectivity strategy for the aforementioned task. To estimate the most important channels and connectivity pairs of MI, a preliminary analysis based on the differences between resting and execution was performed. After the selection, MIs were estimated at higher temporal resolution, and separated in alpha and beta bands, from which a set of features was extracted and used as input for a Support Vector Machine (SVM) classifier to estimate the motor tasks (wrist pronation and wrist supination). For validation, we also estimated motor tasks using a conventional method for sensorimotor analysis, extracting significant ERD components and classified the data using SVM.

The results showed higher accuracies when using the proposed model in beta band and MI features (89.65%). Alpha band resulted in 73.68% accuracy. On the other hand, using ERD, the accuracy of the classifier was 60.73% and 62.49% for alpha and beta bands, respectively. We conclude that the proposed method using functional connectivity and a proper model for the selection of important pairs over specific frequency bands has better response in identifying wrist movements. This strategy could be potentially applied in BMIs that control prosthetic devices at various levels.

Keywords: *Brain Connectivity, Mutual Information, Motor task, Electroencephalography, Event-Related Desynchronization, Brain-Machine Interfaces.*

LIST OF FIGURES

LIST OF TABLES

SUMMARY

ACRONYMS

AR – Autoregressive Model

ALS - Amyotrophic Lateral Sclerosis

ASD – Autism Spectrum Disorder

aIPS – Anterior Intraparietal sulcus

BA – Brodmann Area

BMI – Brain-Machine Interface

BN – Bayesian Network

CAR – Common Average Reference

CV – Cross Validation

CST – Corticospinal Tract

DAG – Directed Acyclic Graph

DLPFC – Dorsolateral prefrontal cortex

dDTF – direct Directed Transfer Function

DTF – Directed Transfer Function

DTI – Diffusion Tensor Imaging

ECog – Electrocorticography

EEG – Electroencephalography

EOG – Electrooculogram

ERD – Event-Related Desynchronization

ERS – Event-Related Synchronization

ERSP – Event-Related Spectral Potential

FES – Functional Electric Stimulation

fMRI – Functional Magnetic Resonance Imaging

fNIRS – Functional Near-Infrared Spectroscopy

GCI – Granger Causality Index

ICA – Independent Component Analysis

ITR – Information Transfer Rate

JPD – Joint Probability Distribution

LFP – Local Field Potential

M1 – Primary Motor Cortex

MEG – Magnetoencephalography

MI – Mutual Information

MIm – Motor Imagery

MRI – Magnetic Resonance Imaging

MVAR – Multivariate Autoregressive

MUA – Multi-Unit Activity

NIRS – Near-Infrared Spectroscopy

NMI – Normalized Mutual Information

PDC – Partial Directed Coherence

PLV – Phase-Locking Synchronization

PMC – Premotor Cortex

PPC – Posterior Parietal Cortex

RSS – Repetitive Tactile Stimulation

S1 – Primary Somatosensory Cortex

SCP – Slow Cortical Potentials

SCI – Spinal Cord Injury

SEP - Somatosensory Evoked Potentials

sDTF – short-time Directed Transfer Function

SL – Synchronization Likelihood

SMA – Supplementary Motor Area

SMC – Sensorimotor Cortex

SMR – Sensorimotor Rhythm

SNR – Signal-to-Noise

SUA – Single-Unit Activity

TC – Total Correlation

TE – Execution Time

TMS – Transcranial Magnetic Stimulation

TV-DBN – Time-Varying Bayesian Networks

VA – Ventral Anterior Nuclei

VL – Ventral Lateral Nuclei

VPL – Ventral Posterior Lateral

1. INTRODUCTION

In the last decades, we have seen an explosion in research attempting to explain how the brain executes and coordinates the various tasks it deals with, from complex cognitive functions to the contraction of a muscle, to speaking and understanding language, etc.

In the 19th century, there were two main study streams of thinking and researching brain function, localizationists and connectionists [1]. Localizationists researchers believed that specific functions are attributed to gray matter brain areas, and impairments occur due to lesions in these areas. Historical examples of localizationist points of view are the findings of Broca and Wernicke, that related speech production with specific cortical areas, and the work of Brodmann, that proposed a map of 46 cortical regions (known as Brodmann Areas) and their functionality [2,3]. According to the connectionists, the neurons are the central processing element of the brain, and large numbers of neurons operate simultaneously and integrate to process the information [4].

Currently, those standpoints are complementary and are incorporated in what we now call functional specialization and functional integration. Functional specialization implies that a cortical area is responsible for some cognitive and functional aspects and can be anatomically segregated within the cortex. Thus, the brain supports functions related to sensory information, memory, learning, and perception by integrating many of those specialized areas, with the coordinated activity of interconnecting neurons, characterizing the so-called functional integration [1,5].

It is known that the integration between sensory and motor systems is essential for motor control. Thus, the so-called sensorimotor integration is defined as the capability of the central nervous system to integrate different sources of stimuli and to transform such inputs in motor actions [6].

The neural processes involved in the coordination of the voluntary movement are divided into three sequential phases: perception of the external environment and the individual itself, the use of the external information to decide the necessary action (cognitive process); and, the execution of the chosen motor plan [7].

Another example of sensorimotor integration is when an individual reads a written word out loud. First, light (visible electromagnetic waves) reaches the eyes; then, the photoreceptors from the retina convert these waves into electrochemical

signals, which are sent to the brain. The Primary Visual Cortex is the first stage of cortical processing of visual information, and it is responsible for decoding the data. For speech production, visual information is transmitted to the posterior language area, including Wernicke's area, travels to Broca's area, and then to the Primary Motor Cortex [8,9].

The areas of Wernicke and Broca generate the necessary motor control for breathing, vocalization, and articulation of speech; thus, body parts, such as lips, tongue, jaw, vellum and the larynx must have precise and simultaneous movements so that the sound does not get distorted [8].

Another example of the coordinated activity of cortical areas is when we reach and hold a glass of water. First, the subject identifies the target (glass) in space. In a simplified description, the aim (move the arm and open hands to get the glass) is identified by the Posterior Parietal Cortex, which receives input from somatosensory, visual, vestibular, and auditory systems, to construct the sense of the body position concerning the target. This information travels to the Supplementary Motor and Premotor Areas, where movement is planned. In this stage, the required muscles, the series of contractions, and the required force and trajectory are planned. Lastly, the motor plan is transmitted to the Primary Motor Cortex, which is responsible for the execution of the voluntary movement. From there, neural information is sent to descending pathways and, finally, to interneurons, motor neurons, and muscles [7,10].

It is assumed that the nervous system has an internal model to predict the environmental changes that result from a motor action. This model is part of the sensorimotor learning process, in which the individual can learn behavioral abilities or learn new skills, e.g., move the cursor of the screen to the desired position, play an instrument, or stop the car on the right moment [11].

The internal models can be classified in inverse or forward model [11]. Given a desired future state, the inverse model generates the motor command that is necessary for this state to happen. In other words, in this model, the nervous system determines the motor command that will reach the target state. The forward model is used by the nervous system to estimate the next state of the motor system and the sensory stimuli that result from a motion. Any difference between this and the feedback received may be used by the motor system to adjust motor control in real-time, as it is required for complex and fast motor activities [12].

Sensorimotor dynamics can be measured through Neuroimaging techniques, such as functional Magnetic Resonance Imaging (fMRI) [13], functional Near-Infrared Spectroscopy (fNIRS) [14], and Electrophysiological methods, such as Electroencephalography (EEG) [15] and Electrocorticography (ECoG) [16].

Neuroimaging techniques have an advantage of high spatial resolution and the possibility to capture the activity in subcortical areas. Although methods such as fMRI have high spatial resolutions (3-4 mm), the temporal resolution is limited by the hemodynamic response time [17]. Typically, it has a width of ~3 s and a peak occurring ~5–6 s after the onset of a neural stimulus. Thus, it is not the best alternative for detecting the temporal changes in sensorimotor integration that occur on a scale of milliseconds (ms) [25].

Electrophysiological methods can be invasive and non-invasive. The most used non-invasive macroscopic recording is EEG, in which the electrodes are placed on the scalp. Mesoscopic invasive methods are ECoG, in which electrodes are placed on the exposed cortex, and Local Field Potential (LFP) recording, where voltage is recorded by a microelectrode inserted in the neuronal tissue [25].

A typical adult human EEG signal is about 10 μV to 100 μV in amplitude and frequency range of 0-100 Hz when measured from the scalp. EEG can be seen as a spatiotemporally smoothed version of the local field potential (LFP), with 50 mm of spatial resolution and with ~1-3 ms of temporal resolution [18]. Also, it is not directly associated with the firing patterns of individual neurons, due to the attenuating effects of the tissues between the current source and the recording EEG electrodes.

The recently introduced high-density EEG, in combination with source modeling, improved the spatial resolution significantly [19]. The spatial and temporal resolution of the ECoG is higher than EEG (i.e., <1 cm/<1 ms, respectively), with a higher signal-to-noise ratio, and it is less susceptibility to artifacts than EEG [20]. Nevertheless, ECoG requires a craniotomy, a risky delicate procedure, and may result in tissue rejection and infection. In that sense, most of the current research groups prefer the use of EEG for research and rehabilitation [21].

EEG has been used in various attempts to better understand the process of sensorimotor integration. Some studies have suggested that the EEG gamma band is responsible for the communication between cortical areas during the performance of sensorimotor integration tasks. These findings indicate that gamma plays an essential

role in the early stages of information processing and of sensorimotor integration process [22]. Oscillations in gamma can be related to cortical operation during recognizing of familiar objects and to the efficiency of forthcoming of sensory information in the relevant sensory cortical areas. Thus, coordinated sensory gamma oscillations play an essential role in direct interactions, cognitive processes involved in the perception and comparison mechanisms related to stored memory content. Also, phase synchronization can promote communication between sensory cortices [23,24].

Alpha and beta bands also play an important role in sensorimotor integration. Verhagen et al. (2012) associated EEG and time-frequency analysis of alpha and beta bands to verify the cortical dynamics of sensorimotor integration during grasp planning [25]. Jenson et al. (2014) examined real-time event-related spectral perturbations, i.e., event-related synchronization and event-related desynchronization, within alpha and beta bands for the comprehension of speech perception and production [26].

Alterations in sensorimotor integration in healthy aging were studied by Brown et al. (2018). Initially, the authors evaluated the baseline neurophysiology of sensorimotor integration using Somatosensory Evoked Potentials (SEPs). Sensorimotor integration was tested in two ways. First, by pairing a hand muscle vibration with single and paired-pulse Transcranial Magnetic Stimulation, to enable a direct comparison between motor circuitry alone and somatosensory influences on motor circuitry. Other techniques such as short-latency afferent inhibition, afferent facilitation, and long-latency afferent inhibition were measured from median nerve stimulation with TMS. In the second experimental session, it was designed a block of sensory training to modulate sensorimotor integration that preceded this neurophysiological assessment. The results suggest that there is a differential aging-related modulation of sensorimotor integration, based on the type of afferent information. Additionally, sensorimotor integration is modifiable with a single session of sensory training, and this ability for neuroplastic change is retained with healthy aging [27].

Despite all these findings and the research related to sensorimotor integration, they according to Tam et al. (2019), although motor decoding performance is improving, we are still very far from the goal of reaching naturalistic and dexterous control of prosthetic limbs in the same manner as we control our natural limbs [28].

A mathematical technique that has been used to study the functional integration of brain areas is based on the use of functional and effective connectivity [4]. Functional

connectivity consists of correlations (statistical dependencies) between spatially distributed neurophysiological time series. On the other hand, effective connectivity refers to the estimation of how two or more brain regions causally influence each other. Effective connectivity is activity-dependent, and provides a model of interactions or coupling between brain time series [4,29,30].

Brain connectivity analysis can be applied to study the effects of a neurological injury and its intrinsic characteristics, elucidating how neurons and neural networks process information. In so doing, it may be possible to contribute towards the development of treatment and monitoring strategies for various neurological dysfunctions caused by Parkinson, Alzheimer's disease, Spinal Cord Injury (SCI), Huntington diseases, and other pathologies or injuries [31,32,33,34]. Thus, this technique enables us to verify the cortical networks involved with sensory, motor, and cognitive functions and explain sensorimotor integration [35]. Other fMRI studies analyzed the brain structure and functional connectivity of sensorimotor integration between known sensory and motor structures within typically developing children and those with Autism Spectrum Disorder (ASD).

EEG-based brain connectivity models have been studied by various researches. Chung et al. (2017) used this approach to find how beta-band activity and connectivity within and between cortical regions are coordinated to enhance motor performance [36]. Freyer et al. (2012) investigated the impact of passive sensory stimulation on the resting-state functional connectivity in the human brain [37]. Additionally, a study from Peterson et al. (2019) investigated cortical connectivity during perturbed balance, since, until now, little information is known about the cortical flow of signals for balance [38] and other movement dynamics [39].

Strategies using EEG-based brain connectivity were also applied for the improvement of Brain-Machine Interfaces accuracy. Daly et al. (2012) mapped phased synchronization levels for EEG channels and achieved higher levels of classification with functional dynamics in relation to traditional features used in the classification of a finger tap BMI [40]. Xu et al. (2020) used EEG connectivity features for affective BMIs in which five types of emotions were discriminated (disgust, fear, sadness, happiness, and neutrality), showing that EEG connectivity combined eye movement data could be used to represent an emotion. Also, the proposed method outperformed the state-of-art ones for emotion classification [41]. In a review of Hamedi et al. (2016), it was

mentioned that most motor imagery (MIm) BMIs are based on temporal, spectral, and spatial single channel features. Nevertheless, there is still not a successful communication for a completely locked-in subject. Thus, since brain connectivity provides cortical dynamic information, it has been considered a promising strategy to improve MIm-BMIs performance [42].

Some important variables related to BMI control signals are the Information Transfer Rate (ITR), the number of possible choices and the requirement of training. ITR is the combination of speed and accuracy of a BMI to determine the amount of information. Sensorimotor Rhythms (SMR) and Slow Cortical Potentials (SCP) do not require an external stimulus (endogenous BMI), but they have less number of choices (possible mental states with reasonable accuracy are 2 or 4 for SCPs and around 2 to 5 for SMRs), lower ITR and requirement of training, differently to the ones that require external stimulus, such as P300 evoked potentials and visual evoked potentials (exogeneous BMI) [21].

Although the great advantages of exogenous BMIs, they require that the user stand in front a screen and keep the eyes fixed on one point to manipulate the BMI, causing fatigue to the user [21]. Thus, due to the fact SMR are readily detectable in healthy as well as individuals with motor impairments, like SCI, amyotrophic lateral sclerosis (ALS), and stroke [43], they are the most common EEG methods implemented for BMIs, especially for imagery of movement [44].

It is important to consider that long-term stability of BMI performance can be affected due to user-related factors, such as aging, lack of motivation or neuropathic pain, and to hardware and technological factors, such as montage difficulty and algorithms for decoding of motor intention [45,46,47,48]. In addition, most BMIs have methods developed mainly in healthy subjects, and it is evident the difficulty in translating them to injured patients [49,50].

Several motor BMI studies are also focused in hand movement. In Cordella et al. (2016), it was shown that around 98% of upper limb prosthetic users are demanding various improvements in the design of those devices, such as to feel the force applied and the temperature of the object been handled by the prosthesis, and also the ability performing additional and more complex movements such as moving individual fingers and increased wrist range of motion and control (flexion/extension and pronation/supination) [51].

Wrist movements are especially important, since they allow for better manipulation of objects and contribute to the mobility of the arm/hand system. In spite of this, most robotic and prosthetic research studies are focused on the development of end effectors/terminal devices (hands, grippers, etc.), and not much has been done to improve and perfect wrist control [52].

Therefore, as shown in literature, brain connectivity could be used potentially as markers of brain activity sensorimotor integration, since it can distinguish and depict temporarily correlated regions and/or causal relations between brain regions, providing richer cortical information for BMIs, despite the user conditions. However, there is not a gold-standard of what is the most appropriate technique and protocol for each kind of analysis well established, such as sensorimotor rhythms.

Additionally, despite the great importance of wrist movements, they are not well explored in prosthetics, with lower classification accuracy in comparison to hand movements. A great difficulty in the classification of these movements is due to the fact they are coordinate by cortical regions very close together.

We hypothesize that, since functional connectivity provides information on how a brain region is temporally correlated to others, it is possible to create an EEG-based strategy to characterize sensorimotor integration, based in the most temporally relevant connections for similar movements, such as wrist movements, without an external stimulus and with a reduced number of electrodes and window of analysis. Consequently, with the proposed strategy, we argue that it can be possible to increase ITR and the accuracy of BMIs.

1.1 Objectives

This work proposes to create a sequential strategy to characterize sensorimotor integration dynamics based on EEG connectivity estimators in order to discriminate similar movements. To do so, the following specific objectives will be pursued in this thesis:

- Define the most suited connectivity technique for cortical activity analyses during the performance of motor tasks.
- Apply the selected connectivity strategy and obtain the neural dynamics during the execution of motor tasks (pronation and supination).

- Devise a model for select the most relevant connections (dimensionality reduction).
- Evaluate the performance of the proposed connectivity strategy using a standard decoder (supervised classifier).
- Compare the performance of the proposed connectivity strategy with conventional models.

2. CORTICAL AREAS RELATED TO HUMAN MOTOR CONTROL

This chapter will present an overview about the cortical areas related to human motor control. For this PhD thesis, cortical response will be mapped by connectivity methods in order to decode motor tasks.

The human motor system can perform different voluntary and non-voluntary motor tasks. For voluntary movements, the process is expressed in a sequential flow of information: Idea – Plan – Select – Move. In this context, the start of movements occurs with the idea, or the goal to be reached, then, this is converted to a plan directing the best way to achieve it; later, muscles are selected to execute the movement. However, this simplified flow does not consider that these elements can be performed in parallel, in time and space, known as brain functional integration. Generally, the areas that comprise the motor system can be organized in hierarchical levels of control, in which the lowest levels are located in primary sensory and motor cortices and higher levels are located at increasing synaptic distance from the periphery summarized as follows [53]:

- Somatosensory system
- Association cortex
- Motor cortical areas
  i. Primary motor cortex
  ii. Dorsal premotor cortex
  iii. Supplementary motor area
- Basal ganglia
- Cerebellum
- Midbrain
- Brainstem
- Pathways of the brainstem
- Spinal cord

The integration between those various levels involves various control mechanisms, such as feedback and feedforward. When the brain alters the ongoing movement based on an outcome, for corrective actions, this is called feedback control. The feedforward control consists of sending signals in advance to prepare the control

region for incoming activity. The main areas responsible for receiving sensory information from ascending pathways are influenced by two subcortical systems: Basal Ganglia and Cerebellum, which connect to the cortex by the thalamic nuclei [54]. Figure 2.1 represents this hierarchical organization of the motor system [55].

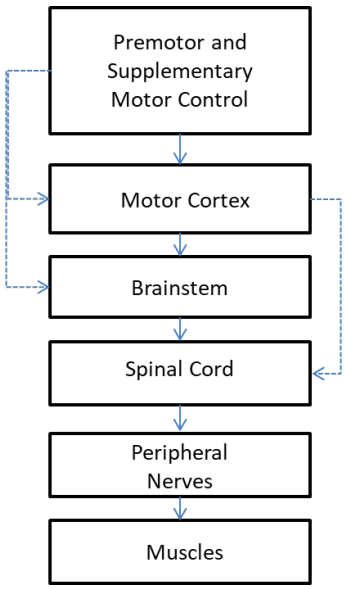

Figure 2.1 – The main levels responsible for the control of the motor system [55].

The motor impulses required for voluntary movement are mainly generated in the primary motor cortex and in the adjacent cortical areas. The motor impulses travel through a descending pathway, especially the corticobulbar and corticospinal tracts, passing by the brainstem and down the spinal cord to the anterior horn of the medulla, where they make synaptic contact with the second motor neuron. Other cortical areas, such as the premotor cortex, and subcortical nuclei, especially the basal ganglia, participate in the control of the movement. These areas form feedback loops with one another and with the primary motor cortex and cerebellum; they exert an influence of the anterior horn cells by means of several distinct fiber pathways in the spinal cord; modulating movement and regulating muscle tone [56].

According to Lent (2010), it is possible to classify the structures involved in the motricity. The muscles responsible for movement execution are called effectors. The motor neurons located in the spinal cord, neural regions of brainstem and motor cortex are denominated coordinators, with the function of transmitting to muscles the commands for action. The basal ganglia and cerebellum are considered controller

structures because they check frequently if the system is working as desired, ensuring that the commands are correct, and if the movement is performed properly. Finally, specific regions of the cortical cortex are called planners, responsible for programing or planning the motor act, creating an ordered and detailed sequence of instructions that the coordinators transmit to the muscles [57].

2.1 Somatosensory System

The somatosensory system deals with proprioceptive and cutaneous events, providing information about bodily sensations, such as touch, temperature, pain, position in space, and movements of the joints [58].

The motor system and the somatosensory system are interrelated at all levels of the nervous system. For example, at the level of the spinal cord, sensory information contributes to motor reflexes; in the neocortex, skilled movements elicited by the motor regions of the frontal lobes require information about actions that have just taken place and about objects that have been or could be manipulated. To produce the movement, it is necessary the integration between both systems, in which motor cortex "decides" what should be done, and the sensory cortex "knows" what has been done [59].

2.1.1 Somatosensory Receptors

The somatosensory system consists of two main elements: somatosensory receptors, found in all parts of the body, and the neurons from these receptors that carry information to the spinal cord. Within the spinal cord, there are two sensory pathways projected to the cortex and, finally, to the somatosensory cortex [59].

The cells that interpret information from the environment can be classified as [60]:

- Free nerve endings: with dendrites embedded in tissue that would receive a sensation, such as pain and temperature receptors in the dermis of the skin;
- Encapsulated ending: the sensory nerve endings are encapsulated by connective tissue that enhances their sensitivity – neurons that respond to pressure and touch;

- Other specialized receptors: such as the cells of the retina that respond to light waves.

The somatosensory receptors in the human body are classified into three groups, according to the type of perception they enable: nocioception, hapsis, and proprioception.

Nocioception consists of the perception of pain and temperature. Free nerve endings characterize nociceptors. Thus, when these endings are stimulated, they release chemicals that stimulate the production of action potentials [59,61].

Hapsis is the perception of fine touch and pressure. These receptors are found in superficial and deep layers of the skin and are attached to body hairs as well. These receptors consist of a dendrite encased in a capsule of connective tissue. Mechanical stimulation of the capsule activates special channels on the dendrite of the neuron, which in turn initiates an action potential [59,61].

Proprioception is characterized as the perception of the location and movement of the body. Proprioception receptors consist of encapsulated nerve endings that are sensitive to stretch of muscles and tendons and the movement of joints [59].

Sensory receptors and the neurons related to those sensations can also be classified into rapidly and slowly adapting types, in which rapidly adapting (phasic) receptors respond maximally, but briefly to stimuli, with the response decreasing fast with time. On the other hand, slowly adapting (tonic) receptors keep firing as long as the stimulus is maintained [62].

Dorsal-root ganglion neurons are somatosensory neurons that reside in ganglions on the dorsal root of the spinal cord. The axons of the dorsal-root ganglion enter the spinal cord, originating the spinal cord's dorsal roots. In the spinal cord, these axons can make synapses with other neurons or continue to the brain, dividing into two main pathways.

The information from haptic-proprioceptive axons reaches the brain by a three-neuron relay in a pathway called posterior column-medial lemniscus. The first synapse is made by the terminals of dorsal root ganglion cells onto neurons in the brainstem nuclei. The axons of these second-order neurons synapse on third-order neurons of the ventral posterior nuclear complex of the thalamus, that send their axons to the primary somatic sensory cortex.

Sensory information about nociceptive pain and temperature takes a different course; the anterolateral system [62]. The anterolateral system, also known as the spinothalamic tract (Figure 2.2), is a sensory pathway that initiates on the skin and runs to the thalamus. When the sensory information reaches the ventral posterolateral nucleus in the thalamus, it is projected up to the somatosensory cortex of the postcentral gyrus [63].

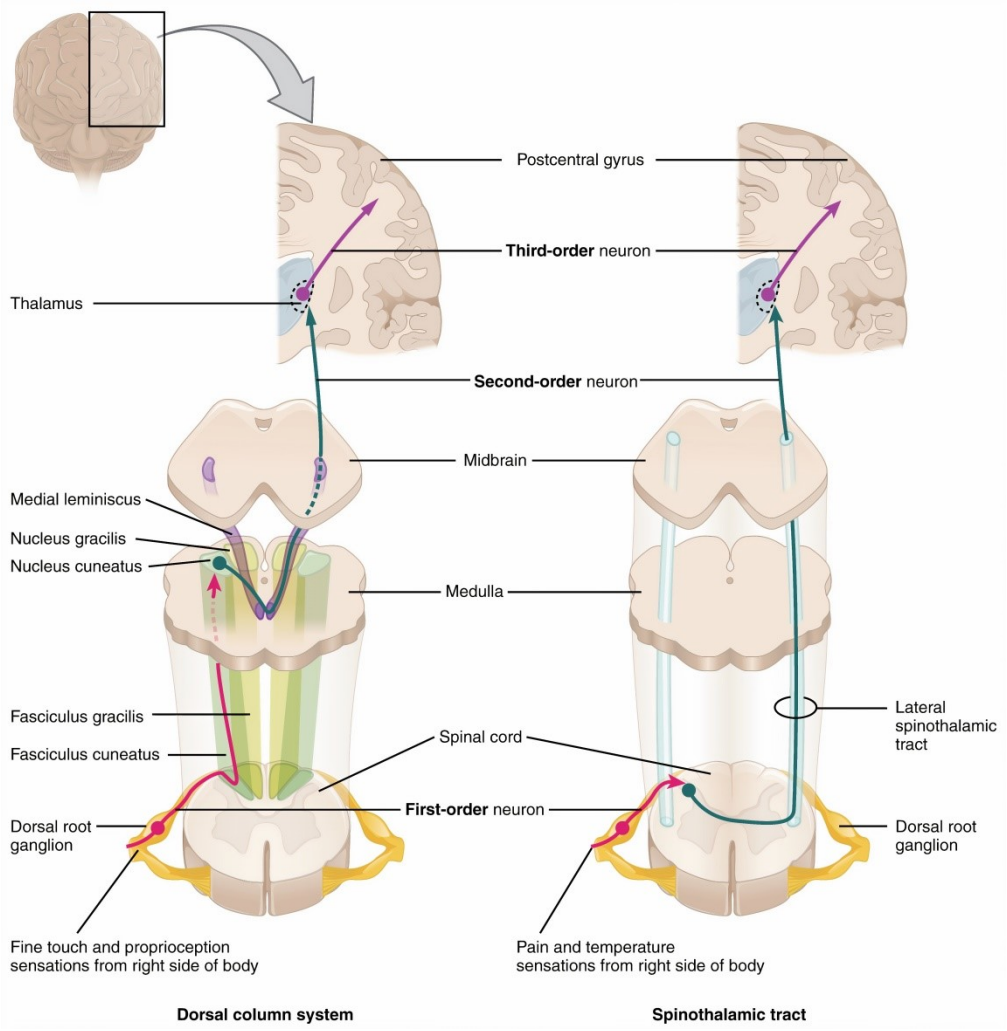

Figure 2.2– Ascending pathways to the Somatosensory Cortex [64] - under CC BY 3.0 attribution license.

2.1.2 Somatosensory Cortex

The somatosensory system is composed by three main cortex areas: primary somatosensory cortex (S1), secondary somatosensory cortex (S2) and somatosensory association cortex.

S1 is in the postcentral gyrus, adjacent to the primary motor cortex, and consists of the Brodmann´s areas 1, 2 and 3 (‘a’ and ‘b’). Brodmann areas (BA) can be seen in Figure 2.3.

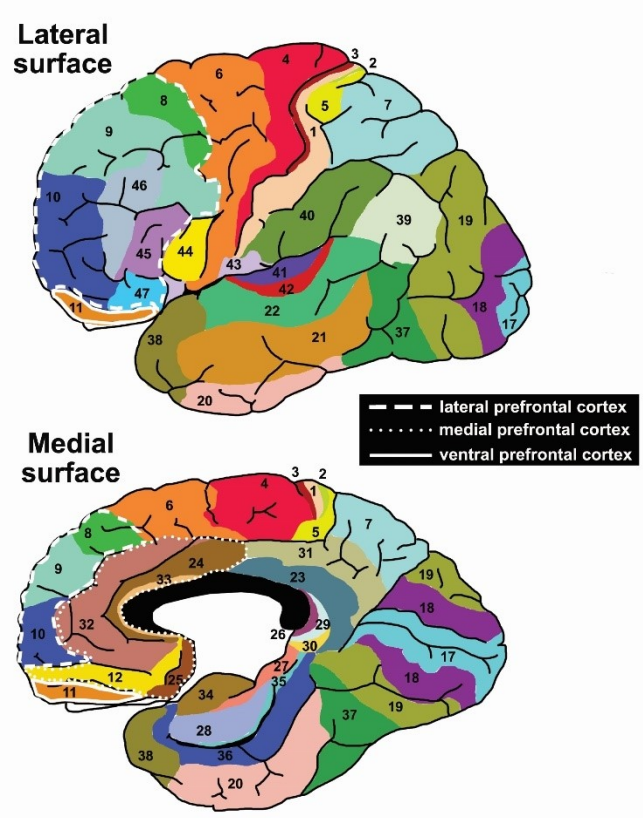

Figure 2.3 – Brodmann areas in lateral and medial views [65] - under CC0 1.0 attribution license.

These areas report about proprioceptive and cutaneous events, such as the position of the limb and contact with objects, in which area 1 receives input from rapidly adapting receptors, area 2 receives input from deep tissue receptors (pressure, joint, position), area 3a receives input from slowly and rapidly adapting skin receptors, and area 3b receives input from deep tissue receptors (muscle stretch receptors) [7].

S1 is somatotopically organized, i.e., specific body part receptors are all grouped and project to a particular region of the cortex. The sensory homunculus includes the cortical representation of the body based on the degree of sensory innervation.

The premotor cortex utilizes the sensory information about the position of the body in the three-dimensional space relative to external objects and organizes appropriate movements.

The secondary somatosensory cortex is located in the parietal lobe, behind S1. S2 includes parts of the Brodmann areas 40 and 43.

The somatosensory association cortex (areas 5 and 7), also known as posterior parietal cortex (PPC), is located posterior to the sensory cortex in the superior parietal lobes. It integrates somatosensory information with visual information, offered by the occipital lobe, to provide spatial awareness. This area also communicates with the premotor cortex and supplementary motor area, as shown in the Figure 2.4.

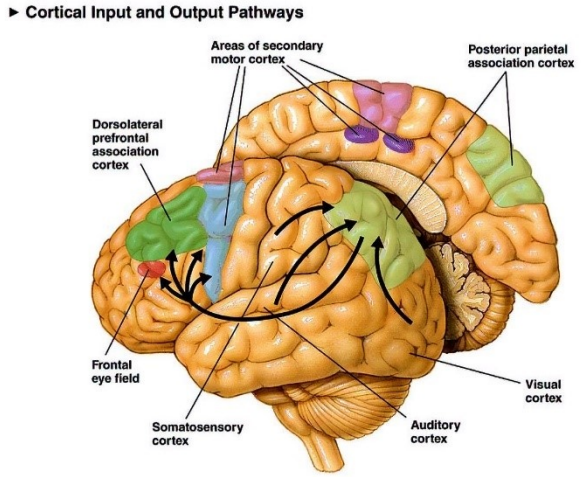

Figure 2.4 – Posterior parietal association cortex representation [66] - under CC BY-SA 3.0 attribution license.

2.2 Motor Cortical Areas

The motor areas are interconnected with each other and send axons to the spinal cord. Those areas consist of the primary motor area (Brodmann's area 4); premotor cortex (lateral area of Brodmann's area 6), which is usually subdivided into dorsal and ventral; supplementary motor area (medial part of Brodmann's area 6) and three regions of the cingulate cortex ventral to the supplementary motor area (SMA), and the prefrontal cortex (Figure 2.5) [56].

The function of the prefrontal cortex is to plan complex behaviors, i.e., the goal towards which movements should be directed. For completion of the target, the prefrontal cortex sends instructions to the premotor cortex, which plans the necessary sequence for the accomplishment of the movement. Finally, the primary motor cortex

(M1) specifies the details of how each motion should be carried out and is the main contributor in generating neural impulses to control the execution of movement [59].

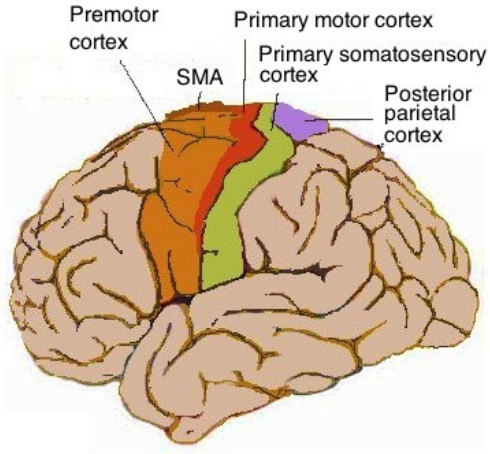

Figure 2.5 – Cortical Motor areas representation [67] - under CC BY-SA 3.0 attribution license.

There is a topographical representation of the different body parts in the primary motor cortex (located on the precentral gyrus), in an arrangement called motor homunculus. In this, the area representing the throat and larynx is located at the inferior end of the primary motor cortex; and regions that represent the face, upper limbs, trunk, and lower limbs are located above it. The homunculus represents the contralateral side. It means that the primary cortex in the right cerebral hemisphere controls the motor activity of the left side of the body and vice-versa. The different body sizes presented in the motor homunculus are related to the density of receptors for various parts of the body [56,57].

The postcentral gyrus, located posteriorly to the central sulcus, includes the somatosensory cortex, which involves the Brodmann's Areas 1, 2 and 3. The topographical representation of the sensory cortex (somatosensory homunculus) shows the tactile representation of the contralateral side, as shown in Figure 2.6. Also, the different sizes of the homunculus reflect the density of receptors for various parts of the body.

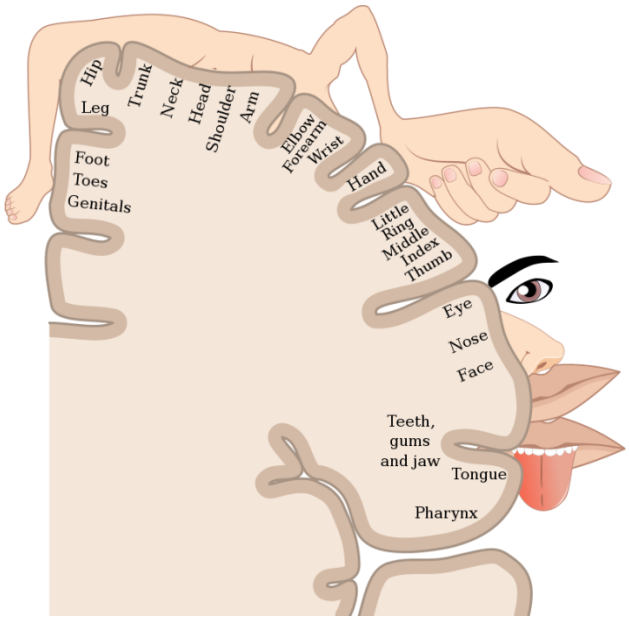

Figure 2.6 – Representation of somatosensory cortex homunculi [64] - under CC BY 3.0 attribution license.

2.3 Concluding Remarks

Considering what was presented in this chapter, we focused on the analysis of EEG electrodes related to cortical areas that strongly contributes to sensorimotor integration areas and reachable with EEG, those are primary motor cortex, posterior parietal cortex and primary somatosensory cortex.

3. PROBING BRAIN ACTIVITY

In this work, we propose to map cortical patterns related to motor movements and discriminate their stages using brain connectivity estimators. This technique is often used in several applications, such as to improve the accuracy of BMIs and help on the understanding of how neurological disorders affect the mobility of individuals at the cortical level. We will present the alternatives for probing brain activity and the reasons why EEG was chosen.

In general, brain activity can be detected by two types of strategies: electrophysiological and hemodynamic response. The hemodynamic response is characterized as a process in which active neurons have increased blood when compared to an area of inactive neurons. The most common techniques to measure this response are fMRI and fNIRS [21].

fNIRS is the use of infrared light to detect fluctuations in cerebral metabolism during neural activity. The infrared light penetrates the skull to a depth of approximately 1–3 cm below its surface. According to the intensity of the light, it is possible to measure alterations in oxyhemoglobin and deoxyhemoglobin concentrations. The spatial resolution is around ~5 mm, and temporal resolution around ~1s [21,68]. The equipment is exemplified in Figure 3.1.

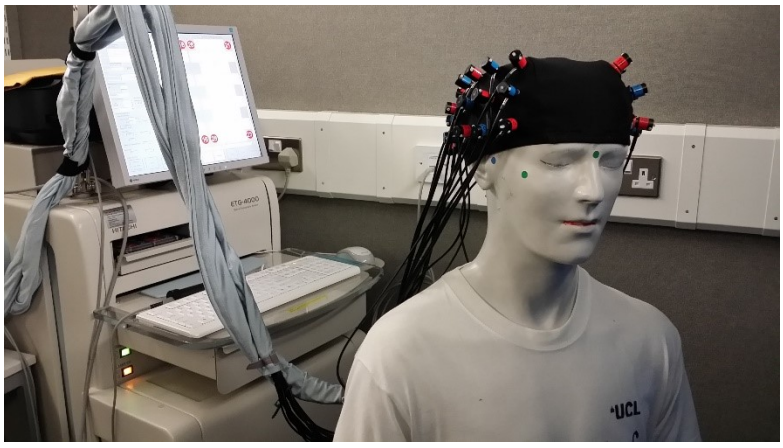

Figure 3.1 – Example of fNIRS equipment setup [69]. - under CC BY-SA 4.0 attribution license.

The main advantage of fMRI over fNIRS is the higher spatial resolution (3-4 mm [17] However, those techniques have similar temporal resolution, since both

measure hemodynamic response, being a little bit lower in fMRI. fMRI's temporal resolution is typically the ~3 s and a peak occurring ~5–6 s after the onset of a brief neural stimulus [17]. A possible disadvantage is that current fMRI devices required a much larger structure, are very expensive and not at all portable [21,70] (Figure 3.2).

Figure 3.2 – Example of fMRI equipment setup [71] - under CC BY 3.0 attribution license.

The electrophysiological activity consists of electrochemical transmitters exchanging information that can be measured through invasive and non-invasive techniques. Invasive methods can be exemplified by intracortical recordings and electrocorticography, and non-invasive by electroencephalography and magnetoencephalography techniques [72].

Intracortical recordings use needle like electrodes that penetrate the brain tissue to measure the activity of multi- (MUA) and single-unit activities (SUA), and local field potentials (LFPs). As described, this technique achieves high temporal resolution (~0.003s) and high spatial resolution (~0.5mm LFP, ~ 0.1 mm MUA and ~0.05mm SUA). MUA and SUA use special signal processing techniques separate the activity of single or multiple units and contain a higher frequency spectrum when compared with LFPs, which are extracted by low-pass filtering (<300Hz) and are the result of the average activity of many neurons in the vicinity of the electrode [21,73].

A disadvantage of intracortical electrodes is limited longevity and a reduction of signal quality with time due to the low biocompatibility of current devices [74].

Another invasive acquisition method is electrocorticography (ECoG) that consists of an intraoperative recording of electrical activity directly over the exposed cerebral cortex, and differently from intracortical recordings, it measures activity underneath the scalp on the surface of the brain, without penetration of brain tissue [28]. The electrodes are implanted subdural, resulting in a high signal-to-noise ratio, high temporal resolution (~0.003 s) and a slightly lower spatial resolution (~1 mm). In the high gamma frequency band, ECoG amplitudes bring relevant information about a task-related activity, such as motor execution and planning, auditory processing, and visual-spatial attention [75]. Since it is an invasive technique, there are also concerns about time rejection and electrode longevity.

Electroencephalography (EEG) is a non-invasive method that captures the sum of electrical fields generated by postsynaptic potentials of neural tissues in the brain on the surface of the scalp with lower spatial in comparison with neuroimaging techniques but provides a high temporal resolution (Figure 3.3). The main disadvantages of EEG are that the skin, skull, dura-matter and cerebrospinal fluids located between the brain and the EEG electrodes attenuate the electrical signal, resulting in low amplitudes and limited bandwidth, typically under 150 μV with frequencies below 100 Hz [15]. The spatial resolution is around ~50 mm and temporal resolution from 1-3 ms [18]. Recent "high density EEG" systems, in combination with source modelling, can significantly improve the spatial resolution [19]. It is also important to highlight that, similarly to all other methods; one single current source can spread to several electrodes due to the volume conduction effect. As such, for precise measurements, special source location methods may be applied to properly define the origin the EEG signals [76].

EEG electrodes are commonly placed on the scalp according to the International 10–20 system, standardized by the American Electroencephalographic Society [77].

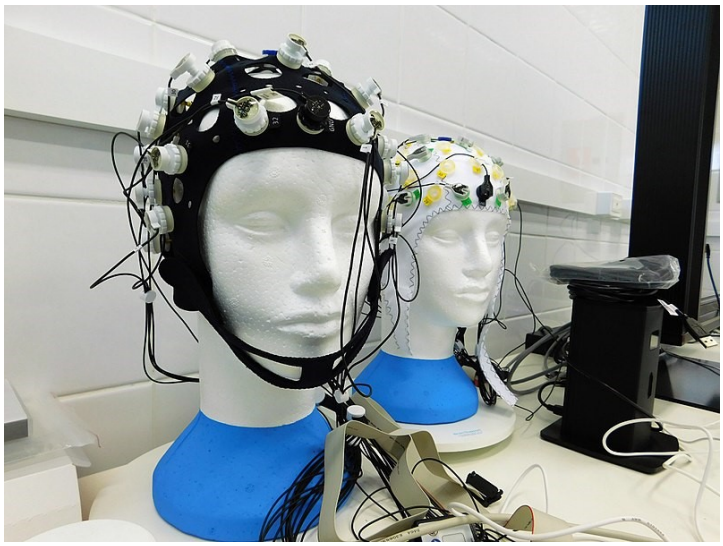

Figure 3.3– Example of Electroencephalography setup [78] - under CC BY-SA 4.0 attribution license.

Magnetoencephalography (MEG) is a non-invasive electrophysiological technique with better spatial resolution (~5 mm) compared to EEG, but differently from the others electrophysiological strategies, it has the lowest temporal resolution (~0.05 s). It is characterized by the measurement of the magnetic field generated by the electrical activity of neurons [79]. Table 3.1 presents the main characteristics about each strategy to measure the dynamic of brain activity presented in this chapter, in order to base the chosen strategy for this PhD thesis.

Table 3.1 – Summary of the main characteristics presented in this chapter.

Technique	**Type (hemodynamic or electrophysiological)**	**Portable (Y/N)**	**Temporal Resolution (s)**	**Spatial Resolution**
fMRI	Hemodynamic	N	3	3-4 mm
fNIRS	Hemodynamic	Y	1	5 mm
ECoG	Electrophysiological	Y	0.003	1 mm
MEG	Electrophysiological	N	0.05	5 mm
Intracortical Recordings	Electrophysiological	Y	0.003	(~0.5 mm LFP, ~ 0.1 mm MUA and ~0.05 mm SUA
EEG	Electrophysiological	Y	0.001-0.003	50mm

3.1 Concluding Remarks

As described, hemodynamic techniques give useful spatial information. However, they require non-portable equipment, in applications such as BMIs, and have a low temporal resolution in comparison to electrophysiological techniques. We argue that, for applications devoted to rehabilitation and BMI, electroencephalography provides the best tradeoff, being non-invasive, portable, and offering good temporal and spatial resolution. As such, for this work, EEG has been selected as the brain activity detection model.

4. EEG-BASED SENSORIMOTOR INTEGRATION STUDIES – STATE OF ART

This chapter aims to explore the existing strategies in literature used to understand the sensorimotor integration. The most found technique will be used to compare with the method proposed in this thesis to verify the accuracy of both in classifying two types of fine movements.

EEG signals can provide useful information of sensorimotor processing and support frameworks like embodied cognition, common coding, and sensorimotor contingency, that do not sequentially separate sensory and motor brain processes [15].

Sensorimotor rhythms (SMRs) have been used to measure sensorimotor integration in EEG signals. SMRs are commonly identified by the occurrence of peaks at ~10 Hz (alpha) and ~20 Hz (beta) across the sensorimotor cortex [80]. It has been observed a reduction of the signal power in the band of 8–13 Hz when a subject is executing an actual or imagined movement. Power alterations can also be found in the lower beta band (12–22 Hz), while the mu-rhythm tends to focus on the bilateral sensorimotor area, and the beta rhythm concentrates mainly on the vertex [28]. The reduction of power coinciding with an event is called Event-Related Desynchronization (ERD). When there is an increase, it is called Event-Related Synchronization (ERS) [81].

ERD and ERS are typically calculated with respect to a reference period, usually when the subject is wakefully relaxed and not executing any task [73]:

$$ERD = \frac{R-A}{R} * 100\% \tag{4.1}$$

where, R is the band power during the reference period, and A is the band power during the period of interest. This formula is similarly applied to ERS.

Verhangen et al. (2012) also used ERS/ERD with combined Transcranial Magnetic Stimulation (TMS) interference and psychophysical methods to test anterior Intraparietal Sulcus (aIPS) causal contributions to sensorimotor integration and characterize the dynamics of those contributions during motor planning. It was shown that the aIPS contributes to the initial planning stage, incorporating both spatial and pictorial evidence into a motor plan, and can even store knowledge of familiar object

configurations. However, it remains to be investigated if these observed effects are exclusively properties of aIPS or if they are shared across a dorsolateral parieto-frontal network (including ventral premotor areas) [82].

In the same year, Nakayashiki et al. (2014) investigated the effect of changes in kinematics and kinetics on resulting ERD during repetitive hand grasping movements. It was found that time differentiation in kinematics (change of hand posture) is correlated with the strength of mu/beta-ERD. However, the maintenance of the current sensorimotor state (i.e., keeping the hand posture in the same condition) was related to the mu/beta rebound [83].

Jenson et al. (2014) evaluated the sensorimotor integration in speech production and perception by examining ERS/ERD and Independent Component Analysis (ICA) associated with Event-Related Spectral Potential (ERSP) patterns in quiet and noisy discrimination conditions. It was observed that ICA successfully identified μ components in speech perception and production. Time-frequency analyses using ERSP showed real-time changes in alpha/beta power that provided indication of premotor cortex/sensorimotor contributions to speech-based dorsal stream activity [80].

The use of ICA and ERSP has also been explored by Cuellar et al. (2016) who intended to map the temporal dynamics of sensorimotor integration relative to the strength and timing of muscular activity during swallowing. It was found that by applying ICA to the whole EEG data successfully resulted in the identification of event-related components during swallowing [84]. Another research investigated the fluctuations of sensorimotor processing in migraine, in which the EEG-activation to non-painful motor and sensorimotor tasks in the different phases of the migraine cycle was found to be longitudinally related to beta event-related desynchronization (beta-ERD) [85] .

A study by Mazurek et al. (2020) combined high-density EEG and motion capture technology with the interaction of objects involving complex sensory stimuli to assess sensorimotor integration. The EEG analysis was also based in Event-Related Potentials, with additional kinematic analysis to detect wrist rotation during the task. The findings indicate that the strategy of object interaction can provide information on how different areas of the brain communicate when different sensory information (visual and auditory stimuli, in the implicit or explicit way) is presented, or different actions are performed [86]. In addition, the authors point out that effective connectivity

techniques could provide information on the flow of sensory information to the motor cortex based on neural recordings [86].

Lau et al. (2014) measured effective connectivity of cortical activity during human standing and walking. The authors used high-density EEG and Granger Causality, and observed that connections involving sensorimotor clusters were weaker for walking than standing, which suggests that cortical involvement during standing is greater than during walking and, also, that these techniques could be used to study gait disorders [87].

Anwar et al. (2016) investigated effective connectivity of cortical sensorimotor networks during finger movement tasks using simultaneous fNIRS, fMRI, and EEG. The analysis showed significant bi-directional information flow between the Contralateral Sensorimotor Cortex (SMC), Contralateral Premotor Cortex (PMC), and Contralateral Dorsolateral Prefrontal Cortex (DLPFC) as determined by the EEG, fMRI and fNIRS modalities for all motor tasks [88]. It was observed that source-level EEG provides the strongest means to characterize the directionality of neural communication within cortico-cortical sensorimotor networks, since the information data flow acquired with source-level EEG showed the largest GCI amplitude values compared to other techniques. Also, this study highlights that linear and nonlinear GCI did not show significant differences in performance. In other words, the less complex linear GCI can detect and quantify changes in coupling strength and direction of activation between different cortical regions [88].

Beta-band activity and connectivity in sensorimotor and parietal cortices were investigated by Chung et al. (2017). High-density EEG and elbow flexor and extensor neuromuscular activity were measured during ballistic movements to verify how visual information could affect movement error. The effective connectivity was measured by direct Directed Transfer Function (dDTF), which revealed that visual gain affected the directional connectivity across broadband frequencies (theta, alpha, and beta frequency bands) from parietal to sensorimotor cortex, but not from sensorimotor cortex to parietal cortex, suggesting the importance of sensorimotor and parietal cortex for accurate motor performance. It was also found that movement errors were reduced, and the number of zero-crossings increased with enhanced visual information [89].

Freyer et al. (2012) evaluated passive Repetitive Tactile Stimulation (RSS) that consists of an alternative to balance the sensory decline after neurological disorders and physiological aging, to improve perceptual abilities without the need for active

participation. The study included healthy human subjects and analyzed resting-state EEG functional connectivity patterns before and after RSS using Imagery Coherence (IC), a functional connectivity estimator. Differently from absolute coherence, phase locking, or synchronization likelihood, this technique does not measure spurious interactions with zero-time lag that occurs due to common references, crosstalk, and volume conduction [37]. This study concludes that 30 min of RSS have significant coherency changes in mu-rhythm, showing that functional connectivity measures provide tools for assessing network interactions in the human brain, and may thus be used to study efficacy of different sensory and motor training paradigms.

Another study from Stefano Filho et al (2017) used graphs connectivity matrices (calculated using the motifs' synchronization method [90]) and ERD and ERS to investigate linear correlations between the synchronization patterns induced by MI. The authors concluded that ERSP performed better for distinguishing hands' MI tasks than only using the functional connectivity matrix and recommend exploiting other graph metrics, besides similarity [91].

Brain connectivity has also been applied by Pichiorri et al (2018) to find an EEG index of sensorimotor interhemispheric coupling after unilateral stroke, since these coupling changes have been related to the extent of damage in the corticospinal tract (CST) and thus, to motor impairment. Effective Connectivity estimation was assessed by means of Partial Directed Coherence, and the coupling index was estimated for each patient and each frequency band on the whole network and in three sub-networks relative to the frontal, central (sensorimotor) and occipital areas. It was found that the interhemispheric coupling, as expressed by the index on the whole network, was significantly higher in patients with preserved CST integrity in beta and gamma bands. The authors claim that this index could be applied to evaluate the effects of training focused on re-establishing interhemispheric balance and eventually encourage the design of future connectivity-driven rehabilitation interventions [92].

Peterson et al (2019) studied source-localized electrocortical effective connectivity of healthy subjects, on walking and standing conditions with visual and physical balance perturbations. The main purpose of the research was to quantify differences in group-level corticomuscular connectivity responses to the perturbations. The connectivity estimator used was direct Directed Transfer Function, and the results show that it could effectively expose the network differences following perturbation [38].

4.1 Concluding Remarks

As shown, only a few EEG-based studies investigated sensorimotor integration with connectivity estimators. Furthermore, we still need more studies to find out which estimator (functional/effective) is the most adequate to describe the sensorimotor integration, i.e., the one that provides relevant information about the dynamics and flow of the process. Also, there is not a standard protocol about how to use these techniques in BMIs, besides some studies have shown that it could improve their accuracy [40,42,41].

Considering what was presented in this chapter, the most used technique for sensorimotor integration analysis is sensorimotor rhythms (ERD/ERS). This strategy will be used to estimate similar movements (wrist pronation and supination). The results will be compared with the proposed connectivity strategy in this PhD thesis.

5. BRAIN CONNECTIVITY ESTIMATORS

This chapter will describe several types of brain connectivity estimators and a brief theory of each technique. At the end, the chosen connectivity method to be used in this thesis will be selected.

5.1. Types of Connectivity

Neuroanatomical connectivity refers to the existence of fibers pathways connecting different brain areas (i.e., white matter tracts that connect different cortical regions). The structural networks of the human brain have not yet been fully mapped. Nevertheless, they can be studied by noninvasive methodologies, such as Magnetic Resonance Imaging (MRI) and specially Diffusion Tensor Imaging (DTI), that can discriminate fibers tracts over extended regions of the brain [93,94]. For this work, anatomical connectivity estimation will not be considered, only functional and effective connectivity to measure cortical reorganization patterns.

Functional and effective connectivity try to establish the function of a cortical area, considering the dependence of cerebral activity on underlying connections. Studies in this area started in the 19th century with Friedrich Goltz (1869), who performed many electrical stimulation experiments in dogs' and monkeys' cortices. Goltz (1869) found that the excitation method generated inconclusive results, since the movements elicited could have been originated in other related pathways, or the electrical current could have spread to other centers [94] .

Despite the advances over the past centuries, the questions related to the existence of functional segregation or functional integration has not yet been properly answered. In this scenario, novel functional and effective connectivity techniques were developed to better understand the neurophysiological processes [94].

Functional connectivity consists of the statistical dependencies between different brain regions among remote neurophysiological events, i.e., associations between spatially remote neurophysiological events. For example, associations can result from stimulus-locked transients evoked by a common afferent input, at the level of multiunit micro-electrode recordings, or reflect stimulus-induced oscillations; and phasic coupling of neural assemblies, mediated by synaptic connections [95,94]. On the other hand,

effective connectivity refers to the influence that one neural system (either a synaptic or population level) exerts over another.

It is important to emphasize that effective connectivity does not necessarily leads to functional connectivity. As an example, in cases of neuromodulatory inputs from ascending aminergic neurotransmitter systems or thalamocortical afferents, the temporal correlations are not related to causality. Usually, in case when we notice correlations between effective and function connectivity this is due indirect effects, e.g., polysynaptic relays through multiple areas.

5.2. Classification of Connectivity Estimators

Connectivity estimators can be classified according the quantity of analyzed temporal series (EEG electrodes' signals), being multivariate if consider the analysis of all electrodes or bivariate, if it is considered only two pairs of electrodes. Other possible classification is if the method applied is linear or non-linear [96].

Various works compared the performance of bivariate and multivariate estimators of connectivity. In general, in systems with more than two channels interrelated, bivariate methods can result in misleading information, providing information if there is a link between two signals, and none if one structure drives another or if there is a feedback between these structures.

In other words, bivariate estimations cannot provide robust information if the dependencies between two signals do not come from the influence of a third channel [97,98]. It was demonstrated that when N electrodes are measuring the activity from a certain source, bivariate estimators will detect those N true connections, will also result in a larger number of false connections ($[\frac{N(N-1)}{2} - N]$) [99].

Blinowska et al. (2004), Kus et al. (2004) and Kaminski (2005) compared bivariate and multivariate methods for directionality estimation. In the referenced papers, with the use of simulations and experimental signals, it was verified that bivariate measures can generate misleading results, with directionality in the reverse propagation [97,100,101].

In 1960, a research using linear brain connectivity estimation started using the measure of pairwise Cross-Correlation to investigate the similarity and time delay between two signals, in which higher correlations consist of stronger functional

relationship between two brain regions. Linear estimation can also be performed in the frequency domain using Coherence, which allows the measurement of correlation in different bands; however, it is sensitive to change in power or phase [95]. Coherence has been used for assessing functional coupling, information interaction, temporal coordination between cortical regions in healthy subjects, and for characterizing synchronization between oscillatory cortical motor and muscle activity in the beta band [102,103,104,105,106].

When the main interest of the analysis is to verify waveform and time coupling between two signals, Correlation is the most recommended estimator. On the other hand, if the main objective is to analyze the stability of coupling in relation to power asymmetries and phase, Coherence is more appropriate. However, since strong or abrupt power asymmetries do not occur under normal physiological conditions, the influence of power asymmetry on Coherence can be considered negligible. As such, Correlation and Coherence usually lead to similar results, providing relevant information about the interdependence between those two signals [107]. Nevertheless, those methods measure mainly bivariate linear connectivity. Since neural connectivity can be due to nonlinear and multivariate factors, they can still be insufficient for the study of complex neurophysiological data [102].

Additionally, a study compared bivariate and multivariate synchronization functional methods for EEG studies. Interestingly, it has shown high correlations between many of bivariate or multivariate synchronization measures for EEG signals indicating that they similarly estimate the same synchronization phenomenon. Thus, in terms of output, multivariate measures do not have superiority over bivariate ones for this kind of connectivity measures [108].

As the name implies, linear measures detect the linear relations between signals, as such, they cannot detect nonlinear connections between them. However, before disregarding linear estimators, we must first answer the question of how often we deal with nonlinearities and how they can affect or improve the results.

Traces of nonlinearity were found during certain stages of epileptic in EEG studies [109], and in neonatal electroencephalogram burst/suppression patterns, where nonlinearities occur in 90% and 87% of bursts and suppression, respectively [110].

Stepien (2002) suggests that the EEG signal, in rest with eyes closed, of a healthy person is generated by a linear stochastic process that can be not be rejected for

most of the subjects. However, nonlinearities were found in frontal channels. Hence, the author proposes the use of nonlinear modeling to clarify the existence of weak nonlinear components in EEG signals [111].

Nonlinear methods were designed to measure the dynamics of time series based on deterministic chaos to provide complementary information to linear methods. The emergence of these techniques was motivated by the fact that many neural processes have nonlinear features, as described before. The developments started in the 1980s, within the concept of synchronization, i.e., adjustment of rhythms of oscillating objects because of their weak interaction [95]. It has been shown that, nonlinear dynamics methods can provide good results in pathological states like epilepsy or coma; or can be used for the assessment of a therapy by comparing the recordings before and after the therapy, as well as for diagnosis, to differentiate pathological cases from normal ones.

Several studies compared the performance of linear and nonlinear methods, David et al. (2014) analyzed various measures on the simulated data generated by populations of neurons using different connection patterns, types, and strengths. This work concluded that in most cases, the coupling could be detected by both linear and nonlinear methods; however, the sensitivity may be lower in linear measures, which may lead to missing flows, but not to nonexistent flows [98,112].

Another study confirmed that nonlinear methods are very sensitive for identifying complex correlations between nonlinear systems in noiseless situations. Nevertheless, linear methods were proved more robust to noise [113].

5.3 Functional Connectivity Estimators

In this topic, it will be presented the selected functional connectivity estimators, for signals derived from noninvasive techniques, such as EEG.

Among a range of functional connectivity estimators, we selected those that have been the choice of most impactful researches published over the past few years [114,115,116] and that have bivariate and multivariate approaches: Correlation, Coherence, Mutual Information (MI), Phase-Locking Synchronization (PLV), and Synchronization Likelihood (SL).

5.3.1 Correlation

The analysis of Pearson's correlation is one of the most common correlation coefficients used as a functional connectivity method to capture linear and time-domain dependencies between two signals. Thus, signals from two anatomically separated brain regions could be temporally correlated, indicating that the areas are functionally connected. However, it is important to consider that a strong correlation between two signals does not imply a functional connection of the underlying neurons, e.g., it may have a considerable correlation of neuronal activity of two regions under the influence of external or equal inputs [117].

The result of correlation estimation has a value between +1 and −1, in which +1 is a total positive linear correlation, 0 corresponds to no linear correlation, and −1 implies in total negative linear correlation. The definition of Pearson's correlations (r_{xy}) for two paired data $\{(x_1, y_1), \dots, (x_n, y_n)\}$ with n pairs [118]:

$$r_{xy} = \sum_{i=1}^{n} \frac{(x_i - (y_i - \bar{y})}{\sqrt{\sum_{i=1}^{n}(x_i - \bar{x})^2}\sqrt{\sum_{i=1}^{n}(y_i - \bar{y})^2}} \tag{5.1}$$

where, n is the sample size, x_i and y_i are the individual sample points and $\bar{x}$ is the sample mean.

5.3.2 Coherence

Coherence coefficient is a method used to quantify phase synchronization between a pair of signals. It is equivalent to the frequency domain of the time domain cross-correlation (CC) function [119]. CC is defined by two discrete time series obtained simultaneously, x_n and y_n, where $n = 1, \dots, N$ [120]:

$$c_{xy}(\tau) = \frac{1}{N - \tau}\sum_{i=1}^{N-\tau}\left(\frac{x_i - \bar{x}}{\sigma_x}\right)\left(\frac{y_{i+\tau} - \bar{y}}{\sigma_y}\right) \tag{5.2}$$

where, $\bar{x}$ and σ_x denote mean and variance, and τ is a time lag.

It is a symmetric measure ($c_{xy}(\tau) = c_{yx}(\tau)$) and its value ranges from zero to one, in which zero corresponds to no synchronization and one corresponds to maximum synchronization. Extracting the Fourier Transform of the cross-correlation is obtained the sample cross spectrum as follows [120]:

$$C_{xy}(\omega) = (Fx)(\omega)(Fy) * (\omega) \tag{5.3}$$

where, Fx is the Fourier Transform of x, and ω are the discrete frequencies ($-\frac{N}{2} < \omega < \frac{N}{2}$) and * is the complex conjugation. Thus, the coherence function can be obtained by:

$$T_{xy}(\omega) = \frac{|\langle C_{xy}(\omega)\rangle|}{\sqrt{\langle C_{xx}(\omega)\rangle}\sqrt{\langle C_{yy}(\omega)\rangle}} \tag{5.4}$$

Coherence is a measure of linear synchronization in function of the frequency ω. It is used when the measure of synchronization is limited by a frequency band, as in EEG signals. The interpretation of the phase difference spectrum in terms of a temporal delay (and consequently as an indicator of directionality) is only valid under rather ideal conditions, in which the connection is predominantly unidirectional and well-represented under the assumption of linearity. In non-ideal circumstances, the phase difference spectrum is not recommended to assign directionality [119].

5.3.3 Mutual Information

Mutual information is a higher-order information-theoretic measure of temporal synchrony that has been used to measure information encoding in stimulus-response experiments [121]. Nonlinear dynamical analyses of EEG have been found to be useful for detecting relative changes between different brain states that cannot be detected using conventional analytic techniques, such as waking/deep sleep state and to analyze cortical differences between patients with Alzheimer's disease and healthy controls [122].

As the name implies, MI measures the mutual information between two variables, by quantifying the information that can be obtained from a random variable when observing another variable. This technique is based on probabilistic distributions, sensitive to second and higher-order correlations. However, MI does not offer causal coupling information because it lacks directional and dynamic information [123].

MI provides a dimensionless quantity with units of bits, and it is understood as the reduction in uncertainty of one random variable within the knowledge of another. High value of mutual information implies on a large reduction in uncertainty; and low mutual information indicates a small reduction; and zero mutual information between two random variables means the variables are independent [120].

Supposing a discrete random variable X with M possible outcomes $1, \ldots, X_M$, obtained, e.g., by a partition of X into M bins. Each outcome has a probability pi, $i = 1, \ldots, M$, with $pi > 0$ and $\sum pi = 1$. First, consider $pi = ni\ /N$, where ni is the number of occurrences of Xi after N samples. Then, Shannon entropy can be defined as [113,120]:

$$I(X) = -\sum_{i=1}^{M} pi \log pi \tag{5.5}$$

If there is a second discrete random variable Y, whose degree of synchronization with X we want to measure. The joint entropy is defined as:

$$I(X,Y) = -\sum_{i,j} p_{ij}^{xy} \log p_{ij}^{xy} \tag{5.6}$$

where p_{ij}^{xy} is the joint probability of $X = Xi$ and $Y = Yj$. Independent variables will have $p_{ij}^{xy} = p_i^x . p_j^y$, then $I(X,Y) = I(X) + I(Y)$.

Thus, MI will be obtained as follows:

$$MI(X,Y) = I(X) + I(Y) - I(X,Y) \tag{5.7}$$

$MI(X,Y)$ corresponds to the amount of information of X we obtain given the knowledge of Y and vice versa. If both variables are independent, $MI(X,Y) = 0$.

Otherwise, it will assume positive values with a maximum of $MI(X,X) = I(X)$ for identical signals. Importantly, MI is a symmetric measure, i.e., $MI(X,Y) = MI(Y,X)$.

There is no upper limit for MI(X,Y), thus to facilitate interpretation and comparisons between parameters, a normalized version of I(X, Y) that ranges from 0 to 1 is preferable. There are several normalization strategies based on the observation that:

$$MI(X,Y) \leq \min\big(I(X), I(Y)\big) \tag{5.8}$$

Some Normalized Mutual Information (NMI) methods are listed in the Table 5.1, with their respective references.

Table 5.1 – Main methods of mutual information normalization.

NMI	**Expression**	**References**
$\mathrm{NMI_{sum}}$	$\frac{2.\,\mathrm{MI(X,Y)}}{\mathrm{I(X)+I(Y)}}$	[124]
$\mathrm{NMI_{joint}}$	$\frac{\mathrm{MI(X,Y)}}{\mathrm{I(X,Y)}}$	[125]
$\mathrm{NMI_{max}}$	$\frac{\mathrm{MI(X,Y)}}{\max\{(\mathrm{I(X)},\mathrm{I(Y)}\}}$	[124]
$\mathrm{NMI_{sqrt}}$	$\frac{\mathrm{MI(X,Y)}}{\sqrt{\mathrm{I(X)I(Y)}}}$	[126]
$\mathrm{NMI_{min}}$	$\frac{\mathrm{MI(X,Y)}}{\min\{(\mathrm{I(X)},\mathrm{I(Y)}\}}$	[124]

As observed in Table 5.1, normalized use the arithmetic or geometric mean of I(X) and I(Y).

Extensions of pairwise Mutual Information to multivariate networks of more than two random variables exist in the literature. The first extension has been described

by Watanabe (1960) and Timme et al. (2014) as a total correlation (TC). TC is defined in terms of the entropies of n random variables $(X_1, X_2, \dots, X_n)$ [127].

$$TC(X_1;\ X_2;\ \dots; X_n) = h(X_1) + h(X_2) + \cdots + h(X_n) - h(X_1, X_2, \dots, X_n) \quad (5.9)$$

Another multivariate extension of mutual information called Multiple Mutual Information (MMI), elaborated by McGill (1954), says that the quantity may be expressed as the alternating sum/difference of permutations of joint entropies of the random variables, as shown in Eq. (5.10) [121]:

$$MMI(X_1;\ X_2;\ \dots; X_n) = \sum_{k=1}^{n} (-1)^{k+1} \sum_{\substack{M \subseteq \{1,\dots,n\} \\ |M|=k}} h(X_{M1}, X_{M2}, \dots, X_{Mn}) \quad (5.10)$$

where, the interior sum is taken over all possible indices formed from integer subsets of$\{1, \dots, n\}$ of cardinality k.

Ball et al. (2017) proposed a normalization of TC called Normalized Multi-information (NMI) that consists of a scalar measure that estimates shared information content in a multivariate network, and it is characterized by being robust to changes in network size. For n random variables, the normalized multi-information is defined as [121]:

$$NMI(X_1;\ X_2;\ \dots; X_n) = \frac{1}{n-1}\ TC(X_1, X_2, \dots, X_n) \quad (5.11)$$

$$NMI(X_1;\ X_2;\ \dots; X_n) = \frac{1}{n-1}\ [\sum_{i=1}^{n} h(X_i) - h(X_1, X_2, \dots, X_n)] \quad (5.12)$$

5.3.4 Phase-Locking Synchronization Index (PLSI)

The analysis of the synchronization phenomena has been used for studying cortical activity with EEG, providing relevant information about the communication process between different brain regions. Different distributed brain areas communicate to provide integration of sensory information and to support functions related to learning, memory, information processing, and perception [128]. Therefore, phase synchronization between two regions indicates correlations of neural excitability and

spike timing. It was found that phase synchronization in the gamma band supports two major functions, neural communication, and plasticity. Nevertheless, it is still unclear how phase synchronization supports memory-related processes and other functions simultaneously without interference [129].

Phase synchronization is a functional connectivity technique that can be estimated in two steps: extraction of instantaneous phase and quantification of the phase synchronization index. The instantaneous phase extraction from a time series can be performed by Hilbert Transform or by Complex Wavelet Transform [112] [130].

1) Hilbert Transform

The instantaneous phase of a narrowband signal can be properly extracted by Hilbert Transform. Considering a continuous signal in time $x(t)$, it is possible to define an analytic signal $Z_x(t)$, in which $Z_x(f) = 0$ for $f < 0$, where $Z_x(f)$ is the Fourier Transform of $Z_x(t)$. An analytic signal is the one in which the imaginary part is the Hilbert Transform of the real part [131].

$$Z_x(t) = x(t) + i\hat{x}(t) = A_x^H(t)e^{-i\theta_x^H(t)} \tag{5.13}$$

where $\hat{x}(t)$ is the Hilbert Transform of $x(t)$:

$$\hat{x}(t) = \frac{1}{\pi} p.v \int_{-\infty}^{\infty} \frac{x(\tau)}{t-\tau} d\tau \tag{5.14}$$

and, p.v is the principal Cauchy value for the improper integral. In a similar way, another continuous signal can be defined as:

$$Z_y(t) = A_y^H(t)e^{-i\theta_y^H(t)} \tag{5.15}$$

For these signals, the phase synchronization index (γ) for two instantaneous phases, θ_x and θ_y is defined as:

$$\gamma = \left|\langle e^{-i(n\theta_x - m\theta_y}\rangle\right| \in [0,1] \tag{5.16}$$

where m and n are integers and generally $n = m = 1$ and $\langle . \rangle$ refers to the average in time.

The estimated index (γ) can vary between 0 (two cortical regions do not present a degree of synchronization) and 1 (maximum synchronization).

2) Wavelet Transform

Another phase synchronization estimator is by Wavelet Transform (γ_w), where the instantaneous phase is obtained with the convolution of each signal with a Complex Wavelet function, (t) [120]:

$$\Psi(t) = \left(e^{-i\omega_0 t} - e^{-\frac{\omega_0^2 \sigma^2}{2}} \right) . e^{-t^2/(2\sigma^2)} \tag{5.17}$$

where ω_0 is the center frequency of the wavelet and σ indicates its rate of decay and its frequency span.

The convolution of a pair of signals $x(t)$ and $y(t)$ with $\Psi(t)$ results in two complex time series of wavelet coefficients:

$$W_x(t) = (\Psi \circ x)_{(t)} = \int \Psi(t') x(t' - t) dt' = A_x^W(t) . e^{-i\emptyset_x^W(t)} \tag{5.18}$$

$$W_y(t) = (\Psi \circ y)_{(t)} = \int \Psi(t') y(t' - t) dt' = A_y^W(t) . e^{-i\emptyset_y^W(t)} \tag{5.19}$$

The phase synchronization index between two signals is given by the difference of the phases:

$$\emptyset_{xy}^W = \emptyset_x^W - \emptyset_y^W \tag{5.20}$$

The estimated PLSI (γ_w) varies from 0 to 1, and just as the previous method, 0 indicates nonexistent synchronization and one indicates that both regions have maximum synchronization.

The bivariate phase synchronization is suitable for the analysis of pairs of signals, but they become less efficient as the number of pairs is increased.

5.3.5 Synchronization Likelihood

Synchronization likelihood (SL) is a functional connectivity method based on the concept of generalized synchronization and detects nonlinear coupling between multivariate signals (two or more simultaneously recorded time series). It is characterized as a measure of synchronization between nonstationary signals without the influence of dimensionality and other properties such as system complexity. In this method, the similarity of the states in a common temporal window to a reference state is computed. Thus, the number of coincidences of the states in different trajectories determines how much they are synchronous. An overall synchronization is obtained sliding the window and averaging the synchronization in all windows [132].

The synchronization likelihood $S_{k,i}$ describes how strongly a channel k is synchronized with other $M-1$ channels at time i. This measure ranges between the values $pref$ and 1. When $S_{k,i} = pref$, the M time series do not show any synchronization, and when $S_{k,i} = 1$, the time series are synchronized. The value of $pref$ can be a low value set arbitrarily and does not depend on the properties of the time series [133].

Therefore, considering M time series recorded simultaneously, $x_{k,i}$, in which k indicates the channel number ($k = 1, \dots, M$), and i refers to the discrete time ($i = 1, \dots, N$), and taking each one of the M time series, it is possible to build a vector $X_{k,i}$ that represents the state of signal X at time i:

$$X_{k,i} = (x_{k,i}, x_{k,i+l}, x_{k,i+2l}, \dots, x_{k,i+(m-1)l}) \tag{5.21}$$

where l corresponds to the time lag, and m is the embedding dimension.

The probability that embedded vectors are closer to each other within a certain distance ε, for each time series k and each time i, is defined as:

$$P_{k,i}^{\varepsilon} = \frac{1}{2.(w_2 - w_1)} \sum_{\substack{j=1 \\ w_1 < |i-j| < w_2}}^{N} \theta(\varepsilon - |X_{k,i} - X_{k,j}|) \tag{5.22}$$

where $|.|$ is the Euclidean distance and θ is the Heaviside step function ($\theta(x) = 0, for\ x \leq 0\ \ and\ \theta(x) = 1, for\ x > 0$). In Eq. (5.22), $w_1$and w_2 are two windows; w_1 is the Theiler correction for autocorrelation effects and should be at least of the order of the autocorrelation effects and should be at least of the order of the autocorrelation time; w_2 is chosen such that $w_1 \ll w_2 \ll N$, and sharpens the time resolution of the synchronization measure.

For each pair k/i, the critical distance can be determined by $P_{k,i}^{\varepsilon}$=pref, in which $pref \ll 1$. Thus, for each discrete pair in the window ($w_1 < |X_{k,i} - X_{k,j}| < w_2$), the number of channels $H_{i,j}$ can be estimated in which the vectors $X_{k,i}$ and $X_{k,j}$ are closer than the critical distance $\varepsilon_{k,i}$:

$$H_{i,j} = \sum_{k=1}^{N} \theta(\varepsilon - |X_{k,i} - X_{k,j}|) \tag{5.23}$$

The values of $H_{i,j}$ varies between 0 and $M - 1$ and elucidates how many embedded signals are like each other. Therefore, it is possible to estimate the synchronization likelihood $S_{k,i,j}$ for each channel k and each discrete timer pair (i, j) as:

$$if |X_{k,i} - X_{k,j}| < \varepsilon_{k,i}: S_{k,i,j} = \frac{H_{i,j} - 1}{M - 1} \tag{5.24}$$

$$if |X_{k,i} - X_{k,j}| \geq \varepsilon_{k,i}: S_{k,i,j} = 0 \tag{5.25}$$

The synchronization likelihood $S_{k,i}$ is finally obtained by averaging all j [133]:

$$S_{k,i} = \frac{1}{2.(w_2 - w_1)} \sum_{\substack{j=1 \\ w_1 < |j-i| < w_2}}^{N} S_{k,i,j} \tag{5.26}$$

where $S_{k,i}$ is a measure which describes how strongly channel k at time i is synchronized to all the other M − 1 channels. Values can range between $pref$ and 1, and $S_{k,i} = pref$ (set at an arbitrarily low level) corresponds with the case where M

time series are uncorrelated and $S_{k,i}$= 1 corresponds with maximal synchronization of M time series.

5.4 Effective Connectivity Estimators

Effective connectivity is defined as the impact that one neural system exerts over another, showing causal influence between regions [4]. In this topic, linear, multivariate effective connectivity estimators will be presented, for signals derived from noninvasive techniques, such as EEG.

5.4.1 Autoregressive Model

Most linear effective connectivity methods are based on autoregressive models (AR), that represent a random process in which the output result depends linearly on its previous values and on a stochastic term. Thus, an AR model can be defined by a group of k-channels recorded simultaneously, as [134]:

$$X(t) = \sum_{j=1}^{p} A(j)X(t-j) + E(t) \tag{5.27}$$

where $X(t) = [X_1(t), X_2(t), \dots, X_k(t)]^T$ is a vector of k samples recorded at time t, $E(t) = [E_1(t), E_2(t), \dots, E_k(t)]^T$ is a vector of k white noises in time t and $A(j)$ is defined as a matrix of parameters of the model, in which $A(j) = \begin{pmatrix} A_{11}(j) & \dots & A_{1k}(j) \\ \vdots & \ddots & \vdots \\ A_{k1}(j) & \dots & A_{kk}(j) \end{pmatrix}$, where $j = 1, \dots, p$ and $A(0)$ is considered the identity matrix and the value of p is the order of the model.

AR can be written in the frequency domain as:

$$E(f) = A(f).X(f) \tag{5.28}$$

$$X(f) = A^{-1}(f).E(f) = H(f).E(f) \tag{5.29}$$

$$H(f) = \sum_{m=0}^{p} A(m) \exp(-j2\,\pi f \Delta t)^{-1} \tag{5.30}$$

As shown in Eq (5.29) in the frequency domain, the model can be considered as a linear filter with white noises $E(f)$ on its input and the signals $X(f)$ on its output. The matrix of filter coefficients $H(f)$ is called the transfer matrix of the system, and it contains spectral and phase information [98].

5.4.2 Granger Causality Index

The Granger Causality Index (GCI) analysis provides effective connectivity estimation without spurious connections [98]. In 1956, Norbert Wiener introduced the concept of causality: one variable is causal to another when the ability to predict the second variable is enhanced by including information about the first. The implementation of this concept was introduced in 1969 by Clive Granger, with linear autoregressive models of stochastic processes [135].

The advantage of GCI is that it allows a researcher to point directional influences of certain regions on another, without necessarily any a priori hypothesis regarding which areas are involved in particular subnetworks [136].

In statistics, explained variance measures the proportion to which a mathematical model represents the dispersion of a given data. The unexplained (residual) variance is the complementary part of the total variation. A causal influence could help to improve the prediction of the driven process when the driving process is observed. Thus, the existence of a causal influence from $x_1(n)$ to $x_2(n)$ in the time domain occurs when a measurable reduction in the unexplained variance of the driven process $(x_2(n))$, results from the inclusion of the causal (driving) process $((x_1(n))$ in linear autoregressive modeling. Hence, pairwise linear GCI is defined as [137]:

$$F_{x_1 \to x_2} = ln\,(\Sigma_1/\Sigma_2) \tag{5.31}$$

where Σ_1 is the unexplained variance (prediction error covariance) of $x_2(n)$ in its own autoregressive model, and $\Sigma_2$is the unexplained variance when a joint AR model for both $x_1(n)$ and $x_2(n)$ is constructed. When $x_1(n)$ influences $x_2(n)$, it is expected that $F_{x_1 \to x_2} > 0$, and when there is no influence, it is expected that $F_{x_1 \to x_2} = 0$. Generally, $F_{x_1 \to x_2}$ is compared to a threshold value.

Bivariate causal analysis does not distinguish direct and indirect influences in more complex connectivity schemes, such as trivariate networks. Bivariate Granger causality can only be assessed by Eq. (5.31), if the pairwise time series have all relevant information and the source of activities. Therefore, in the neurophysiology context, two channels are not suitable for this requirement, due to the influence of other cortical regions over a certain region [138].

Hence, to address inference in this scenario, a series of "leave-one-out" can be performed using the multivariate extension of the linear GCI. For example, in a neural data where p is the number of recording channels, the direct influence exerted by x_m on x_n can be given by [137]:

$$F_{x_m \to x_n} = ln \frac{\sum_{x_n | x_{1\ldots}, x_{m-1}, x_p}}{\sum_{x_n | x_{1\ldots}, x_p}} \tag{5.32}$$

5.4.3 Directed Transfer Function

Directed Transfer Function (DTF) is a multivariate spectral method that gives pairwise directional information from one autoregressive model fit to a larger number of channels. DTF is a linear estimator of connectivity that has a very robust performance to noise [98]. A number of researches using DTF can be found in the literature in areas such as localization of epileptic foci, estimation of EEG propagation in many sleep stages and wakefulness and estimation of cortical connectivity [139,140,141].

Considering the transfer matrix of a system ($H(f)$), defined in Eq (5.30), the non-normalized DTF from channel j to channel i, representing the causal influence from j to i, is defined as:

$$\theta_{ij}^2(f) = \left|H_{ij}(f)\right|^2 \tag{5.33}$$

The normalized DTF is defined as the ratio of influence of channel j in channel i to the joint influences from all the other channels in channel i:

$$\gamma_{ij}^2(f) = \frac{|H_{ij}(f)|^2}{\sum_{m=1}^{k}|H_{im}(f)|^2} \tag{5.34}$$

where $\gamma_{ij}^2(f)$ has a value between 0 and 1 [142].

DTF is not able of distinguishing direct and indirect connections between the signals, i.e., in case of propagation $1 \rightarrow 2 \rightarrow 3$, it only shows the propagation $1 \rightarrow 3$.

To differ indirect and direct flows, the direct Directed Transfer Function (dDTF) has been developed [143]. The dDTF ($X_{ij}(f)$) is defined as a multiplication of a modified DTF by the partial coherence:

$$X_{ij}^2(f) = F_{ij}^2(f).C_{ij}^2(f) \tag{5.35}$$

$$F_{ij}^2(f) = \frac{|H_{ij}(f)|^2}{\sum_f \sum_{m=1}^{k}|H_{im}(f)|^2} \tag{5.36}$$

in which, $C_{ij}^2(f)$ is the partial coherence, and when both functions $F_{ij}^2(f)$ and $C_{ij}^2(f)$ are non-zero values, there exists a direct causal relation between channels $j \rightarrow i$.

5.4.4 Partial Directed Coherence

Partial Directed Coherence (PDC) is a measure of effective connectivity in the frequency domain of multivariate processes developed by Baccala and Sameshima (2011), which shows only the direct flows between channels. It is a method based on the autoregressive model showed in Eq. (5.27) and can be defined as [98]:

$$\pi_{ij}(f) = \frac{A_{ij}(f)}{\sqrt{\sum_{k=1}^{N} A_{ij}(f)A_{kj}*(f)}} \tag{5.37}$$

This measure is normalized so that $0 \leq \left|\pi_{ij}(f)\right|^2 \leq 1$ and $\sum_{i=1}^{N}\left|\pi_{ij}(f)\right|^2 = 1$, for all values $1 \leq j \leq N$. $A_{ij}(f)$ is the Fourier Transform of the multivariate AR model coefficients $A(t)$, shown in Eq. (5.29) and $A_{kj}^*(f)$ represents the conjugate transpose of $A_{kj}(f)$.

The main differences between PDC and DTF is that PDC represents a ratio between the outflow from channel j to i in respect to all outflows from j, whereas DTF

is a ratio related to all inflows to i. Also, PDC does not involve an inversion of the matrix A, which has computational advantages and increase its ability to distinguish direct and indirect connections [144].

5.4.5 Time-Varying Effective Connectivity Estimators

There are also time-varying effective connectivity estimators that aim to explore the dynamics in the effective connectivity, such as Short-time DTF and Time-Varying Dynamic Bayesian Networks.

5.4.5.1 Short-time DTF

Short-time DTF (SDTF) is the time-varying version of DTF, providing the dynamic changes of propagation, based on the application of a short sliding data window and ensemble averaging over realizations that are obtained by repetition of an experiment. First, the non-stationary data should be divided into short time windows (of N_S data points); this division needs to be short enough, so that the data within the window is considered quasi-stationary.

The estimation of Multivariate Autoregressive (MVAR) coefficients is based on the calculation of the correlation matrix R_{ij} of k signals X_i from a multivariate set. The correlation matrix between channels is calculated for each trial separately, then, it is averaged over N_T trials. The resulting correlation matrix can be defined as [98]:

$$\tilde{R}_{ij}(s) = \frac{1}{N_T}\sum_{r=1}^{N_T} R_{ij}^{(r)}(s) = \frac{1}{N_T}\sum_{r=1}^{N_T}\frac{1}{N_S}\sum_{t=1}^{N_S} X_i^{(r)}(t)\, X_j^{(r)}(t+s) \tag{5.38}$$

5.4.5.2 Time-Varying Dynamic Bayesian Networks

Time-Varying Dynamic Bayesian Networks (TV-DBN) models the directed time-evolving network structures subjacent in non-stationary biological time series [145].

A Bayesian Network (BN) is a graph model describing the statistical relationship of n random variables $X = \{X_i\}_{i=1\ldots n}$. A BN is composed of a directed acyclic graph G

and a distribution parameter Θ, in which G has n nodes corresponding to random variables X $(X_1, X_2, \dots, X_n)$, and their edges represent the direct dependencies between these variables. BN represents a joint probability distribution (JPD) over a set of random variables V [146].

The nodes of a Directed Acyclic Graph (DAG) represent random variables and are usually described in graphs as circles labeled by the variable names. The edges correspond to direct dependences between variables and are represented by arrows between nodes. For example, an edge from node X_i to node X_j represents a statistical dependence between both variables, i.e., if it is possible to affirm that X_i influences X_j, thus X_i is referred to as a parent of X_j and, similarly, X_j is referred to as the child of X_j [147].

The second component of BN, Θ, denotes the set of parameters of the network. This set contains the parameter $\theta_{xi|\pi i} = P_B(x_i|\pi_i)$ for each realization x_i of X_i conditioned on π_i, the set of parents of X_i in G. BN defines a unique JPD over V, namely [147]:

$$P_B(X_1, X_2, \dots, X_n) = \prod_{i=1}^{n} P_B(X_i|\pi_i) = \prod_{i=1}^{n} \theta_{xi|\pi i} \tag{5.39}$$

A Dynamic Bayesian Network (DBN) is the extension of a BN for temporal processes. In DBN, a set of random processes are represented by the $X = \{X_i\}_{i=1\dots n}$, and $X_i[t]$ is the random variable of process X_i at discrete time t. The network structure G in DBN is defined by the dependency between variables over a period as well as those within the same time epoch. The processes X are Markovian, causal and the conditional distributions are assumed to be stationary. A C node in a graph G can be linked to other nodes in the same or in the previous epoch, i.e., $Pa(X_i[t] \subset \{X[t-1], X[t]\})$. The parameter Θ is defined similarly as in BN. In addition, G and Θ are kept constant over time, because of the assumption of stationarity. Thus, it is possible to conclude that:

$$p(X[t+1]|X[0:t]) = p(X[t+1|X[t])_{t=0,1,2\dots} \tag{5.40}$$

The assumption of stationarity cannot always be applied in biomedical signal analyses. Therefore, a time-varying dynamic Bayesian network (TV-DBN) approach has been developed. Here, the network structure G and the parameter Θ vary as the distribution of temporal sequence changes, being modeled as $G[t]$ and $\Theta[t]$, respectively.

At each time epoch t, there are n parameters nodes: $\Theta[t] = \{\Theta[t]\}_{i=1\dots n}$. Each $\Theta_i[t]$ determines its conditional distribution jointly with other data nodes linked to it. Therefore, in TV-DBN, the parents of a data node $X_i[t]$ are defined as:

$$Pa(X_i[t]) \equiv \{\widetilde{Pa}(X_i[t]), \Theta_i[t]\} \tag{5.41}$$

where, $\widetilde{Pa}(X)$ is the set of data nodes that are linked to X. The linkage between data nodes, i.e., their probabilistic dependency, is determined by the network structure $G[t]$:

$$G[t] \subset \{e_{ji}, e'_{ji} | i, j = 1 \dots n\}) \tag{5.42}$$

where, e_{ji} corresponds to an edge pointing from $X_j[t]$ to $X_i[t]$, and e'_{ji} is an edge pointing from $X_j[t-1]$ to $X_i[t]$.

As required by Markovian property, nodes at time $t-1$ and t are considered as the potential parents of $X_i[t]$. Given $G[t]$, we can retrieve the non-parameter parents of $X_i[t]$ as:

$$\widetilde{Pa}(X_i[t]) = \{X_j[t] | e_{ji} \in G[t]\} \cup \{X_j[t-1] | e'_{ji} \in G[t]\} \tag{5.43}$$

The dependency of $X_i[t]$ on $\Theta[t]$ is fixed and will not be eliminated over time. To model the changing processes of $\Theta[t]$ and $G[t]$ in TV-DBN we adopt a first order Markov model $p(\Theta[t+1], G[t+1] | \Theta[t], G[t])$ as the joint transition distribution. For a given structure $G[t]$, we can assume that each parameter $\Theta_i[t]$ transits independently, as follows [145]:

$$p(\Theta[t+1], G[t+1] | \Theta[t], G[t])$$

$$= p(G[t+1]|G[t])p(\Theta[t+1]|\Theta[t], G[t+1])$$
$$= p(G[t+1]|G[t]) \prod_{i=1}^{n} p(\Theta_i[t+1]|\Theta_i[t], G[t+1]) \quad (5.44)$$

It is possible to see a dependency of $\Theta[t+1]$ on $G[t+1]$ and $G[t]$ since the dimension of the distribution parameter is affected by network structure.

5.5 Concluding Remarks

We search the literature for possible connectivity methods capable of providing meaningful information on cortical flow during motor tasks. Various studies have shown that effective connectivity models, such as Granger Causality [88], direct Directed Transfer Function [89], Imagery Coherence [37], Partial Directed Coherence [92] can provide information on the flow of sensory information to the motor cortex [86]. The main advantage of effective techniques is to provide information about causality and define which brain regions have indirect/direct connection to others. However, functional connectivity models related to sensorimotor integration has not been well explored. As discussed in this chapter, there are two types of functional connectivity techniques, linear and nonlinear. According to some researchers, although nonlinear methods are more robust to properly detect the connections when compared to linear methods [98,112], they can be very sensitive for identifying complex correlations between nonlinear systems in noiseless situations, not a real issue for most EEG setups [113].

As such, for this study, we propose the use of a nonlinear functional connectivity, MI, to assess sensorimotor integration. MI has been shown to be capable of measuring the encoding of stimulus within the behavioral information from individual neurons. Timme et al. (2018) showed this feature by using simulations of simple models of neurons, and analyzing the stimulus encoding trough time using MI in four types of stimulus (on/off, weak/strong, delayed stimulus and nonlinear filter). The spike count during the pulses was compared using the MI to the spike count during a period without pulses. The same strategy was applied to weak/strong stimulus and to the other two. In all cases, large amounts of mutual information were observed between the spike counts and the stimuli state, but not when there were not stimuli [127].

The implementation of the normalized pairwise method for MI is described in topic 5.3. For this work, it was chosen NMI_{sqrt}, that has been used for clustering ensemble analysis [126]. In this normalization, since I(X) = MI(X, X), it is used the geometric mean due to the analogy with a normalized inner product in Hilbert space, i.e., it is analogous to the correlation coefficient $\rho = Cov(X;Y)/\sqrt{Var(X)Var(Y)}$, where cov is the covariance and var is variance [126].

$NMI_{sqrt}(X,Y)$ varies from 0 to 1, in which when variables are identical $NMI(X,Y) = 1$, and when they are totally independent $NMI(X,Y) = 0$ [126].

In this PhD thesis, the dynamics of MI connectivity over time will be evaluated, and in addition, we will verify how this is relevant to compare two types of similar movements. Besides the great advantages of multivariate measures, it was chosen a bivariate technique, since a study has shown high correlations between many of bivariate or multivariate synchronization measures, such as PLSI and MI, indicating that they similarly estimate the same synchronization phenomenon [108].

6. MATERIALS AND METHODS

This thesis presents a proposal to create an EEG-based strategy to characterize sensorimotor integration, based in the most temporally relevant connections for similar movements, such as wrist movements, without an external stimulus and with a reduced number of electrodes and window of analysis. As mentioned in Chapter 5, the chosen strategy to reach this objective is the normalized MI. Next, the selected method is to apply a sequential strategy to extract MI from EEG signals acquired from healthy individuals while performed motor tasks, to verify the neural dynamics. Finally, the proposed method is compared to traditional methods (ERD).

6.1 Using MI to Decode Motor Tasks

6.1.1 Dataset

We used a set of EEG data from the BNCI horizon 2020 open-access database entitled “Upper limb movement decoding from EEG” [148,149]. The data set consists of EEG signals from 15 healthy subjects aged between 22 and 40 years, with mean age of 27 ± 5 years. From all, nine subjects were female, and except by Subject 1, all were right-handed.

6.1.2 Experimental Design

EEG data were acquired for 61 channels, placed on the volunteers scalp according to the 10/05 system, with a sampling frequency of 512 Hz. Electrooculographic (EOG) signals also were acquired, and the information about elbow flexion/extension, forearm supination/pronation, and hand open/close was monitored by encoders and simultaneously acquired during the experiments.

The subjects were seated on a chair, with the right arm fully supported by an exoskeleton with anti-gravity support to avoid muscle fatigue. A screen was positioned in front of the participant to indicate which movement to perform. The volunteers were

required to perform six types of movements with the right upper limb: elbow flexion/extension, forearm supination/pronation and hand open/close.

The data were acquired from each subject in two sessions, in different days, but no more than a week apart. In the first section, the subjects performed motor execution (ME) tasks, and motor imagery (MIm) in the second session. The movements started from a neutral position: hand half-open, lower arm extended to 120 degrees and thumb on the inner side (neutral rotation). A rest class was also recorded, in which the subjects were instructed to avoid any movement and to stay in the starting position.

Figure 6.1 describes the sequence used for the experimental paradigm. At time equal to 0 second, a beep was released, and a cross appeared on the computer screen. After 2 seconds, a cue was presented on the screen, indicating the class of movement (or rest) to be executed. At the end, the subjects moved the limb back to the starting position.

Figure 6.1 – Diagram of a trial sequence used in the motor-task experiments [149] - under CC BY 4.0 attribution license.

To the purpose of this thesis, we considered only the data related to forearm pronation and supination - for each movement there were six trials per run, 24 trials per subject.

6.1.3 Preprocessing

The preprocessing phase consisted of two mains steps: removal of eye movement artifact and filtering.

1) Eye Movement Artifact Removal

Independent Component Analysis (ICA) was chosen for the removal of eye movement artifact removal. Figure 6.2 exemplifies how ICA works, in which the mixture signal passes through an unmixing process and the results are the extracted components.

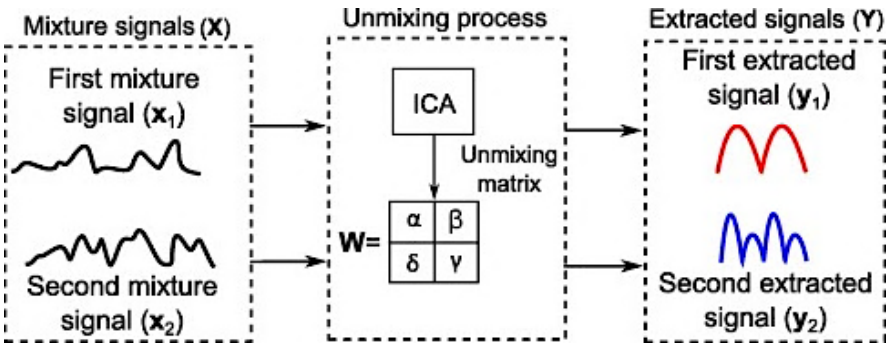

Figure 6.2 – Representation of ICA functionality [150] - under CC BY-NC-ND 4.0 attribution license.

The EEG signals were visually inspected. If during the unmixing process was observed that one or more of the source components were similar to undesired signals (EOG signal), they were eliminated, and the artifact-free EEG was reconstructed [151].

Figure 6.3 shows a fragment of ICA components extracted from the EEG data from one of the volunteers. The ellipsis denotes the component (purple color) removed due to its similarity with blinking behavior.

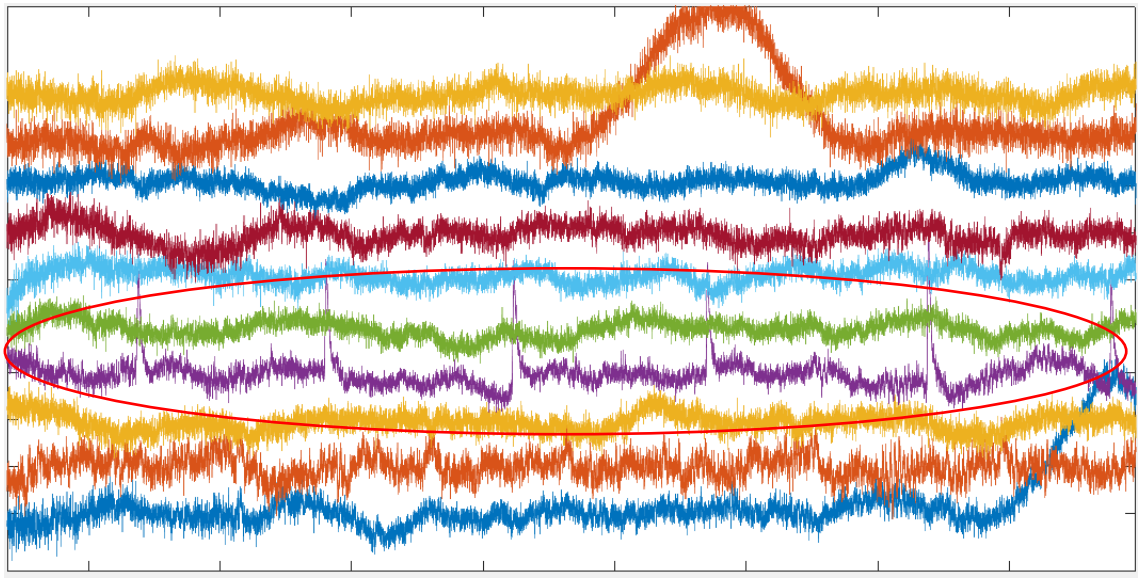

Figure 6.3 – Fragment of the ICA components where it can be observed possible blinking trend marked by an ellipsis.

After the reconstruction of the EEG signal without the corresponding component, we obtained a signal without the blinking patters exposed in Figure 6.4.

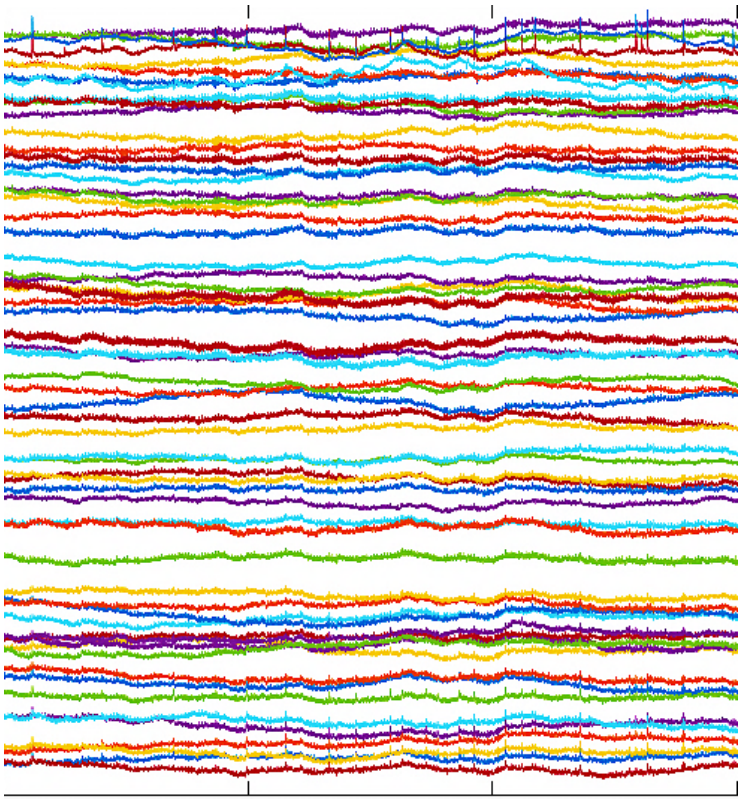

Figure 6.4 – Fragments of EEG signals without blinking artifacts.

2) Bandpass Filtering

After removing eye artifact, the next phase was to limit the frequency range of the signal and remove power line interferences. A third order 50Hz notch Butterworth filter was used to removed 50Hz artifacts (data acquisition performed in Europe). Second, a third-order bandpass Butterworth filter (1-40Hz) was applied to select the frequencies of interest (delta, theta, alpha, beta). Figure 6.5 represents an example of filtered signal.

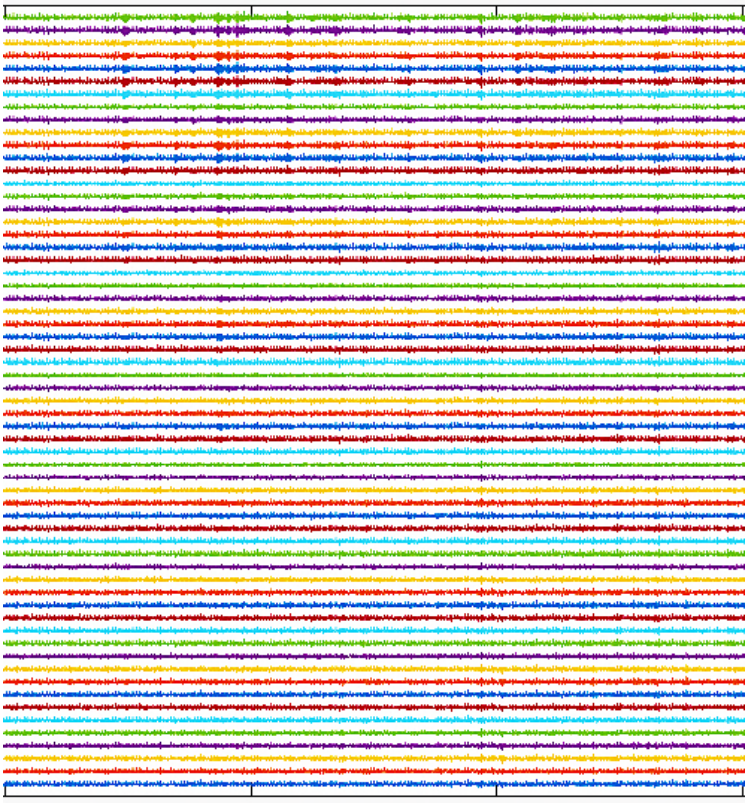

Figure 6.5 – Representation of fragments of EEG signals after EOG artifact removal and bandpass filtering.

6.1.4 Delimitation of EEG Electrodes

In line with the main aim of this research, which is to investigate sensorimotor integration, among all 61 channels we chose those closely related to the activity of the

M1 (Broadman Area (BA) 4), PPC (BA 5 and 7) and S1 (BA 1, 2 and 3), as described in Chapter 2. A total of 20 channels were selected, as shown in Table 6.1.

Table 6.1 – EEG electrodes corresponding to Brodmann areas [152].

Brodmann Areas	Left Hemisphere	Right Hemisphere
1	C3, C1, CP3, CP1	C4, C2, CP4, CP2
2	C3, C1, CP3, CP1	C4, C2, CP4, CP2
3	C3, C1, CP3, CP1	C4, C6, CP4, FC4
4	C3, FC3, C1, FC1	C4, FC4, C2, FC2
5	C1, CZ, CP1, CPZ	C2, CP2, CPZ, CP4
7	P1, CP1, P3	PZ, P2, CP2, P4

For processing, a 4-second window was chosen, starting 1 s before the cue and finishing 3 s after, as shown in Figure 6.6.

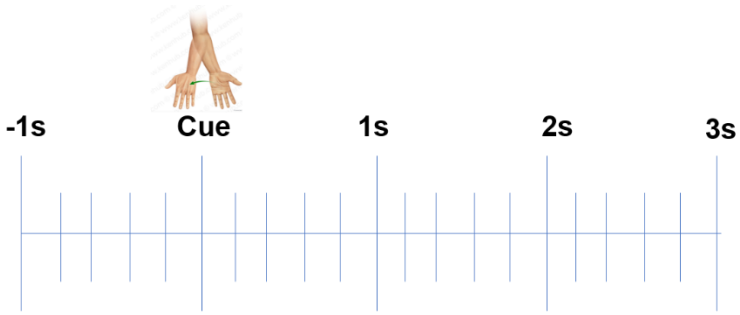

Figure 6.6 – Representation of how the epochs of processing were defined based on the cue of the movement.

6.2 Proposed Method

The proposed method aims to characterize sensorimotor integration EEG-based using MI, using less electrodes, time for training and smaller window of analysis. Thus, we propose a method that firstly, it is responsible for the screening of the most relevant connections, secondly, the relevant connections are selected. At last, NMI with higher temporal resolution is extracted from these connections and the features from the proposed method are compared with the traditional ones. Figure 6.7 represents the sequential stages that were applied.

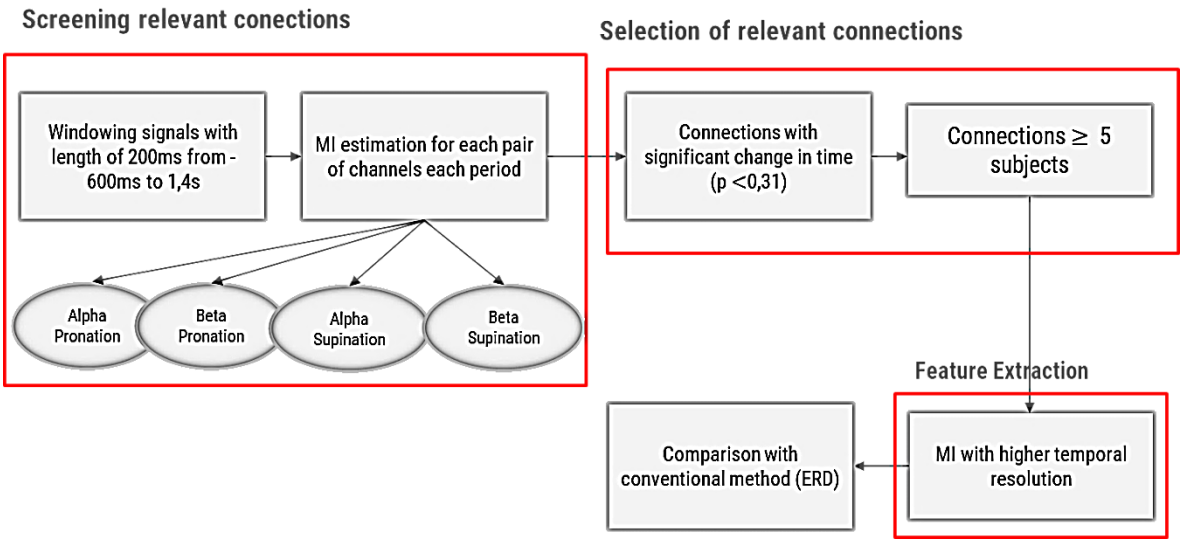

Figure 6.7 – Block diagram that represent the proposed method of this PhD thesis.

6.2.1 Screening Relevant Connections

For the estimation of MI connectivity, the preprocessed signal is filtered in alpha (8-12 Hz) and beta (13-30 Hz) bands, for both types of movement (hand pronation and hand supination).

Bearing in mind that, even with only 20 channels, MI results in a very large number of pairwise connections (20x20), and many of them may not carry important information, we first set to investigate if it was possible to select those that were really more relevant, with a given bonus of reducing the dimensionality of data for the classifier.

To do so, MI was initially processed over 10 non-overlapping windows of 200 ms, in the time range of -600 ms to 1400 ms. The aim was to find which connections show relevant differences between rest and execution of movement, or between the first stages of movement and the end of the movement.

For each subject, MI estimation is performed for each electrode in relation to all other electrodes, resulting in a 20x20 matrix for each window of time, for each trial. The window of time of 200 ms was chosen since it includes both alpha and beta information. Furthermore, the process will be repeated for both frequency bands (alpha and beta) and

each class of movement (pronation / supination). All 24 trials performed by a subject are analyzed in a similar fashion, as shown in Figure 6.8.

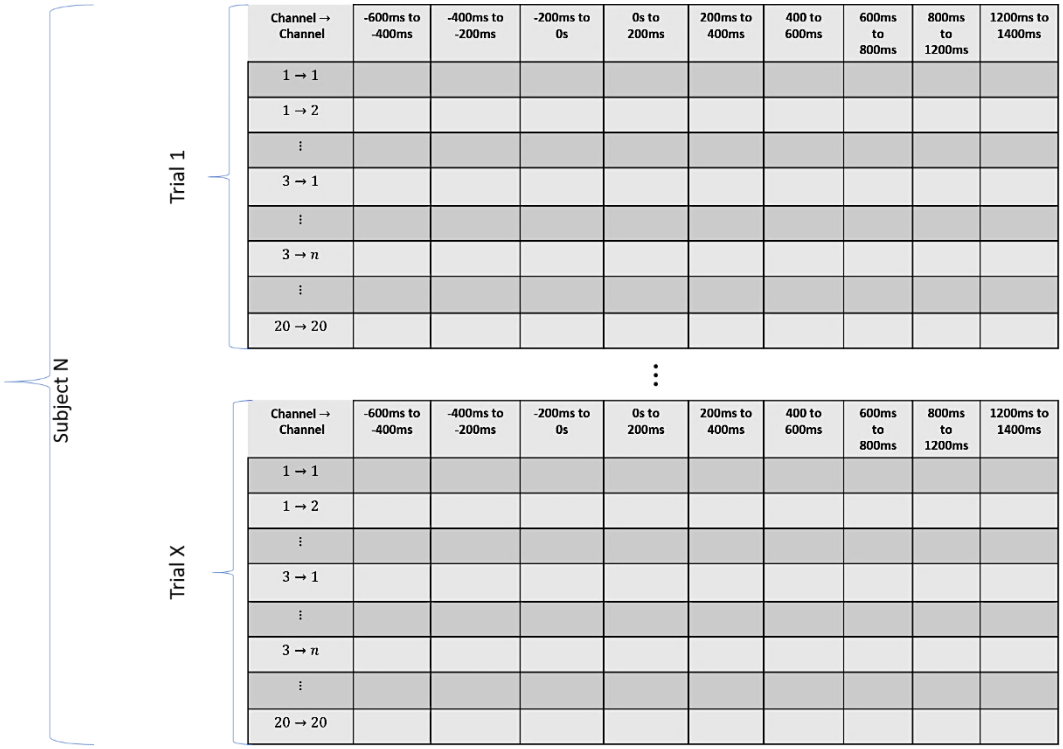

Figure 6.8 – Tables representing how MI estimation is applied over 10 windows of 200ms for all EEG electrode pairs. This procedure is repeated for alpha and beta bands.

6.2.2 Selection of Relevant Connections

As described before, to be able to separate distinct movements using connectivity, it is necessary to select the most relevant pairs of MI connectivity for each band and class of movement. The idea is to see which MI connectivity pairs change significantly over the chosen time windows. These are considered the relevant pairs for each class of movement for alpha and beta bands. To do so, the results were assessed by means of statistical measures.

The first requirement is to verify if the variables have normal distribution. The Shapiro-Wilk test is used and depending on the results a parametric or non-parametric technique will be applied to evaluate which MI pairs show significant changes along the time.

6.2.3 Feature Selection

Once the most relevant pairs are found, MI connectivity is calculated again for those pairs, with higher temporal resolution (moving windows of 50 ms each, with overlapping of 1 ms), to verify the dynamics of the specific connections over time (Figure 6.9). The results are a set of time series showing how the connectivity of each electrode pair changes over the time, for each frequency band.

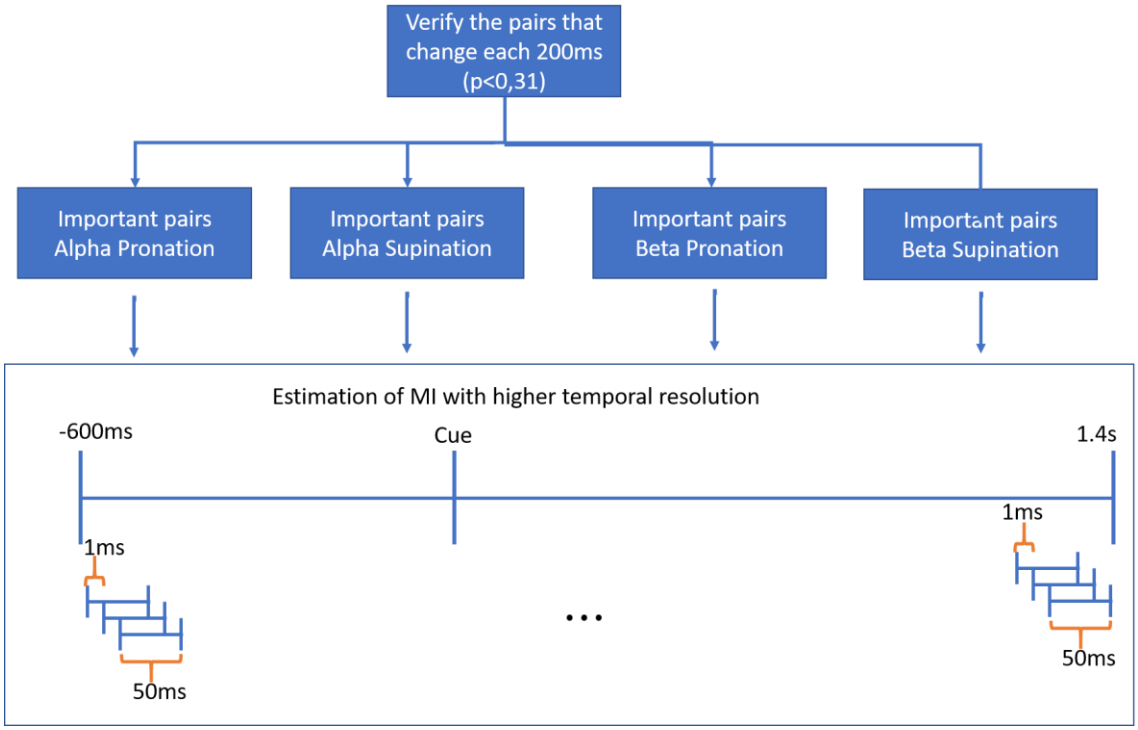

Figure 6.9 – High temporal resolution MI connectivity estimation over the longer time window (-600 ms to 1.4 s). MI measures are calculated over windows of 50 ms, with 1 ms overlap.

Finally, the various "MI connectivity temporal series" of the relevant pairs are used as inputs to the classifier.

6.3 Validation and Comparative Analyses

After obtaining the average connectivity matrices for each class of movement per volunteer, we verify if connectivity information can be more relevant to decode the motor tasks when compared with conventional techniques. We also evaluate if there are specific regions of the connectivity temporal series that can provide better classification

accuracy for predicting class of movement. This is done by using optimization tools aiming to reduce the dimensionality of the data fed to the classifier (see item 2, next).

1) ERD Estimation

The method used for ERD/ERS estimation was based in Pfurtscheller et al. (2001). For this, the estimation consists of the following steps [153]:

1. Bandpass filtering: limit the bandwidth of all event-related signals;
2. Obtain the power of the samples: square the amplitudes;
3. Average the power samples across all trials;
4. If necessary, the power samples over time samples can be averaged to smooth the data and reduce variability.

Finally, it is obtained the percentage values for ERD/ERS. ERD or ERS is defined as the percentage of power decrease or increase given a reference period, respectively (see Eq. 4.1). For the display of the time course of ERD/ERS, a scale displaying either power changes with 0% in the reference period or relative power with 100% in the reference period is recommended.

An ERD/ERS map can be generated for better visualization of increase and decrease of amplitude. It consists basically of a matrix whose rows correspond to ERD/ERS calculations for specific frequency bands. To improve the clarity of the maps, it is also important to display only significant patterns [154].

The problem with selecting the most significant patterns is that majority of statistical techniques assume that the size of the set of sample values is sufficiently large so that asymptotic results can be applied, i.e., it assumes that it is possible (in principle) to continue collecting more data, thus the sample size grows infinitely. Thus, under this assumption, many results obtained are unavailable for samples of finite size [155]. In the case of ERD/ERS calculations, the probability distribution is not known, and the number of trials can be rather limited, thus standard statistical methods to calculate the significance of the ERD estimates may not bring appropriate results.

As an alternative to asymptotic methods for estimating ERS/ERD, we adopted in this PhD thesis the Bootstrap techniques described by Davision and Hinkley et al (1997). This technique consists of substituting the unknown population distribution with the known empirical distribution. Other advantage of this strategy is that it is not necessary to assume Gaussian or other parametric distributions on the data [154].

The percentile bootstrap applied to calculate confidence intervals for ERD/ERS estimates are described below. Considering N be the number of trials, Y_j denotes the set of all Y_{ij} of the jth sample and of all trials, and B is the number of bootstrap resamples. The sample mean and the sample variance of Y_j are denoted by $\overline{y_j}$and ${s_j}^2$, respectively. Therefore, for each sample j:

1) Get N values from Y_j, in which each value is selected randomly, with replacement. The N values are the bootstrap resample $\widehat{Y_j}$.
2) Calculate the mean $\hat{\mu}_{\hat{y}_j}$ and the standard deviation $\hat{\sigma}_{\hat{y}_j}$ of all N values in $\widehat{Y_j}$.
3) Calculate the following: $\hat{\mu}_j = (\hat{\mu}_{\hat{y}_j} - \bar{y}_j)/\,\hat{\sigma}_{\hat{y}_j}$.
4) The first three steps should be repeated to obtain B bootstrap estimates $\hat{\mu}_{j(1)}, \ldots, \hat{\mu}_{j(B)}$. B should be larger than 500.
5) To approximate the distribution of $\hat{\mu}_j$, sort all estimates so that $\hat{\mu}_{j(1)} \leq \hat{\mu}_{j(2)} \leq \cdots \leq \hat{\mu}_{j(B)}$.
6) The 100(1-α)% confidence interval is determined by $[\bar{y}_j - s_j\hat{\mu}_{j(k_2)}, \bar{y}_j - s_j\hat{\mu}_{j(k_1)}]$, where $k_1 = \frac{\beta\alpha}{2}$ and $k_2 = \beta - k_1 + 1$.

ERD represents a decrease of the EEG signal amplitude and indicates the activation of cortical motor and premotor areas that are related to motor tasks. It occurs in mu and beta bands, in average about 1.5 s before the movement initiates, and can be detected over the sensorimotor cortical areas contralateral to the movement, reaching a maximum value at movement onset. This ERD has been observed before and during self-paced voluntary movements, reaction time paradigms, passive movements, or motor imagery [156]. ERS corresponds to an increase of amplitude of the EEG signal after the movement is finished, indicating sensory reafferentation. Both ERD and ERS are strongly used in literature for studying cortical processing and motor control [156].

Since we are interested in the dynamics associated with movement planning and execution, in this study we did not address ERS, as its power is higher only at late/end stages of the movement. Therefore, we compare the decoding performance of the classifier using MI features versus using ERD features.

2) Classification

Intending to verify which the set of features (connectivity or ERD) are more relevant for identifying the classes of movement (pronation and supination) with higher accuracy, the aforementioned set of features will be feed to a classifier, separately.

There are several well-known classifiers described in the literature such as, Naive Bayes, Decision Tree, Logistic Regression, K-Nearest Neighbor, Artificial Neural Networks and Support Vector Machine (SVM). In this study, it was chosen to use SVM. The choice is due to its robust classification accuracies for this class of problem, as reported by numerous studies [157,158,159,160].

SVM constructs a hyper-plane or a set of hyper-planes in a high or infinite-dimensional space, and it can be used for classification, regression, for example. A good separation of data is obtained by the hyperplane that has the greatest distance to the closest points of training data of any class (functional margin). More about its mathematical formulation can be found in Malon et al. (2008) [161].

The main steps applied for SVM classification are the separation of the group of characteristics into training and testing sets, according to the 80%-20% Pareto Principle - 80% of effects are due to 20% of the causes.

Training and testing data sets are usually scaled by Z-score to standardize the distribution. After that, in the training data set, a 5 k-fold cross validation (CV) will be applied. CV is used to estimate the ability of a learning model to predict unseen data. It consists of using a limited sample to estimate how the model is expected to perform in general, especially when used to make predictions on data not used during training. The separation of the dataset is exemplified in Figure 6.10.

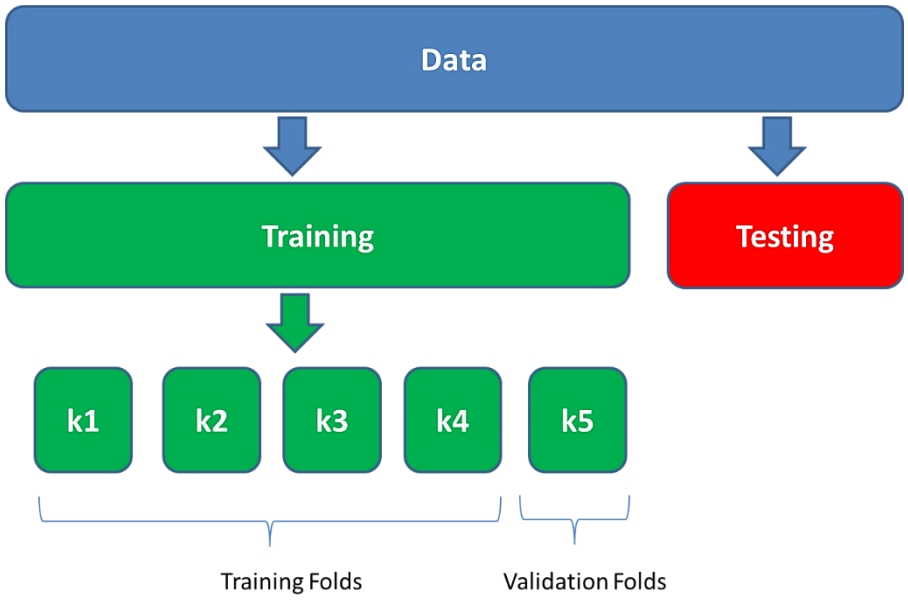

Figure 6.10 – Representation of how the data was separated and final cross validation.

Afterwards, a sequential feature selection method selects the most significant attributes. This technique contains an objective function (criterion), which seeks to minimize the feasible feature subsets. The criterion for classification models is the misclassification rate. It also contains a sequential search algorithm, that includes or removes features from the subset while evaluating the criterion. The model is advantageous, since it moves in only direction, growing or shrinking the set. Usual optimization models perform the task by exhaustive comparisons - compare the criterion for all 2^n subsets of a n-elements data set [162].

Finally, within the selected features, a binary SVM model with radial basis function kernel is trained using *fitcsvm* function from MATLAB [163], and the test set is evaluated. At last, accuracy and Information Transfer Rate (ITR) are measured, in order to see the efficiency of the proposed method for a BMI application. Accuracy is measured by the total correctly predicted answers by the classifier in relation to all predictions.

ITR consists of a measure of the amount of information that is conveyed by a system's output. Firstly, it is defined the mutual information between the selected option (y) and the desired target (x), i.e., information transferred in bits per trial (B) [164]:

$$B = logN + PlogP + (1 - P)log\frac{(1-\mathrm{P})}{N-1} \quad (6.1)$$

where, N is the number of targets and P is the classification accuracy, obtained by the total number of classified commands. Then, to obtain the ITR, B is divided by the average time (T) to select a single symbol.

$$ITR = B/T \quad (6.2)$$

7. RESULTS

In this chapter, the results of the experiments designed to evaluate the hypothesis of this work are shown. The results of the application of the MI to improve decoding motor tasks will be described, followed by the comparative analyses with traditional

7.1 Windowing

After the preprocessing stages, the first step of feature extraction is windowing the EEG signal according to the region of interest. The cues for movement are coded as events in the dataset (Figure 7.1). In this figure, it was plotted the cues over the signal of accelerometer from the exoskeleton used in data acquisition. Accelerometer data was used to verify the average beginning of supination/pronation peaks (~1 s after the cue), then the window of analysis. We defined the time of cue as zero. We selected the events related to the tasks of pronation and supination of the wrist that lasted around 1.2 seconds.

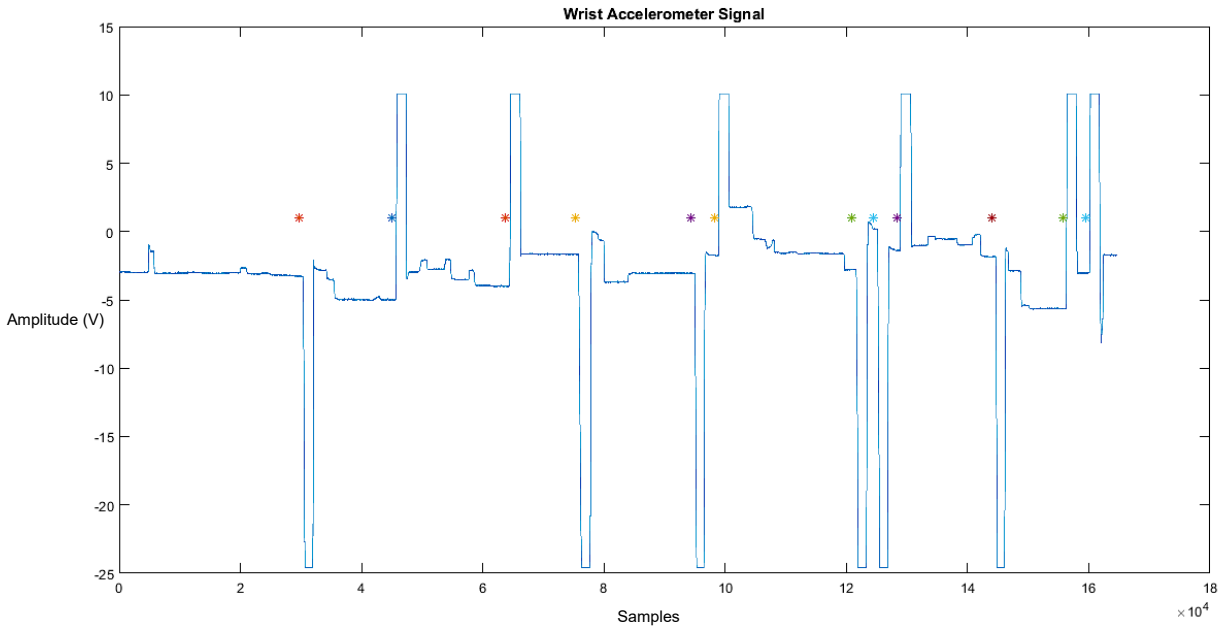

Figure 7.1 – Fragment of the signal corresponding to wrist pronation and supination in the dataset. The onsets of movement are marked with an asterisk. In this case, there were six pronation and six supination movements. The ascending signals correspond to pronation, and descending ones correspond to supination.

The EEG signal was windowed (main epochs) starting 600 ms before and ending 1.4 s after the movement. This period includes the stages of rest, motor planning, and motor execution.

7.2 Proposed Method

7.2.1 Screening Relevant Connections

1) Non-normalized MI

Initially, non-normalized MI was estimated for ten consecutive windows 200 ms within the main epochs. Figure 7.2 depicts box plots showing the density of the average non-normalized MI values across all trials, for each frequency band for pronation and supination movements, for one of the volunteers. In the figures, the windows of time (horizontal axes) are defined as:

- Window 1: -600 to –400 ms
- Window 2: –400 to –200 ms
- Window 3: –200 to 0 ms
- Window 4: 0 to 200 ms
- Window 5: 400 to 600 ms
- Window 6: 600 to 800 ms
- Window 7: 800 to 1000 ms
- Window 8: 1000 to 1200 ms
- Window 9: 1200 to 1400 ms
- Window 10: 1400 to 1600 ms

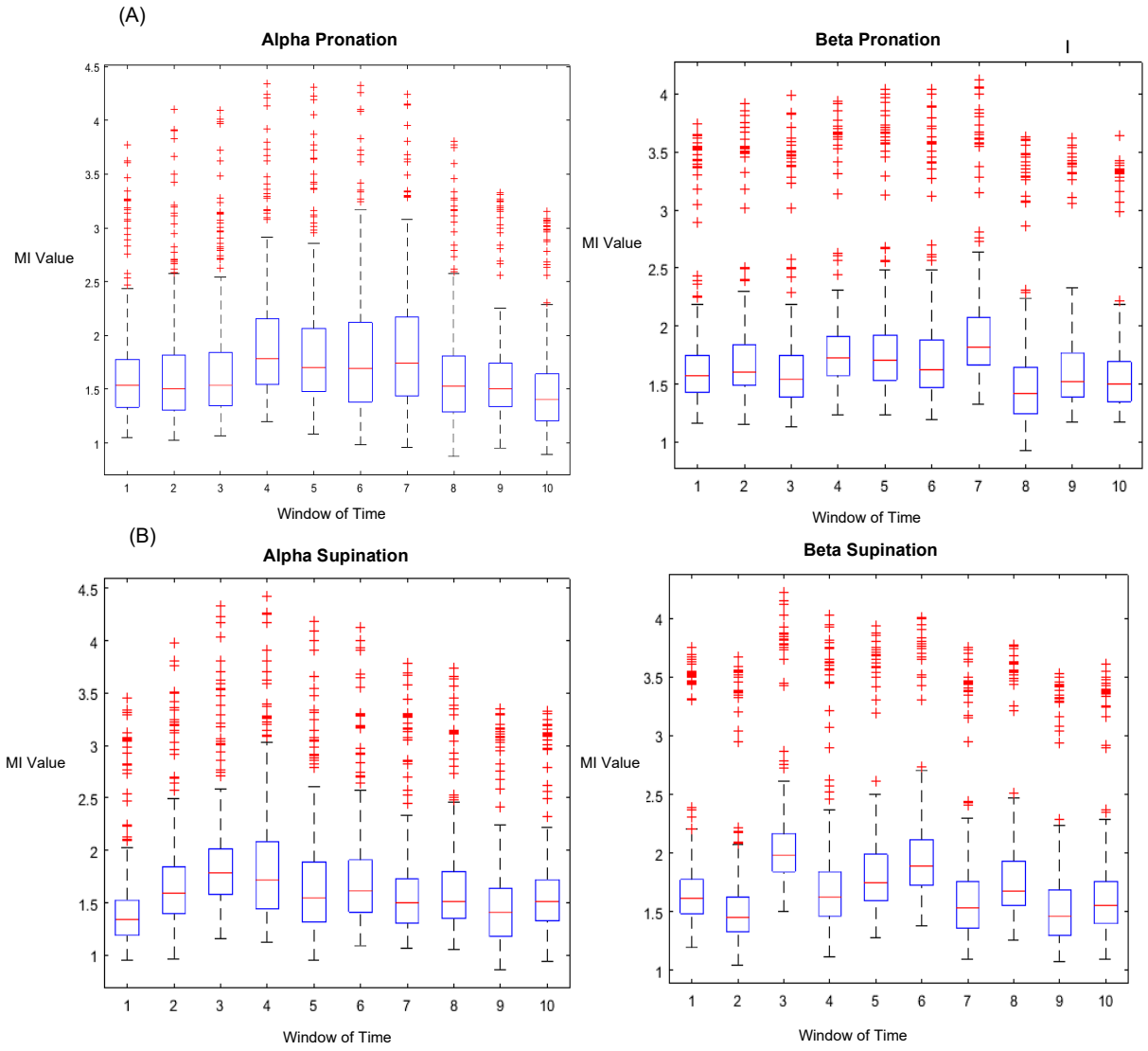

Figure 7.2 – Box plots representing the variability between the average density of non-normalized MI values for all trials for each window of time. (A) represents the MI density for pronation in the alpha and beta bands and (B) represents the MI density for supination in the alpha and beta bands.

It is possible to notice substantial variability of MI values across all windows, making it very hard to pinpoint which level of MI would be a possible candidate to select suitable MI connections (stronger pair). Furthermore, as explained in topic 5.3.3, since there is not an upper bound value for MI, it is not simple to decide if a certain MI values is significant or not. Therefore, a normalization approach has been applied to allow for proper comparisons.

2) Normalized MI

Normalized MI was estimated for ten consecutive windows 200 ms within the main epochs. As explained, this first step was designed to select the relevant pairs of connectivity.

Figure 7.3 and Figure 7.4 depict 3D histograms showing the density of the average MI values across all trials, for the per frequency band for pronation and supination movements, for one of the volunteers. In the figures, the sub-windows are separated by color:

- Dark Blue: -600 to –400 ms
- Orange: -400 to –200 ms
- Yellow: -200 to 0 ms
- Purple: 0 to 200 ms
- Green: 400 to 600 ms
- Light Blue: 600 to 800 ms
- Red: 800 to 1000 ms
- Dark Blue: 1000 to 1200 ms
- Orange: 1200 to 1400 ms
- Yellow: 1400 to 1600 ms

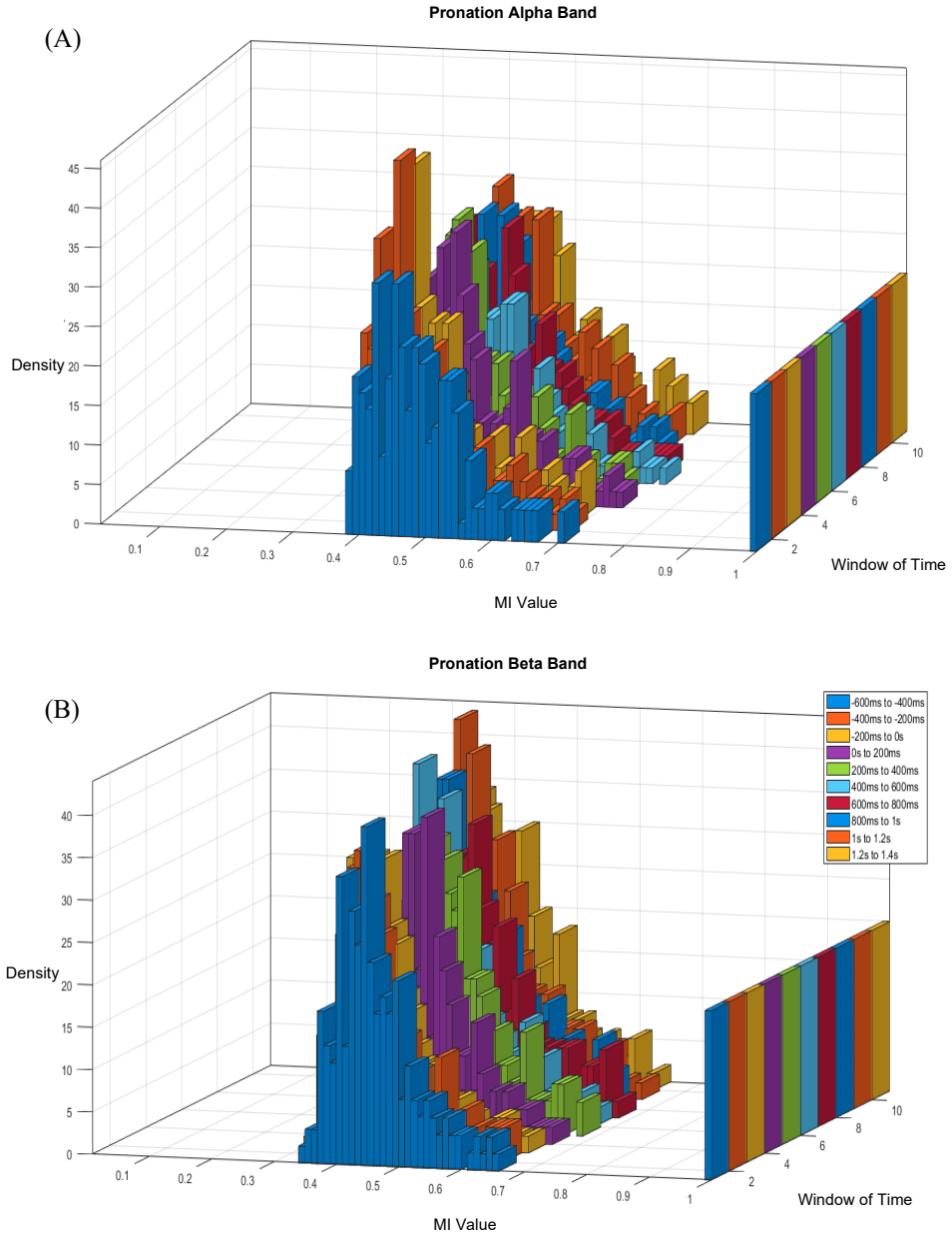

Figure 7.3 – Histograms representing the average density of MI values for all trials for each window of time. (A) represents the MI density for pronation movement in the alpha band, and (B) represents the MI density for pronation movement in the beta band.

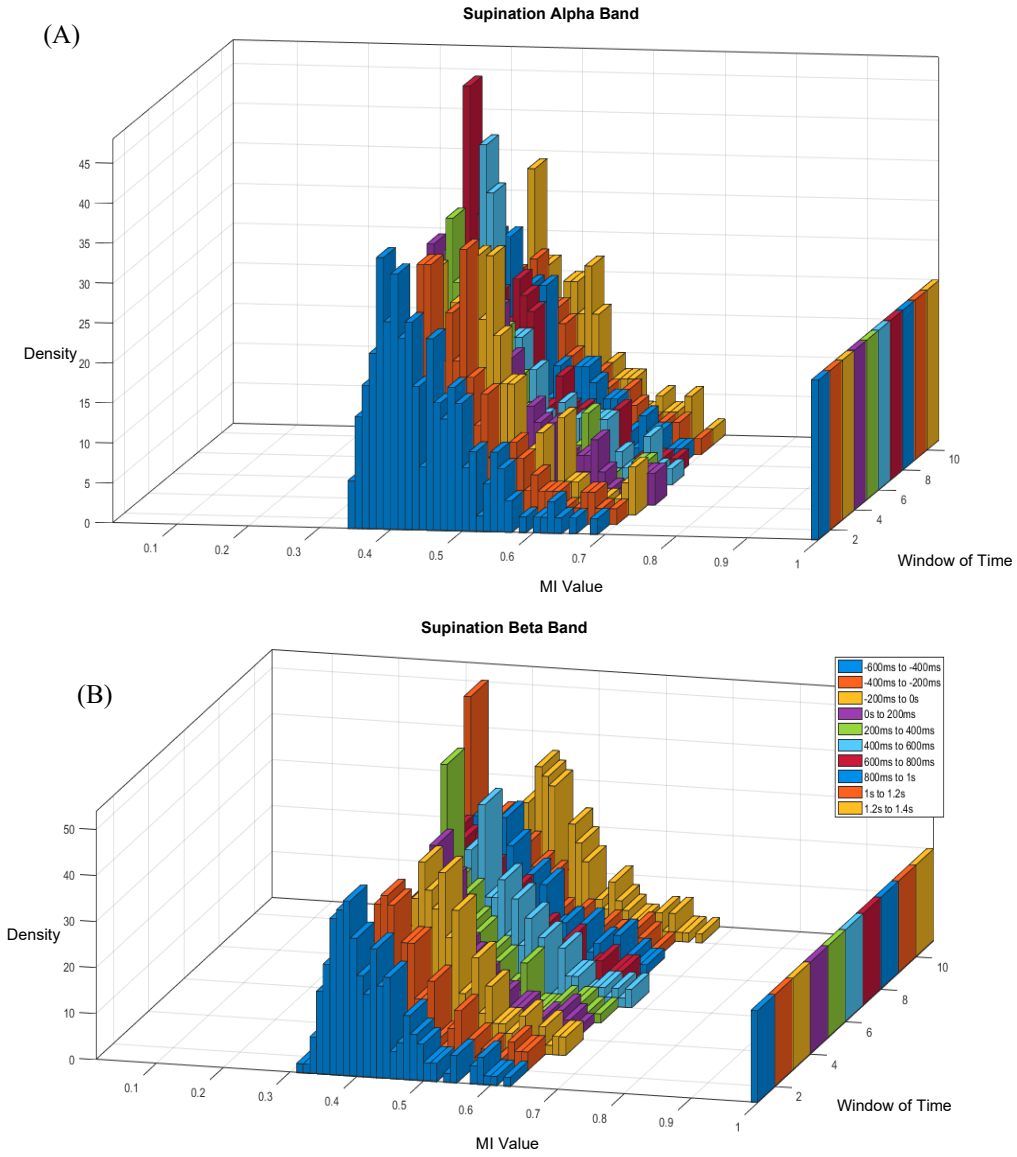

Figure 7.4 – Histograms representing the average density of MI values for all trials for each window of time. (A) represents the MI density for supination movement in the alpha band, and (B) represents the MI density for supination movement in the beta band.

The histograms show the distribution of connectivity values for each period. It is possible to notice that for supination and pronation in alpha and beta bands, the values are distributed between 0.3 to 0.7. The values equal one corresponds to the connectivity of the channel with itself, since MI is a symmetric and non-directed measure. As there are 20 channels of analysis, this is the density of values equal to one.

Within the histograms, it was possible to notice that there were some changes in connectivity values over time and that just visualizing it was not possible to estimate a threshold or the changes patterns. To reinforce this idea of variability over time, it was

plotted box plot graphs for each type of movement and their corresponding band (Figure 7.5). The windows of time were defined in the same way as in Figure 7.2.

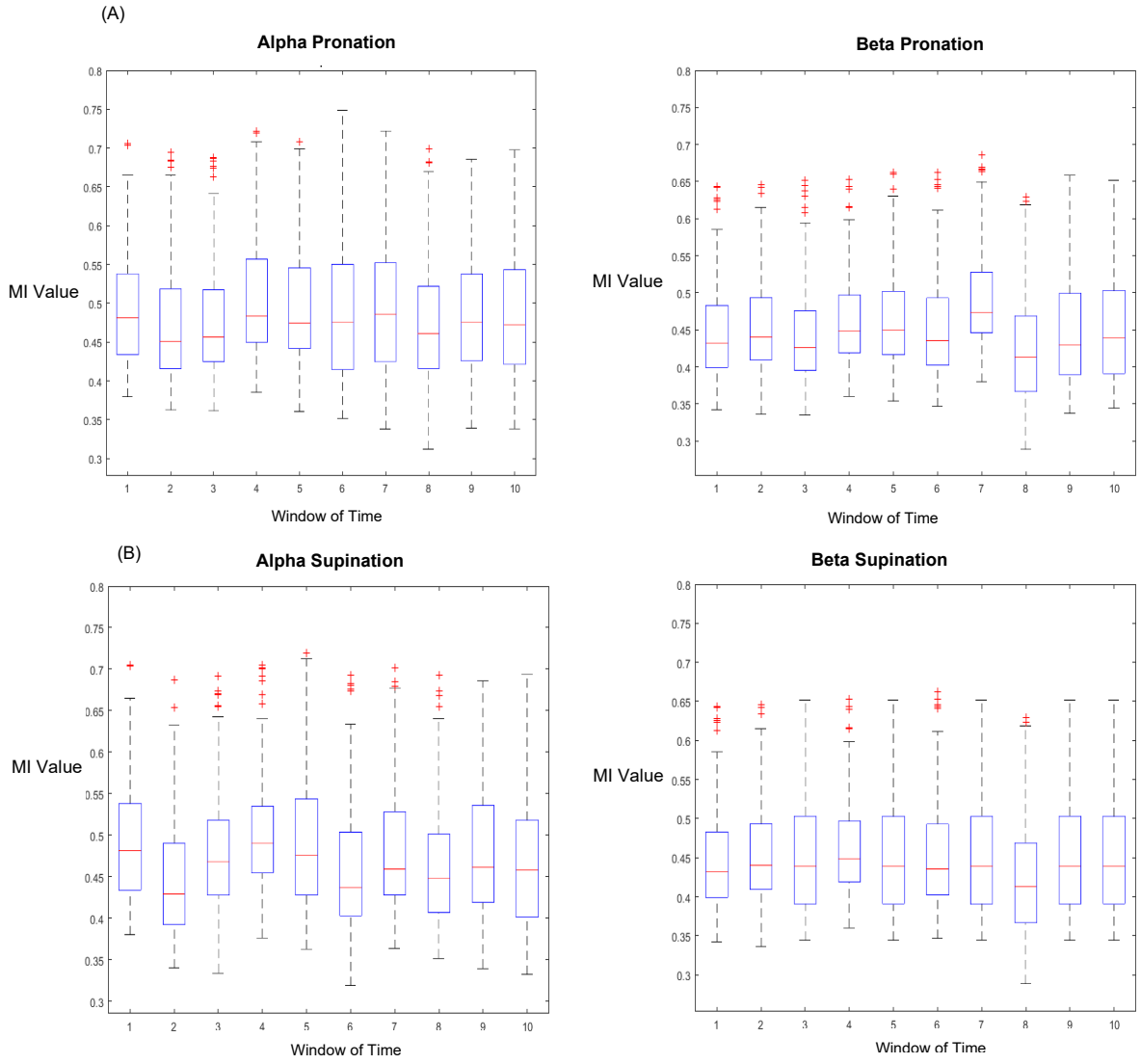

Figure 7.5 – Box plots representing the variability between the average density of normalized MI values for all trials for each window of time. (A) represents the MI density for pronation movement in the alpha and beta band. (B) represents the MI density for supination movement in the beta band.

With the help of the histograms and the above box plots, we set out to investigate which pairs of electrodes are more relevant.

7.2.2 Selecting Relevant Connections

The most relevant pairs of MI connections, among all 400, are the ones that show statistically significant changes over time (from rest to planning and the execution of the movement), across the population.

For that, we evaluated the normality of our variables (pairs of connections for a window of time) for each band (alpha and beta) and for each subject. The results rejected the null hypothesis of normality. Therefore, a non-parametric test for related variables was applied (Friedman's test). This test is used to detect differences in treatments across multiple test attempts, as in the example of Table 7.1. In our case, each treatment is the window of time, and the blocks are the MI intensity of a pair of electrodes. Therefore, k=1 to 10 (total of windows of time) and blocks = 1 to 24 (total of observations of MI values from a pair of electrodes). The test will verify the windows of time that had significant change for the corresponding MI pair.

Table 7.1 – Example of use of the Friedman's test [165].

Blocks	**Treatments**			
	1	2	…	k
1	X_{11}	X_{11}	…	X_{1k}
2	X_{21}	X_{12}	…	X_{2k}
⋮	⋮	⋮	⋮	⋮
B	X_{b1}	X_{1b}	…	X_{kb}

For each subject, each pair of electrodes was evaluated according to the frequency band. We selected the pairs with $p<0.31$, which is equivalent to one standard deviation for a Gaussian distribution. Furthermore, to discover which window of time showed significant differences for a pair of electrodes, a multiple comparison test was chosen and executed using the *multcompare* function from MATLAB [166].

The pairs of electrodes that had significative changes between any two windows of time during the period of -600 ms to 1.4 s and for more than five subjects were considered the most relevant pairs. Table 7.2 and Table 7.3 show the most frequent pairs for supination and pronation, respectively.

Table 7.2 – Pairs of EEG channels that showed significative changes across any two windows of time and the number of subjects for whom that significance appeared, for supination in the alpha and beta bands.

Supination			
Alpha Band		**Beta Band**	
Pairs of Channels	**Repetitions**	**Pairs of Channels**	**Repetitions**
FC3 – FC4	6	C6 – C2	5
FC3 – C2	5	FC3 – P1	5
FC3 – C4	5	FC3 – PZ	5
FC3 – CZ	5	FC3 – P2	5
C6 – FC4	5	CP3 – C1	5
FC3 – P4	5	CP3 – CZ	6
CP1 – P1	5	CP2 – FC2	5
P1 – PZ	5	C6 – CP1	5
		CP3 – CP2	5
		C6 – CP4	5
		CP1 – PZ	5
		P1 – PZ	5
		CPZ – P1	5
		CP1 – CP2	5
		CPZ – PZ	5
		CPZ – P2	5
		CP4 – P2	5
		CP4 – P3	5
		CP4 – PZ	5
		CP1 – CPZ	5

Table 7.3 – Pairs of EEG channels that showed significative changes across any two windows of time and the number of subjects for whom that significance appeared, for pronation in the alpha and beta bands.

Pronation			
Alpha Band		**Beta Band**	
Pairs of Channels	**Number of subjects**	**Pairs of Channels**	**Repetitions**
FC3 – C3	5	FC3 – FC4	6
C6 – FC4	5	FC3 – CZ	5
FC3 – CPZ	6	C6 – CZ	5
CP3 – C3	5	FC3 – CP1	5
CP2 – FC1	5	CP3 – FC2	5
CP2 – C3	6	CP3 – FC4	7
CP3 – CP4	5	CP3 – C3	5
CP1 – P2	5	FC3 –P1	5
CPZ – P4	6	CP4 – P4	5
CP2 – CP4	6		

Observing the above tables, it is possible to notice that for supination and pronation there were relevant connections between primary somatosensory cortex (BA 1,2 and 3) and primary motor cortex (BA 4), and between primary somatosensory cortex and posterior parietal cortex (BA 5 and 7), see Table 6.1 of Chapter 6 to check corresponding electrodes (Figure 7.6). However, alpha band supination has different relevant connections in number and hemisphere from alpha band pronation, and the same is observed in beta band.

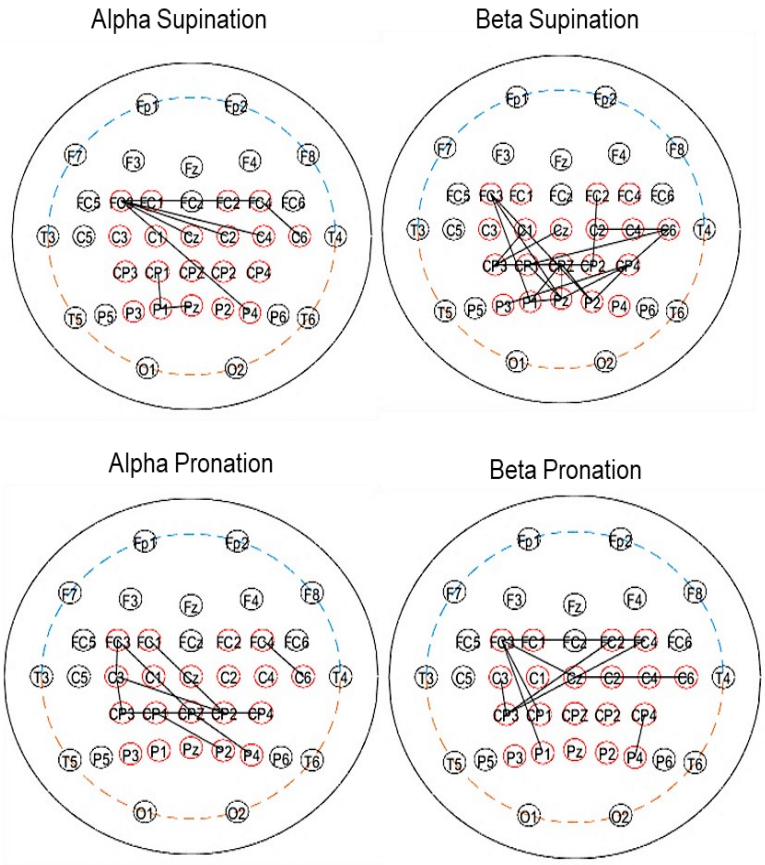

Figure 7.6 – Plots of the relevant pairs of connections over a 2D representation of scalp.

7.2.3 High Resolution MI Connectivity Estimation

Once the most relevant pairs were found, the MI connectivity of these pairs were estimated, now with improved temporal resolution using sliding windows of 50 ms with overlapping of 1 ms. In other words, we are calculating the MI connectivity every 1 ms. The aim was to assess the dynamics of connections over time (-1.0 sec to 1.3 sec). Figure 7.7 and Figure 7.8 represent the resulting time series for the MI connections for pronation and supination, for the alpha and beta bands, respectively.

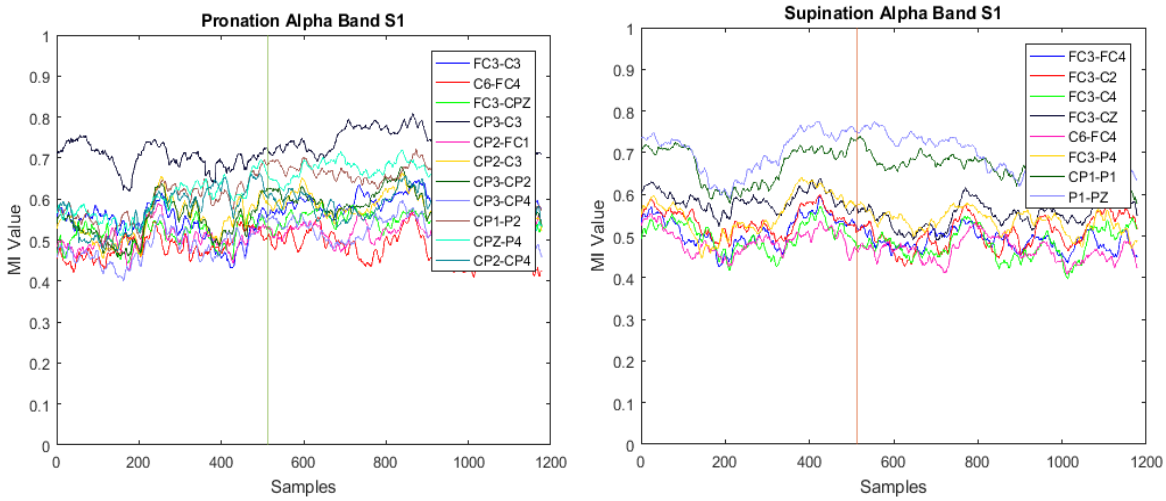

Figure 7.7– Plots of the MI connectivity estimates for alpha band of pronation and supination movements for Subject 1, with resolution of 1ms. Vertical lines represent the cue.

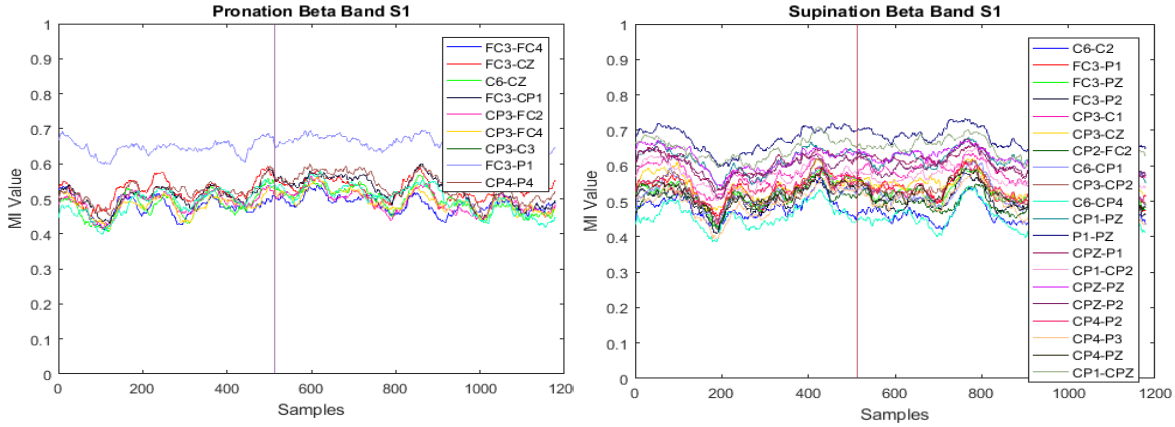

Figure 7.8– Plots of the MI connectivity estimates for beta band of pronation and supination movements for Subject 1, with resolution of 1ms. Vertical lines represent the cue.

Within the plots, it is possible to notice that between-subjects there was a trend of the pairs of channels with higher and lower amplitude and that right after the cue some pairs of channels had a decrease or increase of values. These represent the dynamic MI from rest to execution of the movement.

7.3 Comparative Evaluation

1) ERD Estimation

As described earlier, we will evaluate the performance of an SVM classifier using features extracted by the MI method with the performance using a standard ERD method. Since we are focused on the sensorimotor activity, the significant ERDs were estimated for channels C3, Cz and C4. The estimations were calculated over time windows within -1 s to 3 s (baseline from -1 s to 0 s), with frequency resolution of 1 Hz and time resolution of 0.2s. Before ERD estimation, a Common Average Reference (CAR) filter was applied using the mean of the entire electrode montage as the virtual reference. Spatial filters, such as CAR, minimize volume conduction problems and enhance highly focal distributions [167]. Figure 7.9 shows the obtained ERD maps for channels C3, Cz and C4 during the execution of pronation and supination movements of one of the volunteers.

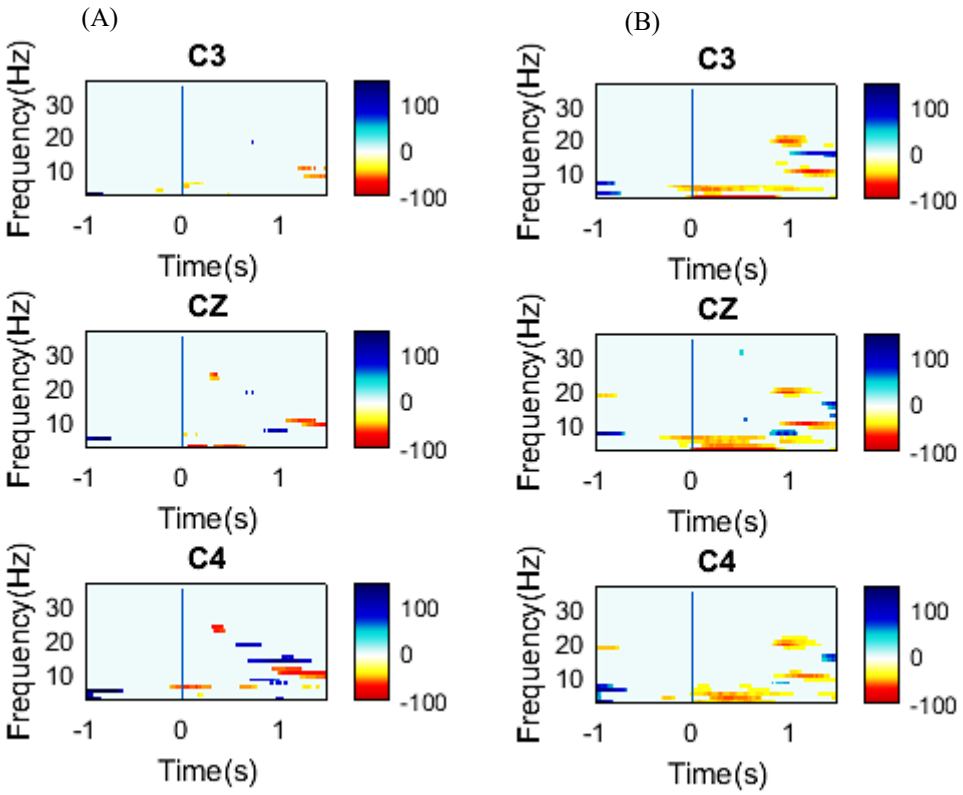

Figure 7.9 – Time-frequency maps of most significant ERD components for one subject. The blue vertical lines indicate when the cue was presented. (A) ERD maps for pronation; (A) ERD maps for supination.

As shown in literature, Mu/Beta ERD precedes voluntary motor movements, mostly 1.5 s seconds before the movement execution (~one second after the cue). When the cue is presented is possible to notice significant ERD in these frequency band, and that the significant ERD (frequency bins) for pronation were different from the supination.

7.4 Validation and Comparative Analyzes

7.4.1 SVM Classifier Using MI Features

For this analysis, the high-resolution MI connectivity series of the most relevant pairs were used as the features to feed the SVM classifier. Those features were extracted for all subjects using sliding 50 ms windows with 1 ms overlapping over the entire period of 0 to 1 s after cue, as explained in item "7.2.3 High resolution MI connectivity estimation" (Table 7.4). This period was chosen because it should contain the most relevant features related to motor planning and the onset of motion. EEG signals collected during the experiments were averaged for all trials and all subjects to define the onset of motion, around 1s.

Table 7.4 – Organization of rows and columns for SVM classification. The first row corresponds to MI estimated for a selected connection A to B from 0 to 1 s, each with 1 ms resolution, using 50 ms sliding windows. Pronation and supination were found to be better represented by distinct MI pairs, even for the same band. Similar tables were developed for both alpha and beta bands.

Feature 1	**Feature 2**	**Feature n**	**…**	**Feature 512**	**Label**
MI $(ch\ A \rightarrow ch\ B)$ 0-50 ms	MI $(ch\ A \rightarrow ch\ B)$ 1-51 ms	MI $(ch\ A \rightarrow ch\ B)$ n-(n +50) ms	…	MI $(ch\ A \rightarrow ch\ B)$ 1000-1000.05 ms	0 (supination)
⋮	⋮	⋮	⋮	⋮	⋮
MI $(ch\ C \rightarrow ch\ D)$ 0-50 ms	MI $(ch\ C \rightarrow ch\ D)$ 1-51 ms	MI $(ch\ C \rightarrow ch\ D)$ n-(n +50) ms	…	MI $(ch\ C \rightarrow ch\ D)$ 1000-1000.05ms	0 (supination)
MI $(ch\ E \rightarrow ch\ F)$ 0-50 ms	MI $(ch\ E \rightarrow ch\ F)$ 1-51 ms	MI $(ch\ E \rightarrow ch\ F)$ n-(n +50) ms	…	MI $(ch\ E \rightarrow ch\ F)$ 1000-1000.05ms	1 (pronation)
⋮	⋮	⋮	⋮	⋮	⋮
MI $(ch\ G \rightarrow ch\ H)$ 0-50 ms	MI $(ch\ G \rightarrow ch\ H)$ 1-51 ms	MI $(ch\ G \rightarrow ch\ H)$ n-(n +50) ms	…	MI $(ch\ G \rightarrow ch\ H)$ 1000 ms ~ 1000.05ms	1 (pronation)

As shown in Figure 6.8, the number of possible features is very large (about 1000 features per MI pair), which would lead to very high processing time and even overfitting of the classifier. A preliminary measure to counter those problems, a sequential feature selection method, was used to select the most significant attributes. The algorithm was set to choose an unlimited number of optimized features, if necessary. This optimization led to a much lower number of MI features for both frequency bands, as shown in Table 7.5.

Table 7.5 – MI features selected by the sequential feature selector for alpha and beta bands. Feature index indicates the index in the high-resolution MI time series.

Alpha Band		**Beta Band**	
Feature index	**Corresponding Window of time**	**Feature index**	**Corresponding Window of time**
131	255.85ms ~305.85ms	3	5.8ms ~50ms
209	408.2ms ~ 458.2ms	86	167.96ms ~ 217.96ms
254	496.09ms ~546.09ms	130	253.91ms ~303.91ms
348	679.68ms ~ 729.68ms	184	359.38ms ~ 409.38ms
371	724.61ms ~774.61ms	248	484.38ms ~ 535.38ms
373	728.52ms ~ 778.52ms	332	648.43ms ~ 698.43ms
383	748.04ms ~798.04ms	409	798.82ms ~ 848.82ms
503	982.42ms ~ 1.03s	411	802.73ms ~ 852.73ms
		428	835.94ms ~ 885.94ms

Head plots for the selected features can be seen in Figure 7.10 (alpha pronation), Figure 7.11 (alpha supination), Figure 7.12 (beta pronation) and Figure 7.13 (beta supination). Each selected feature represents normalized MI values of the relevant connections for the corresponding window of 50 ms.

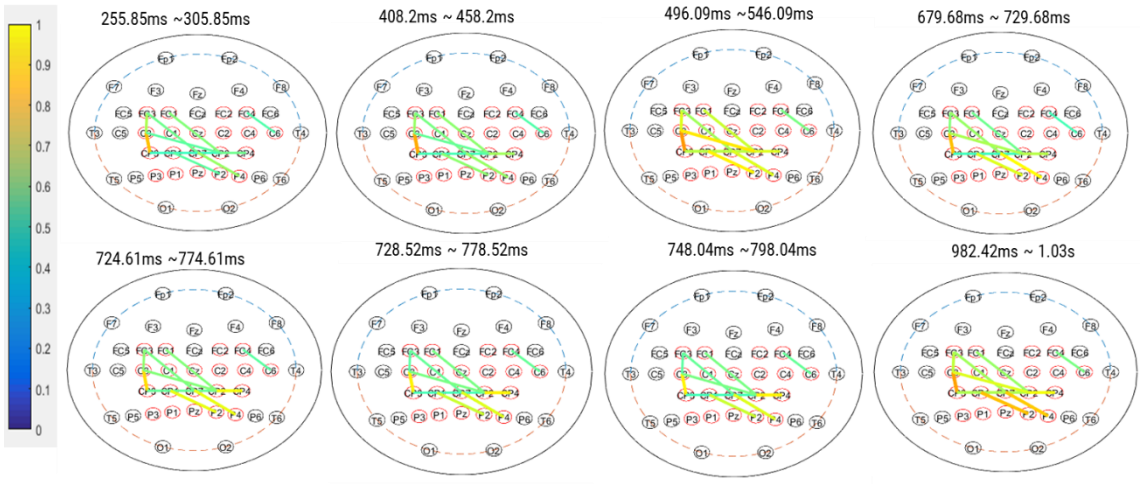

Figure 7.10 – Head plots of the selected MI features by the sequential feature selector for alpha pronation.

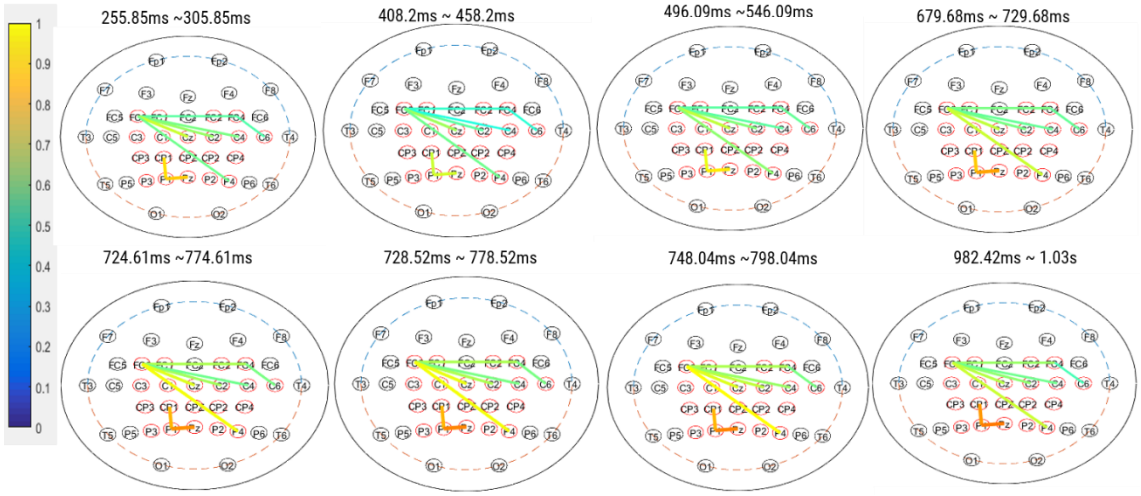

Figure 7.11 – Head plots of the selected MI features by the sequential feature selector for alpha supination.

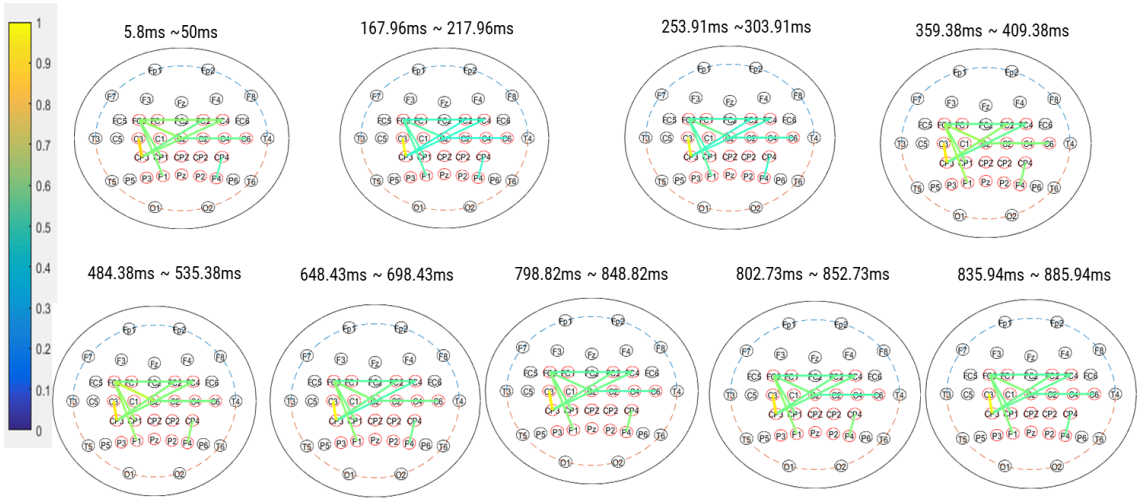

Figure 7.12 – Head plots of the selected MI features by the sequential feature selector for beta pronation.

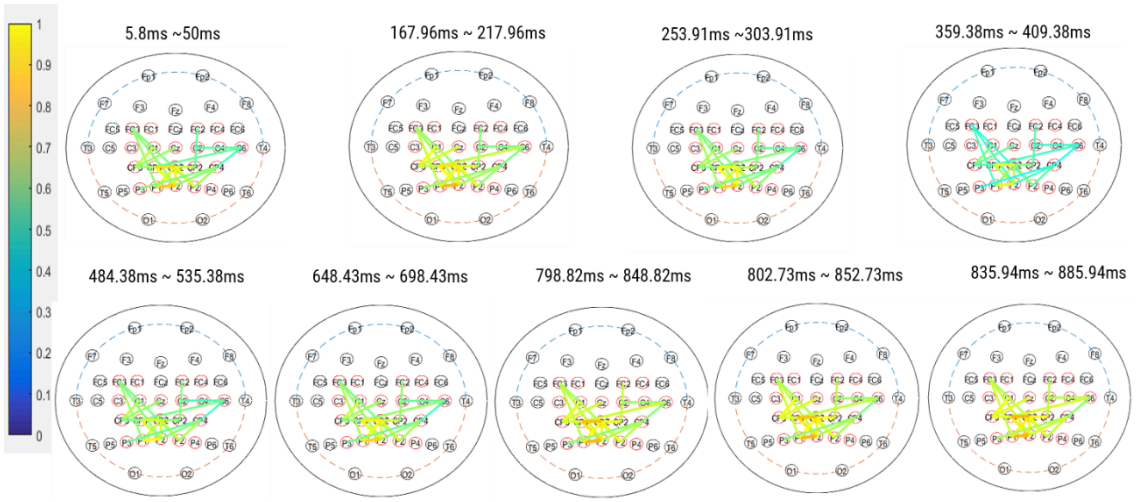

Figure 7.13 – Head plots of the selected MI features by the sequential feature selector for beta supination.

The classification accuracy of the classifier was tested for the alpha and beta bands separately. Before classification, the dataset was randomized, and a 5-fold cross-validation was applied. The classification accuracies obtained for alpha and beta bands are shown in Table 7.6. Accuracies were obtained by the ratio of the correctly predicted class from all trials and for all of subjects by the number of trials available. As seen, beta band features were able to separate both classes of movement with 89.65% of accuracy. Alpha and beta features were tested separately to compare how well each band describes the movement as sensorimotor rhythms.

Table 7.6 – MI SVM classification accuracy using alpha and beta band features.

MI SVM Accuracy	
Alpha Band	Beta Band
73.68%	89.65%

7.4.2 ERD Classification

ERD component with frequency resolution of 1 Hz were used to extract the features to be fed to the SVM classifier. This frequency resolution was selected in order to use a similar time window as that used when the SVM classifier processed MI features. We selected the significant components for alpha and beta bands for pronation and supination classes of movements, from -0.5 s to 1 s, since ERD component initiates, in average, 1.5 seconds before the movement. As features for the classifier, it was selected the significant component for each corresponding frequency bin, as shown in Table 7.7.

Table 7.7 – Organization of the alpha band ERD dataset. A similar table was developed for the beta band, with the difference that the beta band has 18 frequency bins from 13Hz to 30Hz.

Feature	**Label**	
	0 (supination)	**1 (pronation)**
8Hz	Correspondent ERD time values from -0.5 to 1s.	Correspondent ERD time values from -0.5 to 1s.
9Hz	Correspondent ERD time values from -0.5 to 1s.	Correspondent ERD time values from -0.5 to 1s.
10Hz	Correspondent ERD time values from -0.5 to 1s.	Correspondent ERD time values from -0.5 to 1s.
11Hz	Correspondent ERD time values from -0.5 to 1s.	Correspondent ERD time values from -0.5 to 1s.
12Hz	Correspondent ERD time values from -0.5 to 1s.	Correspondent ERD time values from -0.5 to 1s.

As shown in Figure 6.8, the number of possible features is very large, which would lead to very high processing time and even overfitting of the classifier. Similarly to the procedure used for the MI classifier, a sequential feature selection method was used to select the most significant attributes. The algorithm was set to choose an

unlimited number of optimized features, if necessary. This optimization led to a much lower number of ERD features for both frequency bands, as shown in Table 7.8.

Table 7.8 – Features selected by the sequential feature selector for alpha and beta bands.

Selected features	
Alpha band (Hz)	***Beta band (Hz)***
8	13
9	14
10	15
11	16
	17
	18
	19
	20
	21
	22
	23
	24
	25

The classification accuracy of the classifier was tested for the alpha and beta bands separately. Before classification, the dataset was randomized, and a 5-fold cross-validation was applied. The classification accuracies obtained for alpha and beta bands are shown in Table 7.9. Accuracies were obtained by the ratio of the correctly predicted class from all trials and for all of subjects by the number of trials available.

Table 7.9 – ERD SVM classification accuracy using alpha and beta band features.

ERD SVM Accuracy	
Alpha Band	Beta Band
60.73%	62.49%

Here, alpha and beta band presented similar accuracy values to distinguish both classes. And similar as to MI, both bands were tested separately to verify how well each one describes both bands.

7.4.3 Information Transfer Rate

1) Proposed method – MI Connectivity measures

Experiments using the proposed method resulted in P = 89.65% when the SVM classifier used beta features and P = 73.68% using alpha features with two targets (pronation/supination). Processing required data extracted from of one second of EEG data. Therefore, we can calculate ITR as follows:

- SVM using MI beta band features:

$$B_{MI\_Beta} = log2 + 0.8965log0.8965 + (1 - 0.8965)log\frac{(1-0.8965)}{2-1} \quad (7.1)$$

$$B_{MI\_Beta} = \log 2 + 0.8965 \log 0.8965 + 0.1035 \log 0.1035 \quad (7.2)$$

$$B_{MI\_Beta} = 0.1565\ bits/trial \quad (7.3)$$

Considering T = 1 s:

$$ITR_{MI\_Beta} = \frac{0.1565}{1\ s} = 0.1565\ bits/s \quad (7.4)$$

$$ITR_{MI\_Beta} = 0.1565\ bits/s\ x60\ =\ 9.36\ bits/min. \quad (7.5)$$

- SVM using MI alpha band features:

$$B_{MI\_Alpha} = log2 + 0.7368 \log 0{,}7368 + (1 - 0.7368)log\frac{(1-0.7368)}{2-1} \quad (7.6)$$

$$B_{MI\_Alpha} = \log 2 + 0.7368 \log 0.7368 + 0.2632 \log 0.2632 \quad (7.7)$$

$$B_{MI\_Alpha} = 0.0507\ bits/trial \quad (7.8)$$

Considering T = 1 s:

$$ITR_{MI\_Alpha} = \frac{0.0507}{1\ s} = 0.0507\ bits/s \quad (7.9)$$

$$ITR_{MI\_Alpha} = 0.0507\ bits/s\ x60\ =\ 3.042\ bits/min. \quad (7.10)$$

2) Standard ERD features

Experiments using the proposed the ERD method resulted in P = 62.49% when the SVM was fed with ERD beta features and P = 60.73% using alpha features, for two targets (pronation/supination). Processing required data extracted from of 1.5 second of EEG data. Therefore, we can calculate ITR as follows:

- SVM using ERD beta band features:

$$B_{ERD\_Beta} = log2 + 0.6249log0.8965 + (1 - 0.6249)log\frac{(1-0.6249)}{2-1} \quad (7.11)$$

$$B_{ERD\_Beta} = \log 2 + 0.6249 \log 0.6249 + 0.3751 \log 0.3751 \quad (7.12)$$

$$B_{ERD\_Beta} = 0.0137\ bits/trial \quad (7.13)$$

Considering T = 1.5 s:

$$ITR_{ERD\_Beta} = \frac{0.0137}{1.5\ s} = 0.0091\ bits/s \quad (7.14)$$

$$ITR_{ERD\_Beta} = 0.0091\ bits/s\ x60\ =\ 0.546\ bits/min \quad (7.15)$$

- SVM using ERD alpha band features:

$$B_{ERD\_Alpha} = log2 + 0.6073 \log 0.6073 + (1 - 0.6073)log\frac{(1-0.6073)}{2-1} \quad (7.16)$$

$$B_{ERD\_Alpha} = \log 2 + 0.6073 \log 0.6073 + 0.3927 \log 0.3927 \quad (7.17)$$

$$B_{ERD\_Alpha} = 0.01\ bits/trial \quad (7.18)$$

Considering T = 1.5 s:

$$ITR_{ERD\_Alpha} = \frac{0.01}{1.5\ s} = 0.0067\ bits/s \quad (7.19)$$

$$ITR_{ERD\_Alpha} = 0.0067\ bits/s\ x60\ =\ 0.4\ bits/min \quad (7.20)$$

8. DISCUSSIONS

This thesis aimed to verify the existing methods of evaluation of sensorimotor integration and propose a new approach based on functional connectivity. The importance of understanding sensorimotor integration is that with the comprehension of motor planning and motor execution, it is possible to improve the accuracy of BMIs and understand cortical reorganization after an injury.

According to Tam et al. (2019), although it is possible to intercept and decode the motor intention at several points in the neuro-muscular control pathway and use that information to drive a prosthetic device to restore movement, we are still far from the goal of reaching naturalistic and dexterous control like our native limbs [28]. Thus, it is still necessary to find strategies that could improve motor decoding and, consequently, better BMIs. One of the main challenges that make it harder to use BMIs in the clinical environment is the need for specialized hardware, such as dry electrodes, that should also be comfortable to wear and easy donning beyond laboratories and hospitals. Besides, BMI systems still have poor reliability for most applications, and another important consideration is the tiredness caused by the training process [168].

Also, it is essential to mention that most neural prostheses do not offer wrist motion of range. Wrist movements are important because they allow better manipulation of objects and contribute to the arm/hand system's mobility. Cordella et al. (2016) report that most of the prosthesis users (around 98%) long for improvements such as to feel the force applied and the temperature of the object being handled by the prosthesis, additional movements, such as pointing the index finger, moving individual fingers and increased wrist range of motion (flexion and extension/ pronation and supination/ radial and ulnar) [51].

A current review by Bajaj et al. (2019) shows that most robotic and prosthetic research studies are focused on the development of end effectors/terminal devices (hands, grippers, and others) over wrists [52].

One strategy that could help with the comprehension of sensorimotor integration is the use of functional and effective connectivity analyses. Those strategies have been extensively applied to study the effects of a neurological injury and its intrinsic characteristics, elucidating how neurons and neural networks process information. Also, those methods have provided contributions for the development of treatment and

monitoring strategies for various neurological dysfunctions caused by Parkinson, Alzheimer's disease, Spinal Cord Injury, Huntington diseases, and similar pathologies or injuries [31,32,33,34].

Previous studies have shown that effective techniques could provide information on the flow of sensory information to the motor cortex [87]. There were reports of studies using effective connectivity for the understanding of sensorimotor integration such as Granger Causality [89], direct Directed Transfer Function [90], Imagery Coherence [37], Partial Directed Coherence [93].

However, in the literature on sensorimotor integration, we observed that the nonlinear functional connectivity approach had not been widely explored. Functional connectivity consists of statistical dependencies between different brain regions related to distant neurophysiological events, i.e., associations between spatially remote neurophysiological events [4].

Therefore, to investigate and decode information associated with the sensorimotor system, we propose using a functional connectivity strategy, so-called normalized pairwise Mutual Information, to decode motor activities during the motor planning phase. MI is a nonlinear higher-order information-theoretic measure of temporal synchrony that quantifies the information obtained from a random variable, by observation of another [114]. MI has been used previously in attempts with BMIs [169], but here we proposed a selection of MI features based on their changes over time.

As shown in the previous chapter, non-normalized MI features could not be used since there is no upper bound for MI estimation. Also, as shown in Figure 24, all windows of time have different scales and many outliers, making it harder to compare different movements in various bands.

In this research, we were able to identify the normalized MI pairs of connections that show significant change over time and used them to obtain the MI dynamic changes. The estimation of the best pairs for alpha-band pronation was different from alpha-band supination, and the same was observed for beta-bands. Since relevant connectivity pairs were different for each movement, even though they represent the same regions (posterior parietal cortex, primary somatosensory cortex, and primary motor cortex), we hypothesize that the nonlinear functional connectivity measures could have detected subtle differences between movements. For instance, alpha supination showed a relevant connection between FC3 and FC4, with strong links between the primary motor cortices of both hemispheres. Similar behavior was also found for alpha

pronation, beta supination, and beta pronation. There is evidence that both brain hemispheres are active during the execution of bimanual and unimanual movements, supporting our findings [170].

Importantly, another example of a relevant connection found in alpha supination was FC3 and C4, representing a connection between the primary motor cortex and the somatosensory cortex. This finding is coherent with the literature. It is expected that sensory information processed by S1 is sent to the prefrontal cortex, which in turn sends instructions to the premotor cortex to plan the necessary sequence for the movement's accomplishment. Finally, the premotor area and M1 carried out the final tasks to generate neural impulses to control movement execution [10].

The posterior parietal cortex (PPC) is active during the planning of motor tasks and can anticipate the visual consequence of the intended action during the planning period, i.e., the stimulus-driven attention. As the dataset used in the experiments used visual cues to indicate the movement's type, it was likely that relevant pairs related to PPC areas were also found. Indeed, we found, for both classes (pronation and supination) and bands, the presence of a relevant pair of connections to PPC areas, such as P1 and Pz in beta supination and CPz and P4 in alpha pronation [171].

To evaluate if the proposed method could improve decoding of cortical activity during motor tasks, we compared its performance against the performance of a conventional sensorimotor integration Event-Related Desynchronization methods, in which Mu/Beta ERDs are usually observed before and during voluntary movement execution [26,84]. This comparative approach was chosen because sensorimotor rhythms (SMR) are among the most common EEG methods implemented for BMIs, especially for imagery of movement. MIm-BMIs have been used to control devices such as orthosis, drones, wheelchairs, and software for communication. According to Neuper et al. (2002), most of the neural activity related to fist movements is found in channels C3, C4, and Cz [172]. The ERD was then estimated for these channels, and we compared their results to the MI method.

Classification using SVMs showed that it is possible to separate pronation and supination. When the classifier used only MI alpha-band features, we achieved performances of up to 73.68%. Using only MI beta-band features, much higher performance was achieved (89.65%). Using the conventional method (ERD), the accuracy of the classification of the two classes of movement was 60.73% and 62.49% for alpha and beta bands, respectively.

In literature, some studies have also attempted to decode wrist movements based on EEG signals. Khan et al. (2010) investigated single-trial EEG classification for wrist movement imagery based on spatial filtering in the gamma band. The authors reported accuracy of around 89%. However, their experimental procedure required the volunteer to keep a sustained movement for 3 seconds. In this regard, an advantage of our study is the use of the motor planning window, not execution. As such, a BMI using our approach would not require tentative movements, and, consequently, the BMI would be able to achieve faster and more natural control [173].

Kiguchi et al. (2013) proposed a method to identify pronation and supination motion based on an artificial neural network. In this work, forearm angle, angular velocity, or angular acceleration were estimated using a neural network. The authors showed that higher motion frequency is correlated with higher error values, except in the case of when the estimation is made based on angular acceleration. The smaller error value obtained to estimate angular velocities was in the range of 2% for motions with a frequency of 0.25 Hz [174]. Unlike our study, [174] estimated angular forearm velocities based on the EEG signals. However, the sample was composed of only three subjects, so it is not possible to assure the error values will be the same for a more substantial population.

Ofner et al. (2019) proposed a strategy to decode upper limb movements based on the low-frequency EEG time-domain. Their approach had a 61% chance of predicting the correct pronation of the forearm. For forearm supination, the obtained accuracy was only 57%. Higher accuracies were obtained for hand closing (84%) and hand opening (79%) [150]. In contrast, our method provided accuracies of up to 89.65% when classifying pronation and supination movements. Also, it is important to mention that the study has found that movement vs. movement average classification became significant between -0.56 s and 0.81 s (window size ~1.37 s). In our research, we achieved higher results with a 1 s window size.

Besides high accuracy, the MI-based method also had higher ITR when compared with the ERD method. Dynamic MI beta features could deliver ITR of 9.36 bits/min. On the other hand, ERD was only capable of achieving 0.546 bits/min. It is crucial to point out that the performance of the MI-based method was achieved without any training.

ERD is based on the average of the power samples across all trials, and it considers the decrease of the amplitude existing for Mu/Beta bands. The statistical

dependency between spatially distant electrodes is not taken into consideration. The main drawback of ERD BMI-based is that it requires substantial training on the user side to lead to the most precise and most distinct ERD/ERS. This type of BMI can currently only be used with a maximum of 3 or 4 different tasks to guarantee maximal performances; with more tasks, the decoding accuracy becomes even lower [21,175].

In our method, the selection of relevant connections based on time brought information about how one channel is strongly related to other spatially distant over time. It uses information theory to explain how a channel exerts influence over others during the time. This dynamic may explain why the proposed method separated the movements better than ERD. Also, we have evidence that the proposed method could respond better to separate more types of tasks since that for each task; their specific relevant connections will be estimated, being adjustable according to the task.

Finally, the possibility of decoding cortical information during the planning phase can be valuable for real-time applications. Our research also provided evidence that it is not necessary to use high-density EEG systems and large processing windows to obtain acceptable accuracy and ITR for motor task decoding.

9. CONCLUSIONS

In this PhD thesis, we presented a method for decoding cortical response during wrist rotation motor-tasks based on functional connectivity. Our results overcome conventional strategies (ERD). Therefore, it could potentially be used for achieving better results in BMIs, due to the inclusion of dynamic information and selection of relevant channels that could increase computational efficiency and accuracy.

The methods implemented in this research focused on the classification of wrist movements, which are not well-explored motions in the neural prosthesis field. Good accuracy in distinguishing this subtle movement could help the prosthesis' user to have the possibility of the wrist rotation while using the prosthesis for manipulating objects.

The main contribution of this work is the proposal and validation of functional connectivity as the main feature for separating wrist movements. Besides, we provide a method to select relevant connections based on the connectivity change over time, with the intent to minimize the computational cost.

The main limitations of this study are associated with the low number of subjects in our sample. Also, the volume conduction could have interfered with the results since the most relevant pairs were close to each other. In addition, it was not measured how the cross-talking could impact the connectivity results.

As future work, we could list the following:

- Verify the impact of volume conduction and use techniques to minimize it.
- Comparison of this method with other kinds of wrist movements, such as, radial/ulnar deviation and flexion and extension, and other hand/arm movements.
- Comparison of the applied method with MI multivariate and other multivariate methods.
- Comparison of the different kinds of normalization of MI, and to verify the effects on the selection of relevant channels.
- Comparison of the relevance of other EEG bands (theta, delta and gamma) that were not explored in this study.
- Comparison of the applied method with effective connectivity ones and verify if the causal information could complement functional features.

- To verify the effect of different windows of time and implement adaptive windows.

9.1 Publications

Below, there is the list of all publications generated during the doctorate program.

1) National and International Scientific Journals

First author:

- MELO, M.C.; Macedo, D.R.; SOARES, A.B. Divergent findings in brain reorganization after spinal cord injury: a review**. Journal of Neuroimaging**. v. 20, n.4, p. 410-427, 2020.

Co- author:

- VIEIRA, D; SILVA, M. B.; MELO, M. C.; SOARES, A.B. Effect of Myofeedback on the Threshold of the Stretch Reflex Response of Post-Stroke Spastic Patients. **Disability and Rehabilitation**, v. 39, p. 458-467, 2017.
- AZEVEDO, M. R.; SILVA, M. B.; MELO, M. C.; MACIEL, M; SOARES, A.B. Bruxismo do sono e o padrão neurocomportamental - Proposta de protocolo de biofeedback multimodal. **Ortodontia,** v. 48, p. 270-283, 2015.

2) National and International Scientific Conferences:

First author:

- MELO, M. C.; MACEDO, D. R.; SOARES, A. B.; KRISHNAN, S. Technological aspects of traumatic spinal cord injury rehabilitation. In: 2017 IEEE Canada International Humanitarian Technology Conference (IHTC),

2017, Toronto. 2017 IEEE Canada International Humanitarian Technology Conference (IHTC), 2017. v. 1. p. 11-15.

Co-author:

- ALMEIDA, M. Q. S. A.; MELO, M. C.; MACEDO, D. R.; DYONISIO, G.; CARVALHO, E. D.; SOARES, A. B. Functional Connectivity Analysis After Sci - A fMRI Study. Congresso Brasileiro de Engenharia Biomédica (CBEB 2018). IFMBE Proceedings. 1ed.: Springer Singapore, 2019, P. 589-596.
- MACEDO, D. R.; B. CARVALHO, E.; MELO, M. C.; M. LUPPI, A.; A. A. MACEDO, T.; DYONÍSIO, G.; SOARES, A. B. Alterações Corticais em Indivíduos Portadores de Lesão Medular - Um Estudo Baseado em Ressonância Magnética Funcional. In: Congresso Brasileiro de Eletromiografia e Cinesiologia (COBEC) e o Simpósio de Engenharia Biomédica (SEB) COBECSEB, Uberlândia. Anais do V Congresso Brasileiro de Eletromiografia e Cinesiologia e X Simpósio de Engenharia Biomédica, 2017.
- MACEDO, D. R.; CARVALHO, E. B.; MELO, M. C.; LUPPI, A. M.; MACEDO, T. A. A.; SOARES, A. B.. Evidências de Alterações Neuroanatômicas Após Lesão Medular com Uso de Ressonância Magnética. In: XXII Congresso Brasileiro de Física Médica, 2017, Ribeirão Preto - SP. Anais do XXII Congresso Brasileiro de Física Médica, 2017. v. 1. p. 1-1.
- SEGATTO, L. G.; MELO, M. C.; DA SILVA, G. M. Proposal of an educational game for improvement of cognitive performance of intellectually disabled people. In: 2017 IEEE Canada International Humanitarian Technology Conference (IHTC), 2017, Toronto. 2017 IEEE Canada International Humanitarian Technology Conference (IHTC), 2017. p. 109.
- SCHMIELE, E. F.; SPIRANDELI, A. F.; ARAMAKI, R. S.; OLIVEIRA, F. H. M.; MELO, M. C.; SOARES, A. B. Decodificação de Fonemas da Língua Portuguesa Baseada na Atividade Eletroencefalográfica. In: Anais COBECSEB 2017, Uberlândia. Anais do V Congresso Brasileiro de Eletromiografia e Cinesiologia e X Simpósio de Engenharia Biomédica, 2017.
- DYONISIO, G.; MACEDO, D. R.; MELO, M. C.; SOARES, A. B. Estudo Epidemiológico das Lesões Medulares em Adultos Jovens do Sexo Masculino

no Triângulo Mineiro. In: Congresso Brasileiro de Eletromiografia e Cinesiologia (COBEC) e o Simpósio de Engenharia Biomédica (SEB) COBECSEB, Uberlândia. Anais do V Congresso Brasileiro de Eletromiografia e Cinesiologia e X Simpósio de Engenharia Biomédica. Uberlândia: Even3, 2017.

- SEGATTO, L. G.; MELO, M. C.. Proposta de Jogo da Memória Para Análise de Desempenho Cognitivo de Deficientes Intelectuais. In: IX Simpósio de Engenharia Biomédica, 2016, 2016.
- VIEIRA JUNIOR, P. R.; MELO, M. C.; MIRANDA JUNIOR, L. C. Proposta se um Teclado Virtual Baseado em Eletromiografia Para Comunicação de Pessoas Com Necessidades Especiais. In: XIV Conferência de Estudos em Engenharia Elétrica, 2016, Uberlandia. Anais da XIV Conferência de Estudos em Engenharia Elétrica, 2016.
- DAMASCENO, M. F.; CAMPOS, W. O.; TACON, T. S.; CAPARELLI, K. R. B.; MELO, M. C. Proposta de medidor inteligente de consumo de energia elétrica. In: XIV Conferência de Estudos em Engenharia Elétrica, 2016, Uberlândia. XIV CEEL, 2016. v. 7.

References

1. DAVIDSON, R. J.; HUGDAHL, K. **Brain Asymmetry**. [S.l.]: MIT Press, 1996.
2. BROCA, P. Remarques sur le siege de la faculté du langage articulé, suives d'une observation d'aphemie. **Bull. Mem. Soc. Anatomique Paris 2**, p. 330-357, 1861.
3. WERNICKE, C. **Der Aphasische Sysmtomenkomplex**. Breslau: Cohn and Weingart, 1874.
4. FRISTON, K. J. Functional and Effective Connectivity: A Review. **Brain Connectivity**, v. 1, n. 1, p. 13-36, 2011. https://doi.org/10.1089/brain.2011.0008
5. MOELLER, K.; WILLMES, K.; KLEIN, E. A review on functional and structural brain connectivity in numerical cognition. **Frontiers in Human Neuroscience**, v. 9, 2015. https://doi.org/10.3389/fnhum.2015.00227
6. MACHADO, S. et al. Sensorimotor integration: basic concepts, abnormalities related to movement disorders and sensorimotor training-induced cortical reorganization. **Rev Neurol.**, v. 51, n. 7, p. 427-36, 2010.
7. KANDEL, E. R.; SCHWARTZ, J. H.; JESSEL, T. M. **Princípios da Neurociência**. São Paulo: Manole, 2003.
8. DRONKERS, N.; OGAR, J. Brain areas involved in speech production. **Brain**, v. 127, n. 7, p. 1461-1462, 2004. https://doi.org/10.1093/brain/awh233
9. SIMONYAN, K. et al. New Developments in Understanding the Complexity of Human Speech Production. **Journal of Neuroscience**, v. 36, n. 45, p. 11440-11448, 2016. https://doi.org/10.1523/JNEUROSCI.2424-16.2016
10. GUYTON, A. C.; HALL, J. E. **Tratado de Fisiologia Médica**. [S.l.]: Elsevier / Medicina Nacionais, 2006.
11. LALAZAR, H.; VAADIA, E. Neural basis of sensorimotor learning: modifying internal models. **Current Opinion in Neurobiology**, v. 18, p. 1-9, 2008. https://doi.org/10.1016/j.conb.2008.11.003
12. COOPER, R. P. **Forward and Inverse Models in Motor Control and Cognitive Control**. Proceedings of the Symposium on AI-Inspired Biology. London: [s.n.]. 2010.
13. SYED, M. F. et al. Dynamic Functional Connectivity States Between the Dorsal

and Ventral Sensorimotor Networks Revealed by Dynamic Conditional Correlation Analysis of Resting-State Functional Magnetic Resonance Imaging. v. 7, n. 10, p. 635-642, 2017. https://doi.org/10.1089/brain.2017.0533

14. CHIA, L. C. et al. Functional near-infrared spectroscopy (fNIRS) brain imaging of multi-sensory integration during computerized dynamic posturography in middle-aged and older adults. **Exp Brain Res.**, v. 235, n. 4, p. 1247–1256, 2017. https://doi.org/10.1007/s00221-017-4893-8

15. MELNIK, A. et al. EEG correlates of sensorimotor processing: independent components involved in sensory and motor processing. **Scientific Reports** , v. 7, 2017. https://doi.org/10.1038/s41598-017-04757-8

16. SU, D. K.; OJEMANN, G. Electrocorticographic Sensorimotor Mapping. **Clin Neurophysiol.**, v. 124, n. 6, p. 1044-1048, 2013. https://doi.org/10.1016/j.clinph.2013.02.114

17. GLOVER, G. H. Overview of Functional Magnetic Resonance Imaging. **Neurosurg Clin N Am.**, 22, n. 2, 2011. 133-139. https://doi.org/10.1016/j.nec.2010.11.001

18. KUCEWICZ, M. T.; BERRY, M.; WORRELL, G. A. Simultaneos Macro- and Microrecordings. In: LHATOO, S. D.; KAHANE, P.; LUDERS, H. O. **Invasive Studies of the Human Epileptic Brain:** Principles and Practice. [S.l.]: Oxford University Press, 2019. https://doi.org/10.1093/med/9780198714668.003.0036

19. BUZSÁKI, G.; ANASTASSIOU, C. A.; KOCH, C. The origin of extracellular fields and currents — EEG, ECoG, LFP and spikes. **Nature Reviews Neuroscience**, 13, 2012. 407–420. https://doi.org/10.1038/nrn3241

20. HILL, N. J. et al. Recording human electrocorticographic (ECoG) signals for neuroscientific research and real-time functional cortical mapping. **J Vis Exp.**, 64, 2012. 3993. https://doi.org/10.3791/3993

21. NICOLAS-ALONSO, L. F.; GOMEZ-GIL, J. Brain Computer Interfaces, a Review. **Sensors (Basel)**, v. 12, n. 2, p. 1211-1279, 2012. https://doi.org/10.3390/s120201211

22. TEIXEIRA, S. et al. Gamma band oscillations in parietooccipital areas during performance of a sensorimotor integration task: a qEEG coherence study.

Arquivos de Neuro-Psiquiatria, v. 69, n. 2b, 2011. https://doi.org/10.1590/S0004-282X2011000300007

23. MISSELHORN, J. et al. Synchronization of Sensory Gamma Oscillations Promotes Multisensory Communication. **eNeuro**, v. 6, n. 5, 2019. https://doi.org/10.1523/ENEURO.0101-19.2019

24. HERRMANN, C. S.; DEMIRALP, T. Human EEG gamma oscillations in neuropsychiatric disorders. **Clin Neurophysiol.**, v. 116, n. 12, p. 2719-33, 2005. https://doi.org/10.1016/j.clinph.2005.07.007

25. VERHAGEN, L.; DIJERKMAN, H. C.; MEDENDORP, W. P. Cortical Dynamics of Sensorimotor Integration during Grasp Planning. **Journal of Neuroscience**, v. 32, n. 13, p. 4508-4519, 2012. https://doi.org/10.1523/JNEUROSCI.5451-11.2012

26. JENSON, D. et al. Temporal dynamics of sensorimotor integration in speech perception and production: independent component analysis of EEG data. **Front. Psychol**, v. 5, 2014. https://doi.org/10.3389/fpsyg.2014.00656

27. BROWN, K. E. et al. Sensorimotor integration in healthy aging: Baseline differences and response. **Experimental Gerontology**, v. 112, n. 2018, p. 1-8, 2018. https://doi.org/10.1016/j.exger.2018.08.004

28. TAM, W. K. et al. Human motor decoding from neural signals: a review. **BMC Biomedical Engineering volume**, v. 22, 2019. https://doi.org/10.1186/s42490-019-0022-z

29. TONONI, G.; SPORNS, O. Measuring information integration. **BMC Neuroscience**, v. 4, n. 31, 2003. https://doi.org/10.1186/1471-2202-4-31

30. SCHREIBER, T. Measuring information transfer. **Phys Rev Lett**, v. 85, n. 2, p. 461-464, 2000. https://doi.org/10.1103/PhysRevLett.85.461

31. ROWE, J. et al. Attention to action in Parkinson's disease: impaired effective connectivity among frontal cortical regions. **Brain**, v. 125, n. 2, p. 276-289, 2002. https://doi.org/10.1093/brain/awf036

32. BERTRAND, J.-A. et al. Brain Connectivity Alterations Are Associated with the Development of Dementia in Parkinson's Disease. **Brain Connectivity**, v. 6, n. 3, p. 216-224, 2016. https://doi.org/10.1089/brain.2015.0390

33. DUMAS, E. M. et al. Reduced functional brain connectivity prior to and after disease onset in Huntington's disease. **NeuroImage: Clinical**, v. 2, p. 377-384, 2013. https://doi.org/10.1016/j.nicl.2013.03.001

34. JIANG, L.; XU, H.; YU, C. Brain Connectivity Plasticity in the Motor Network after Ischemic Stroke. **Neural Plasticity**, 2013. https://doi.org/10.1155/2013/924192

35. KALINOSKY, B. T. et al. Tasked-Based Functional Brain Connectivity in Multisensory Control of Wrist Movement After Stroke. **Front. Neurol.**, v. 10, 2019. https://doi.org/10.3389/fneur.2019.00609

36. CHUNG, J. W. et al. Beta-band Activity and Connectivity in Sensorimotor and Parietal Cortex are Important for Accurate Motor Performance. **Neuroimage**, v. 144, p. 164-173, 2017. https://doi.org/10.1016/j.neuroimage.2016.10.008

37. FREYER, F. et al. Repetitive tactile stimulation changes resting-state functional connectivity—implications for treatment of sensorimotor decline. **Front Hum Neurosci.**, v. 6, n. 144, 2012. https://doi.org/10.3389/fnhum.2012.00144

38. PETERSON, S. M.; FERRIS, D. P. Group-level cortical and muscular connectivity during perturbations to walking and standing balance. **NeuroImage**, v. 198, p. 93-103, 2019. https://doi.org/10.1016/j.neuroimage.2019.05.038

39. SILVA, F. et al. Functional coupling of sensorimotor and associative areas during a catching ball task: a qEEG coherence study. **International Archives of Medicine**, v. 5, n. 9, 2012. https://doi.org/10.1186/1755-7682-5-9

40. DALY, I.; NASUTO, S. J.; WARWICK, K. Brain computer interface control via functional connectivity dynamics. **Pattern Recognition**, v. 45, n. 6, p. 2123-2136, 2012. https://doi.org/10.1016/j.patcog.2011.04.034

41. WU, X.; ZHENG, W.-L.; LU, B.-L. Investigating EEG-Based Functional Connectivity Patterns for Multimodal Emotion Recognition. **arXiv:2004.01973v1**, 2020. https://doi.org/10.1109/NER.2019.8717035

42. HAMEDI, M.; SALLEH, S.-H.; NOOR, A. M. Electroencephalographic Motor Imagery Brain Connectivity Analysis for BCI: A Review. **Neural Comput**, v. 28, n. 6, p. 999-1041, 2016. https://doi.org/10.1162/NECO_a_00838

43. YUAN, H.; HE, B. Brain-Computer Interfaces Using Sensorimotor Rhythms:

Current State and Future Perspectives. **IEEE Trans Biomed Eng.**, v. 61, n. 5, p. 1425–1435, 2014. https://doi.org/10.1109/TBME.2014.2312397

44. WIERZGAŁA, P. et al. Most Popular Signal Processing Methods in Motor-Imagery BCI: A Review and Meta-Analysis. **Frontiers in Neuroinformatics** , v. 12, 2018. https://doi.org/10.3389/fninf.2018.00078

45. FRIEDRICH, E. V. C.; SCHERER, R.; NEUPER, C. Long-term evaluation of a 4-class imagery-based brain–computer interface. **Clinical Neurophysiology**, v. 124, n. 5, p. 916-927, 2013. https://doi.org/10.1016/j.clinph.2012.11.010

46. RUPP, R. Challenges in clinical applications of brain computer interfaces in individuals with spinal cord injury. **Front Neuroeng.**, v. 7, n. 38, 2014. https://doi.org/10.3389/fneng.2014.00038

47. LÓPEZ-LARRAZ, E. et al. Evolution of EEG Motor Rhythms after Spinal Cord Injury: A Longitudinal Study. **PLoS One**, v. 10, n. 7, p. e0131759, 2015. https://doi.org/10.1371/journal.pone.0131759

48. XU, R. et al. Movement-related cortical potentials in paraplegic patients: abnormal patterns and considerations for BCI-rehabilitation. **Front Neuroeng.**, v. 7, n. 35, 2014. https://doi.org/10.3389/fneng.2014.00035

49. MÜLLER-PUTZ, G. R.; DALY, I.; KAISER, V. Motor imagery-induced EEG patterns in individuals with spinal cord injury and their impact on brain–computer interface accuracy. **Journal of Neural Engineering**, v. 11, p. 035011, 2014. https://doi.org/10.1088/1741-2560/11/3/035011

50. SALISBURY, D. B. et al. Brain–Computer Interface for Individuals After Spinal Cord Injury. **Rehabilitation Psychology**, v. 61, n. 4, p. 435-441, 2016. https://doi.org/10.1037/rep0000099

51. CORDELLA, F. et al. Literature Review on Needs of Upper Limb Prosthesis Users. **Front Neurosci.**, v. 10, n. 209, 2016. https://doi.org/10.3389/fnins.2016.00209

52. BAJAJ, N. M.; SPIERS, A. J.; DOLLAR, A. M. State of the Art in Artificial Wrists: A Review of Prosthetic and Robotic Wrist Design. **IEEE Transactions on Robotics**, v. 35, n. 1, 2019. https://doi.org/10.1109/TRO.2018.2865890

53. ROTHWELL, J. C. Overview of neurophysiology of movement control. **Clinical**

Neurology and Neurosurgery, v. 114, n. 5, p. 432-435, 2012. https://doi.org/10.1016/j.clineuro.2011.12.053

54. BERNE, R. M. et al. **Fisiologia**. Rio de Janeiro: Mosby, 2004.
55. POPOVIC, D. B.; SINKJAER, T. Central nervous system lesions leading to disability. **Journal of Automatic Control**, 18, n. 2, 2008. https://doi.org/10.2298/JAC0802011P
56. BAEHR, M.; FROTSCHER, M. **Duus' Topical Diagnosis in Neurology**. Stuttgart: Thieme, 2012. https://doi.org/10.1055/b-005-148826
57. LENT, R. **Cem bilhões de neurônios?** [S.l.]: Atheneu, 2010.
58. KAAS, J. H. **The Human Nervous System (Third Edition)**. [S.l.]: Elsevier, 2012.
59. KOLB, B.; WHISHAW, I. Q.; TESKEY, G. C. **An Introduction to Brain and Behavior**. [S.l.]: Worth Publishers, 2016.
60. OPENSTAX. **Anatomy and Physiology**. [S.l.]: OpenStax, 2013.
61. ELLISON, A. **Getting Your Head Around the Brain**. [S.l.]: Palgrave, 2012. https://doi.org/10.1007/978-1-137-27250-8
62. PURVES, D. et al. **Neurociencia**. Madrid: Medica panamericana, 2008.
63. FAGOT, J.; LACREUSE, A.; VAUCLAIR, J. Chapter 13 - Role of Sensory and Post-Sensory Factors on Hemispheric Asymmetries in Tactual Perception. **Advances in Psychology**, v. 123, p. 469-494, 1997. https://doi.org/10.1016/S0166-4115(97)80080-5
64. OPENSTAX COLLEGE. Anatomy & Physiology. **Connexions Web site**, 19 jun. 2013. Disponivel em: <http://cnx.org/content/col11496/1.6/>. Acesso em: 06 jul. 2020.
65. VYSHA. Brodmann areas with the lateral PFC and the ventromedial PFC clearly marked., 2013. Disponivel em: <https://commons.wikimedia.org/w/index.php?curid=78155917>. Acesso em: 21 jul. 2020.
66. PASKARI. **A picture of the posterior parietal lobe**, 02 jul. 2007. Disponivel em: <https://commons.wikimedia.org/wiki/File:Posterior_Parietal_Lobe.jpg>.

Acesso em: 06 jul. 2020.

67. LAMONZY, 14 jul. 2014. Disponivel em: <https://commons.wikimedia.org/wiki/File:Human_motor_cortex.jpg>. Acesso em: 06 jul. 2020.

68. HEROLD, F. et al. Applications of Functional Near-Infrared Spectroscopy (fNIRS) Neuroimaging in Exercise–Cognition Science: A Systematic, Methodology-Focused Review. **J Clin Med.**, v. 7, n. 12, 2018. https://doi.org/10.3390/jcm7120466

69. WALEJ. Functional near-infrared spectroscopy (fNIRS) - Hitachi ETG-4000 (2), 21 out. 2017. Disponivel em: <https://commons.wikimedia.org/wiki/File:FNIRS_head_Hitachi_ETG4000_2.jpg>. Acesso em: 06 fev. 2020.

70. DOMINICO, S. I. D. et al. unctional Near-Infrared Spectroscopy: Proof of Concept for Its Application in Social Neuroscience. In: **Neuroergonomics**. [S.l.]: Academic Press, 2019. p. 169-173. https://doi.org/10.1016/B978-0-12-811926-6.00028-2

71. AINALI, J., 12 fev. 2008. Disponivel em: <https://commons.wikimedia.org/wiki/File:MRI-Philips.JPG>. Acesso em: 06 jul. 2020.

72. MELO, M. C. et al. **Technological aspects of traumatic spinal cord injury rehabilitation**. 2017 IEEE Canada International Humanitarian Technology Conference (IHTC). Toronto: [s.n.]. 2017. https://doi.org/10.1109/IHTC.2017.8058169

73. TAM, W.-K. et al. Human motor decoding from neural signals: a review. **BMC Biomedical Engineering**, v. 22, n. 2019, 2019. https://doi.org/10.1186/s42490-019-0022-z

74. SZOSTAK, K. M.; GRAND, L.; CONSTANDINOU, T. G. Neural Interfaces for Intracortical Recording: Requirements, Fabrication Methods, and Characteristics. **Front. Neurosci.**, v. 11, 2017. https://doi.org/10.3389/fnins.2017.00665

75. JEREMY HILL, N. et al. Recording Human Electrocorticographic (ECoG) Signals for Neuroscientific Research and Real-time Functional Cortical Mapping.

J Vis Exp, v. 64, n. 3993, 2012.

76. PASCUAL-MARQUI, R. D. et al. Low resolution brain electromagnetic tomography (LORETA) functional imaging in acute, neuroleptic-naive, first-episode, productive schizophrenia. **Psychiatry Res.**, v. 90, n. 3, p. 169-79, 1999. https://doi.org/10.1016/S0925-4927(99)00013-X

77. AMERICAN Electroencephalographic Society Guidelines for Standard Electrode Position Nomenclature. **Journal of Clinical Neurophysiology**, v. 8, n. 2, p. 200-202, 1991. https://doi.org/10.1097/00004691-199104000-00007

78. RIDC NEUROMAT, 27 jul. 2017. Disponivel em: <https://commons.wikimedia.org/wiki/File:Random_Structures_in_the_Brain_102.jpg>. Acesso em: 22 jul. 2020.

79. SINGH, S. P. Magnetoencephalography: Basic principles. **Ann Indian Acad Neurol**, v. 17, n. 1, p. 107-112, 2014. https://doi.org/10.4103/0972-2327.128676

80. JENSON, D. et al. **Speech perception, production, and the sensorimotor mu rhythm**. Proceedings of the 2014 Biomedical Sciences and Engineering Conference. [S.l.]: [s.n.]. 2014. https://doi.org/10.1109/BSEC.2014.6867736

81. MCFARLAND, D. J. et al. Mu and beta rhythm topographies during motor imagery and actual movements. **Brain Topogr.** , v. 12, n. 3, p. 177-86, 2000. https://doi.org/10.1023/A:1023437823106

82. VERHAGEN, L. et al. Cortical Dynamics of Sensorimotor Integration during Grasp. **The Journal of Neuroscience**, v. 32, n. 13, p. 4508 – 4519, 2012. https://doi.org/10.1523/JNEUROSCI.5451-11.2012

83. NAKAYASHIKI, K. et al. Modulation of event-related desynchronization during kinematic and kinetic hand movements. **Journal of NeuroEngineering and Rehabilitation**, v. 11, n. 90, 2014. https://doi.org/10.1186/1743-0003-11-90

84. CUELLAR, M. et al. Time-frequency analysis of the EEG mu rhythm as a measure of sensorimotor integration in the later stages of swallowing. **Clinical Neurophysiology**, v. 127, n. 2016, p. 2625-2635, 2016. https://doi.org/10.1016/j.clinph.2016.04.027

85. MYKLAND, M. S. et al. Fluctuations of sensorimotor processing in migraine: a controlled longitudinal study of beta event related desynchronization. **The**

Journal of Headache and Pain, v. 20, n. 77, 2019. https://doi.org/10.1186/s10194-019-1026-8

86. MAZUREK, K. A. et al. Utilizing High-Density Electroencephalography and Motion Capture Technology to Characterize Sensorimotor Integration While Performing Complex Actions. **IEEE TRANSACTIONS ON NEURAL SYSTEMS AND REHABILITATION ENGINEERING**, v. 28, n. 1, p. 287-295, 2020. https://doi.org/10.1109/TNSRE.2019.2941574
87. LAU, T. M.; GWIN, J. T.; FERRIS, D. P. Walking reduces sensorimotor network connectivity compared to standing. **Journal of NeuroEngineering and Rehabilitation**, v. 11, n. 14, 2014. https://doi.org/10.1186/1743-0003-11-14
88. ANWAR, A. R. et al. Effective Connectivity of Cortical Sensorimotor Networks During Finger Movement Tasks: A Simultaneous fNIRS, fMRI, EEG Study. **Brain Topogr** , v. 29, p. 645–660 , 2016. https://doi.org/10.1007/s10548-016-0507-1
89. CHUNG, J. W. et al. Beta-band Activity and Connectivity in Sensorimotor and Parietal Cortex are Important for Accurate Motor Performance. **Neuroimage**, v. 144, p. 164-173, 2017. https://doi.org/10.1016/j.neuroimage.2016.10.008
90. ROSARIO, R. et al. Motif-Synchronization: a new method for analysis of dynamic brain networks with EEG. **Physica A**, 2015, n. 439, 2015. 7-19. https://doi.org/10.1016/j.physa.2015.07.018
91. STEFANO FILHO, A.; ATTUS, R.; CASTELLANO, G. EEG sensorimotor rhythms' variation and functional connectivity measures during motor imagery: linear relations and classification approaches. **Peer J**, 2017. https://doi.org/10.7717/peerj.3983
92. PICHIORRI, F. et al. An EEG index of sensorimotor interhemispheric coupling after unilateral stroke: clinical and neurophysiological study. **European Journal of Neuroscience**, v. 47, p. 158-163, 2018. https://doi.org/10.1111/ejn.13797
93. SPORNS, O. et al. Organization, development and function of complex brain networks. **Trends in Cognitive Science**, v. 8, n. 9, p. 418-425, 2004. https://doi.org/10.1016/j.tics.2004.07.008
94. ASHBURNER, J.; FRISTON, K.; PENNY, W. **Human Brain Function**. [S.l.]:

[s.n.], 2003.

95. SAKKALIS, V. Review of advanced techniques for the estimation of brain connectivity measured with EEG/MEG. **Comput Biol Med**, v. 41, n. 12, p. 1110-1117, 2011. https://doi.org/10.1016/j.compbiomed.2011.06.020

96. BRONZINO, J. D.; PETERSON, D. R. **Biomedical Signals, Imaging, and Informatics**. Boca Raton: CRC Press, 2015. https://doi.org/10.1201/b15468

97. KUS, R.; KAMINSKI, M.; BLINOWSKA, K. J. Determination of EEG Activity Propagation: Pair-Wise Versus Multichannel Estimate. **IEEE TRANSACTIONS ON BIOMEDICAL ENGINEERING**, v. 51, n. 9, p. 1501-1510, 2004. https://doi.org/10.1109/TBME.2004.827929

98. BLINOWSKA, K. J. Review of the methods of determination of directed connectivity from multichannel data. **Medical & Biological Engineering & Computing**, v. 49, n. 5, p. 521-529, 2011. https://doi.org/10.1007/s11517-011-0739-x

99. KAMINSKI, M.; BLINOSWKA, K. J. Directed Transfer Function is not influenced by volume conduction - inexpedient pre-processing should be avoided. **frontiers in Computational Neuroscience**, 8, n. 61, 2014. https://doi.org/10.3389/fncom.2014.00061

100. BLINOWSKA, K. J.; KUS, R.; KAMINSKI, M. Granger causality and information flow in multivariate processes. **Phys. Rev. E**, v. 70, n. 5, p. 050902, 2004. https://doi.org/10.1103/PhysRevE.70.050902

101. KAMINSKI, M. Determination of transmission patterns in multichannel data. **Philos Trans R Soc Lond B Biol Sci**, v. 360, n. 1457, p. 947-952, 2005. https://doi.org/10.1098/rstb.2005.1636

102. JIN, S.-H.; LIN, P.; HALLETT, M. Linear and nonlinear information flow based on time delayed mutual information method and its application to corticomuscular interaction. **Clinical Neurophysiology**, v. 121, n. 3, p. 392, 2010. https://doi.org/10.1016/j.clinph.2009.09.033

103. GERLOFF, C. et al. Functional coupling and regional activation of human cortical motor areas during simple, internally paced and externally paced finger movements. **Brain**, v. 121, n. 8, p. 1513-1531, 1998.

https://doi.org/10.1093/brain/121.8.1513

104. LEOCANI, L. et al. Event-related coherence and event-related desynchronization/synchronization in the 10 Hz and 20 Hz EEG during self-paced movement. **Electroencephalogr Clin Neurophysiol**, v. 104, p. 199-206, 1997. https://doi.org/10.1016/S0168-5597(96)96051-7

105. NAGAMINE, T. et al. Movement-related slow cortical magnetic fields and changes of spontaneous MEG- and EEG-brain rhythms.. **Electroencephalogr Clin Neurophysiol**, v. 99, p. 274-286, 1996. https://doi.org/10.1016/0013-4694(96)95154-8

106. KRISTEVA, R.; PATINO, L.; OMLOR, W. Beta-range cortical motor spectral power and corticomuscular coherence as a mechanism for effective corticospinal interaction during steady-state motor output. **Neuroimage**, v. 36, p. 785-792, 2007. https://doi.org/10.1016/j.neuroimage.2007.03.025

107. GUEVARA, M. A.; CORSI-CABRERA, M. EEG coherence or EEG correlation? **International Journal of Psychophysiology**, v. 23, n. 3, p. 145-153, 1996. https://doi.org/10.1016/S0167-8760(96)00038-4

108. JALILI, M.; KNYAZEVA, M. G.; BARZEGARAN, E. Synchronization of EEG: Bivariate and Multivariate Measures. **IEEE Transactions on Neural Systems and Rehabilitation Engineering**, 2013. https://doi.org/10.1109/TNSRE.2013.2289899

109. PIJN, J. P. et al. Nonlinear dynamics of epileptic seizures on basis of intracranial EEG recordings. **Brain Topogr**, v. 9, n. 4, p. 249-70, 1997. https://doi.org/10.1007/BF01464480

110. MIZAEI, P. et al. Surrogate data test for nonlinearity of EEG signals: A newborn EEG burst suppression case study. **Digital Signal Processing**, v. 70, p. 30-38, 2017. https://doi.org/10.1016/j.dsp.2017.07.010

111. STEPIEN, R. A. Testing for non-linearity in EEG signal of healthy subjects. **Acta Neurobiol. Exp**, v. 62, p. 277-281, 2002.

112. DAVID, O.; COSMELLI, D.; FRISTON, K. J. Evaluation of different measures of functional connectivity using a neural mass model. **Neuroimage**, v. 21, n. 2, p. 659-573, 2004. https://doi.org/10.1016/j.neuroimage.2003.10.006

113. NETOFF, I. T. et al. Detecting Coupling in the Presence of Noise and Nonlinearity. In: **Handbook of Time Series Analysis:** Recent Theoretical Developments and Applications. Weinheim: Wiley, 2006. p. 265-281. https://doi.org/10.1002/9783527609970.ch11

114. CHANGCHENG, S. et al. Mutual Information-Based Brain Network Analysis in Post-stroke Patients With Different Levels of Depression. **Front. Hum. Neurosci**, v. 12, 2018. https://doi.org/10.3389/fnhum.2018.00285

115. PETKOSKI, S.; PALVA, J. M.; JIRSA, V. K. Phase-lags in large scale brain synchronization: Methodological considerations and in-silico analysis. **Plos Computational Biology**, v. 14, n. 7, p. e1006160, 2018. https://doi.org/10.1371/journal.pcbi.1006160

116. WANG, F. et al. Study of the Home-Auxiliary Robot Based on BCI. **Sensors**, v. 18, n. 1779, 2018. https://doi.org/10.3390/s18061779

117. MOHANTY, R. et al. Rethinking Measures of Functional Connectivity via Feature Extraction. **Scientific Reports volume**, 2020. https://doi.org/10.1038/s41598-020-57915-w

118. RODGERS, L. J.; NICEWANDER, W. A. Thirteen Ways to Look at the Correlation Coefficient . **The American Statistician**, 42, n. 1, 1988. 59-66. https://doi.org/10.1080/00031305.1988.10475524

119. BASTOS, A. M.; SCHOFFELEN, J. M. A Tutorial Review of Functional Connectivity Analysis Methods and Their Interpretational Pitfalls. **Front. Syst. Neurosci.**, 9, 2016. https://doi.org/10.3389/fnsys.2015.00175

120. QUIROGA, Q. R. et al. Performance of different synchronization measures in real data: a case study on electroencephalographic signals, 65, n. 4, 2002. https://doi.org/10.1103/PhysRevE.65.041903

121. BALL, K. R. et al. A multivariate extension of mutual information for growing neural networks. **Neural Networks**, v. 95, n. 2017, p. 29-43, 2017. https://doi.org/10.1016/j.neunet.2017.07.009

122. JEONG, J.; GORE, J. C.; PETERSON, B. S. Mutual information analysis of the EEG in patients with Alzheimer's disease. **Clinical Neurophysiology**, v. 112, n. 5, p. 827-835, 2001. https://doi.org/10.1016/S1388-2457(01)00513-2

123. VICENTE, R. et al. Transfer entropy—a model-free measure of effective connectivity for the neurosciences. **Journal of Computational Neuroscience**, v. 30, n. 1, p. 45-67, 2011. https://doi.org/10.1007/s10827-010-0262-3

124. KVALSETH, T. O. Entropy and Correlation: Some Comments. **IEEE Transactions on Systems, Man, and Cybernetics**, 17, n. 3, 1987. 517-519. https://doi.org/10.1109/TSMC.1987.4309069

125. YAO, Y. Y. Information-Theoretic Measures for Knowledge Discovery and Data Mining. In: KARMESHU **Entropy Measures, Maximum Entropy Principle and Emerging Applications.** Berlin: Springer, 2003. p. 115-136. https://doi.org/10.1007/978-3-540-36212-8_6

126. STREHL, A.; GHOSH, J. Cluster Ensembles – A Knowledge Reuse Framework for Combining Multiple Partitions. **Journal of Machine Learning Research**, 3, 2002. 583-617.

127. TIMME, N. M.; LAPISH, C. A Tutorial for Information Theory in Neuroscience. **eNeuro**, v. 5, n. 3, 2018. https://doi.org/10.1523/ENEURO.0052-18.2018

128. GREFKES, C.; FINK, G. R. Reorganization of cerebral networks after stroke: new insights from neuroimaging with connectivity approaches. **Brain**, v. 134, n. 5, p. 1264-1276, 2011. https://doi.org/10.1093/brain/awr033

129. FELL, J.; AXMACHER, N. The role of phase synchronization in memory processes. **Nature Reviews Neuroscience**, v. 12, p. 105-118, 2011. https://doi.org/10.1038/nrn2979

130. LE VAN QUYEN, M. et al. Comparison of Hilbert transform and wavelet methods for the analysis of neuronal synchrony. **J. Neurosci. Methods**, v. 111, p. 83-98, 2001. https://doi.org/10.1016/S0165-0270(01)00372-7

131. BOASHASH, B. **Time-frequency Signal Analysis**. Oxford: Longman Cheshire, 2003.

132. MITRA, A. **Computation of Synchronization for coupled systems by Synchronization Likelihood**. 6th International Conference on Advanced Computing & Communication Technologies (ICCCT-2012). Delhi: [s.n.]. 2012.

133. STAM, C. J.; VAN DIJK, B. W. Synchronization likelihood: an unbiased measure of generalized synchronization in multivariate data sets. **Physica D**, v.

163, p. 236-251, 2002. https://doi.org/10.1016/S0167-2789(01)00386-4

134. MCQUARRIE, A. D. R.; TSAI, C.-L. The Multivariate Regression Model. In: **Regression and Time Series Model Selection**. Singapore: World Scientific, 1998. p. 141-197. https://doi.org/10.1142/9789812385451_0004

135. BRESSLER, S. L.; SETH, A. K. Wiener–Granger Causality: A well established methodology. **NeuroImage**, v. 58, p. 323-329, 2011. https://doi.org/10.1016/j.neuroimage.2010.02.059

136. BEHARELLE, A. R.; SMALL, S. L. **Imaging Brain Networks for Language**. [S.l.]: [s.n.], 2016. https://doi.org/10.1016/B978-0-12-407794-2.00064-X

137. KRUMIN, M.; SHOHAM, S. Multivariate Autoregressive Modeling and Granger Causality Analysis of Multiple Spike Trains, 2010, 2010. https://doi.org/10.1155/2010/752428

138. PEREDA, E.; QUIROGA, R. Q.; BHATTACHARYA, J. Nonlinear multivariate analysis of neurophysiological signals. **Progress in Neurobiology**, v. 77, n. 1-2, p. 1-37, 2005. https://doi.org/10.1016/j.pneurobio.2005.10.003

139. FRANASZCZUK, P. J.; BERGEY, G. J.; KAMINSKI, M. Analysis of mesial temporal seizure onset and propagation using the directed transfer function method. **Electroencephalogr Clin Neurophysiol**, v. 91, p. 413-427, 1994. https://doi.org/10.1016/0013-4694(94)90163-5

140. KAMINSKI, M.; BLINOWSKA, K. J.; SZELENBERGER, W. opographic analysis of coherence and propagation of EEG activity during sleep and wakefulness. **Electroencephalogr Clin Neurophysiol.** , v. 102, p. 216-227, 1997. https://doi.org/10.1016/S0013-4694(96)95721-5

141. ASTOLFI, L. et al. Assessing cortical functional connectivity by linear inverse estimation and directed transfer function: simulations and application to real data. **Clin Neurophysiol**, v. 116, n. 4, p. 920-932, 2005. https://doi.org/10.1016/j.clinph.2004.10.012

142. KAMINSKI, M. et al. Evaluating causal relations in neural systems: Granger causality, directed transfer function and statistical assessment of significance. **Biological Cybernetics**, v. 85, p. 145-157, 2001. https://doi.org/10.1007/s004220000235

143. KORZENIEWSKA, A. et al. Determination of information flow direction among brain structures by a modified directed transfer function (dDTF) method. **Journal of Neuroscience Methods**, v. 125, n. 1-2, p. 195-207, 2003. https://doi.org/10.1016/S0165-0270(03)00052-9

144. FLORIN, E. **Causality measures between signals from invasively and non-invasively obtained local field potentials in humans**. Jülich, p. 257. 2010.

145. WANG, Z. et al. Time Varying Dynamic Bayesian Network for Nonstationary Events Modeling and Online Inference. **IEEE Transactions on Signal Processing**, v. 59, n. 4, p. 1553-1568, 2011. https://doi.org/10.1109/TSP.2010.2103071

146. SONG, L.; KOLAR, M.; XING, E. P. **Time-Varying Dynamic Bayesian Networks**. Neural Information Processing Systems (NIPS). [S.l.]: [s.n.]. 2009.

147. BEN-GAL, I. **Bayesian Networks**. [S.l.]: Wiley & Sons, 2007. https://doi.org/10.1002/9780470061572.eqr089

148. THE Future of Brain/Neural Computer Interaction: Horizon 2020. Disponivel em: <http://bnci-horizon-2020.eu/database/data-sets>. Acesso em: 10 mar. 2020.

149. OFNER, P. et al. Upper limb movements can be decoded from the time-domain of low-frequency EEG. **Plos One**, 2017. https://doi.org/10.1371/journal.pone.0182578

150. THARWAR, A. Independent component analysis: An introduction. **Applied Computing and Informatics**, 2018. https://doi.org/10.1016/j.aci.2018.08.006

151. Disponivel em: <https://sccn.ucsd.edu/~jung/Site/EEG_artifact_removal.html>. Acesso em: 08 abr. 2020.

152. BRAINMASTER 2.0 software. Disponivel em: <http://www.brainm.com/software/pubs/dg/BA_10-20_ROI_Talairach/nearesteeg.htm>. Acesso em: 2020 abr. 13.

153. PFURTSCHELLER, G. Functional brain imaging based on ERD/ERS. **Vision Research**, v. 41, n. 10-11, p. 1257-1260, 2001. https://doi.org/10.1016/S0042-6989(00)00235-2

154. GRAIMANN, B. et al. Visualization of significant ERD/ERS patterns in multichannel EEG and ECoG data. **Clinical Neurophysiology**, v. 113, p. 43–47,

2002. https://doi.org/10.1016/S1388-2457(01)00697-6

155. BALAKRISHNAN, N.; IBRAGIMOV, I. A. V. B.; NEVZOROV, V. B. **Asymptotic Methods in Probability and Statistics with Applications**. [S.l.]: Birkhäuser, 2001. https://doi.org/10.1007/978-1-4612-0209-7

156. ZELLER, D.; ROCCA, M. A. **Plasticity in Multiple Sclerosis:** From Molecular to System Level, from Adaptation to Maladaptation. [S.l.]: Front. Neurol., 2015. https://doi.org/10.3389/fneur.2015.00265

157. ILYAS, M. Z. et al. **Classification of EEG signals for brain-computer interface applications:** Performance comparison. International Conference on Robotics, Automation and Sciences (ICORAS). [S.l.]: [s.n.]. 2016. https://doi.org/10.1109/ICORAS.2016.7872610

158. GULLER, I.; UBEYLI, E. D. Multiclass Support Vector Machines for EEG-Signals Classification. **IEEE TRANSACTIONS ON INFORMATION TECHNOLOGY IN BIOMEDICINE**, v. 11, n. 2, 2007. https://doi.org/10.1109/TITB.2006.879600

159. MA, Y. et al. Classification of Motor Imagery EEG Signals with Support Vector Machines and Particle Swarm Optimization. **Computational and Mathematical Methods in Medicine**, v. 2016, p. Computational and Mathematical Methods in Medicine, 2016. https://doi.org/10.1155/2016/4941235

160. AMIN, H. U. et al. Classification of EEG Signals Based on Pattern Recognition Approach. **Front. Comput. Neurosci**, v. 11, 2017. https://doi.org/10.3389/fncom.2017.00103

161. MALON, C.; UCHIDA, S.; SUZUKI, M. Mathematical symbol recognition with support vector machines. **Pattern Recognition Letters**, v. 29, p. 1326-1332, 2008. https://doi.org/10.1016/j.patrec.2008.02.005

162. MATHWORKS. Disponivel em: <mathworks.com/help/stats/sequential-feature-selection.html>. Acesso em: 15 jun. 2020.

163. FITCSVM. Disponivel em: <https://www.mathworks.com/help/stats/fitcsvm.html>. Acesso em: 15 jun. 2020.

164. SPEIER , W.; ARNOLD, C.; POURATIAN, N. Evaluating true BCI Communication through Mutual Information and Language Models. **PLoS ONE**,

8, n. 10, 2013. https://doi.org/10.1371/journal.pone.0078432

165. PORTAL Action. Disponivel em: <http://www.portalaction.com.br/tecnicas-nao-parametricas/teste-de-friedman>. Acesso em: 16 jun. 2020.

166. MULTCOMPARE. Disponivel em: <https://www.mathworks.com/help/stats/multcompare.html>. Acesso em: 17 jun. 2020.

167. GRAIMANN, B.; PFURTSCHELLER, G. Quantification of visualization of event-related changes in oscillatory brain activity in the time frequency domain. In: **Event-Related Dynamics of Brain Oscillations**. [S.l.]: Elsevier, 2006. https://doi.org/10.1016/S0079-6123(06)59006-5

168. PATTNAIK, K.; SARRAF, J. Brain Computer Interface issues on hand movement. **Journal of King Saud University – Computer and Information Sciences**, p. 1319-1578, 2016.

169. SCHIATTI, L. et al. **Mutual Information-Based Feature Selection for Low-Cost BCIs**. 38th Annual International Conference of the IEEE Engineering in Medicine and Biology Society (EMBC). [S.l.]: [s.n.]. 2016. https://doi.org/10.1109/EMBC.2016.7591305

170. RIEHLE, A.; VAADIA, E. **Motor Cortex in Voluntary Movements:** a distributed system for distributed functions. CRC Press: [s.n.], 2004. https://doi.org/10.1201/9780203503584

171. KUANG, S.; MOREL, P.; GAIL, A. Planning Movements in Visual and Physical Space in Monkey Posterior Parietal Cortex. **Cerebral Cortex**, v. 26, n. 2, 2016. https://doi.org/10.1093/cercor/bhu312

172. NEUPER, C.; PFURTSCHELLER, G. Event-related dynamics of cortical rhythms: frequency-specific features and functional correlates. **International Journal of Psychophysiology**, v. 43, p. 41-58, 2001. https://doi.org/10.1016/S0167-8760(01)00178-7

173. KHAN, Y. U.; SEPULVEDA, F. Brain-computer interface for single-trial EEG classification for wrist movement imagery using spatial filtering in the gamma band. **IET Signal Processing**, v. 4, n. 5, 2010. https://doi.org/10.1049/iet-spr.2008.0235

174. KIGUCHI, K.; DULANTHA, T.; HAYASHI, Y. Estimation of Forearm Supination/Pronation Motion Based on EEG Signals to Controle an Artificial Arm. **Journal of Advanced Mechnical Design, Systems and Manufacturing**, 7, n. 1, 2013. 74-81. https://doi.org/10.1299/jamdsm.7.74

175. IBÁNEZ, J. et al. **An EEG-Based Design for the Online Detection of Movement Intention**. IWANN 2011: Advances in Computational Intelligence. [S.l.]: [s.n.]. 2011. https://doi.org/10.1007/978-3-642-21501-8_46